

Tephrochronology of the North Atlantic during the Last Glacial period – a paleoclimate synchronization tool



Sunniva Rutledal

Thesis for the degree of Philosophiae Doctor (PhD)
University of Bergen, Norway
2021

UNIVERSITY OF BERGEN



Tephrochronology of the North Atlantic during the Last Glacial period – a paleoclimate synchronization tool

Sunniva Rutledal



Thesis for the degree of Philosophiae Doctor (PhD)
at the University of Bergen

Date of defense: 09.04.2021

© Copyright Sunniva Rutledal

The material in this publication is covered by the provisions of the Copyright Act.

Year: 2021

Title: Tephrochronology of the North Atlantic during the Last Glacial period – a paleoclimate synchronization tool

Name: Sunniva Rutledal

Print: Skipnes Kommunikasjon / University of Bergen

“It is fair to say that cryptotehpra analysts typically develop and share some common traits, with most being methodical and patient and, above all, showing strong determination and perseverance”

Davies (2015)

Scientific environment

The research leading to this thesis was carried out at the Department of Earth Science and the Bjerknes Centre for Climate Research, University of Bergen, Norway, between September 2017 and December 2020. The laboratory work was conducted at the Tephra Analysis Unit, University of Edinburgh and EARTHLAB, University of Bergen.

This thesis was part of the Ice2Ice (Arctic Sea Ice and Greenland Ice Sheet Sensitivity) project funded by the European Research Council under the European Community's Seventh Framework Programme (FP7/2007-2013) / ERC synergy grant agreement n° 610055.

Main supervisor of this PhD thesis was Professor Eystein Jansen (University of Bergen) and co-supervisors were Professor Haflidi Haflidason (University of Bergen), Dr. Sarah M. P. Berben (University of Bergen) and Dr. Trond. M. Dokken (NORCE, Norwegian Research Centre).



European Research Council
Established by the European Commission



EARTHLAB
Earth Surface Sediment Laboratory

Acknowledgements

First, I would like to thank my supervisors. This thesis would not have been possible without their continuous support and advice. Thank you, Eystein for giving me the opportunity to work on such an exciting topic within the environment of the Ice2Ice project. I am thankful for your many thorough manuscript revisions and for giving me the freedom to explore and design this PhD project. Thank you, Trond for always taking an interest in new tephra findings, especially thank you for believing in the project and always cheering me on along the way. I am forever grateful to Hafliði for jumping on to supervise this PhD project mid-way when I needed extra tephra support. Your knowledge of Icelandic tephra is beyond inspiring! Thank you for believing in me and always having your door open for short and long discussions. Lastly, thank you Sarah for your patience with me both in the lab and in the many rounds of manuscript revisions. Thank you for the many joyful (and exhausting...) trips to Edinburgh.

I also want to thank Jordan Donn Holl for help in sample preparation and for always having a cheerful mood in the lab. I thank Eivind Støren for support whenever I needed something in the lab (often on short notice!). A special thank you to Chris Hayward at the Tephra Analysis Unit in Edinburgh for his assistance with the EPMA analysis.

I want to thank the Ice2Ice project members and especially Team Jansen for inspiring ideas and collaborations. Thank you, Amandine Tisserand for help with Mg/Ca analysis. Especially, I thank my office neighbor Margit Simon for contributions to Paper 2 in this thesis. That paper would not have been possible without your continuous help and support.

Thank you to friends and colleagues at GEO (UiB) and the Bjerknes Centre for interesting discussions and fun lunch breaks. Thank you to my cruise-companion and friend Anna B. H. for an amazing experience up in the frozen Arctic Ocean and for proofreading my thesis. A special thanks to my former office mates Eva, Henrik, Lisa and Evi for the warm welcome to the office. Thank you, Lisa for many encouraging scientific and non-scientific conversations. I also have to thank Jan Magne and Willem

for guidance in using the CT-scanner, and especially Willem for providing invaluable advice along the way.

I would also like to thank my family and friends in Bergen for encouragement and support. A special thank you to Hege Kilhavn for proofreading my thesis.

Finally, thank you Herman for always being there and believing in me.

We made it!

Sunniva Rutledal
Sunniva Rutledal

Bergen, 23rd of December 2020

Abstract

During present time, the global climate is changing at a rapid pace. To understand the future consequences of these changes, studies of past abrupt climate change are essential. A natural analogue to the current climate change is re-occurring abrupt warming episodes first witnessed in Greenland during the Last Glacial period. These events, referred to as Dansgaard-Oeschger (DO) events manifested as rapid warming on decadal timescales of up to 15°C in Greenland air temperature, followed by a gradual decline to colder temperatures. Understanding of the forcing mechanisms behind these events is currently limited by chronological uncertainties and the inability to accurately synchronize disparate climate records.

However, the application of tephrochronology has the potential for testing hypotheses regarding the synchronicity of past climate change events. This by utilizing the near to simultaneous deposition of geochemically distinct tephra material in different climate archives over large geographical distances. That potential is demonstrated in this thesis, by the documentation of previously known and unknown tephra horizons in the North Atlantic Ocean.

Findings presented in this thesis extend the established North Atlantic marine tephra framework by the identification of the well-known Faroe Marine Ash Zone (FMAZ) II-1 and North Atlantic Ash Zone (NAAZ) II (II-RHY-1) tephra horizons in the Irminger and Labrador Seas. A significant discovery, opening for a wider marine-marine cross-correlation of paleoproxy records. Furthermore, this thesis demonstrates the previously unknown tephrochronological potential of the Labrador Sea region by the publication of the first continuous tephrostratigraphic record from this area. Here, five isochronous tephra layers sourced from the Bárðarbunga-Veidivötn and Grímsvötn volcanic systems have the potential to serve as important chronological tie-points, if identified elsewhere in future studies. Collectively, these two studies (**Paper 1 and 3**), document that regions outside the dominant eastward wind direction from Iceland contain records of isochronous tephra layers. A key factor being the rapid transportation of tephra on drifting sea-ice along the East Greenland Current.

Additionally, we show the potential of applying tephrochronology in paleoclimate research by the reconstruction of marine reservoir ages (MRAs) in a transect of marine sediment cores where the FMAZ II-1 tephra horizon had been identified (**Paper 2**). First, the findings document large spatial variability in near-surface MRAs, ranging from 543 to 2523 ^{14}C years across the North Atlantic Ocean, which will have large implications for marine radiocarbon-based chronologies. Moreover, the FMAZ II-1 horizon is perfectly positioned to constrain the onset of the Last Glacial Maximum (LGM) (i.e., $26\,740 \pm 390$ years b2k). Higher than modern near-surface MRAs (i.e., >400 ^{14}C years) representing a vigorous Atlantic inflow, can be interpreted to reflect a weaker flux of Atlantic water. Following this, we reconstruct the spatial configuration of the Atlantic surface inflow branches at that time. The results indicate that the primary pathway of Atlantic advection into the Nordic Seas was probably routed west of the Faroe Islands, over the Iceland-Faroe Ridge, with limited advection through the Faroe-Shetland Channel. In conclusion, coupled mechanisms related to sea-ice variability, subpolar gyre strength and continental ice sheet extent may have caused the observed pattern. Most importantly, we provide evidence for continued inflow of Atlantic waters into the Nordic Seas at the onset of the LGM. As a result, the region was most likely seasonally sea-ice free, and thus could have acted as an important moisture source in the build-up of the LGM ice sheets.

List of Publications

1. **Rutledal, S.**, Berben, S. M. P., Dokken, T. M., van der Bilt, W. G. M., Cederstrøm, J. M. and Jansen, E. 2020: Tephra horizons identified in the western North Atlantic and Nordic Seas during the Last Glacial Period: Extending the marine tephra framework. *Quaternary Science Reviews*, 240, 106247, <https://doi.org/10.1016/j.quascirev.2020.106247>
2. **Rutledal, S.**, Simon, M. H., Haflidason, H., Berben, S. M. P. and Dokken, T. M. Sustained Atlantic inflow into the Nordic Seas at the onset of the LGM revealed by near-surface marine reservoir ages. *Manuscript in review*
3. **Rutledal, S.**, Haflidason, H., Berben, S. M. P., Griem, L., and Jansen, E. 2020: A continuous tephrostratigraphic record from the Labrador Sea spanning the last 65 ka. *Journal of Quaternary Science*, 35, 7, 855-868, <https://doi.org/10.1002/jqs.3241>

The published papers are reprinted with permission from the respective journals. All rights reserved.

Contents

| | |
|---|------------|
| Scientific environment | III |
| Acknowledgements | V |
| Abstract | VII |
| List of Publications | IX |
| 1. Introduction | 1 |
| 1.1 Why study the past climate? | 1 |
| 1.2 The naturally changing climate | 1 |
| 1.3 A tale of time | 3 |
| 1.4 Tephra as a synchronization tool | 5 |
| 1.5 The North Atlantic marine tephra framework covering the Last Glacial period | 9 |
| 2. Objectives | 15 |
| 3. Thesis approach | 17 |
| 3.1 Tephrochronology | 17 |
| 3.2 Paleoclimate proxies | 27 |
| 4. Summary of papers | 29 |
| 5. Synthesis and outlook | 33 |
| 5.1 Future outlook | 34 |
| 6. References | 37 |
| 7. Scientific Results | 43 |
| 8. Appendix I | 115 |

1. Introduction

1.1 Why study the past climate?

The global climate is currently changing at a rapid pace and as time progresses, the Earth's climate is pushed towards a warmer state, never before witnessed in the historical record (Tierney et al., 2020). The state of the future climate is highly uncertain, in particular, our understanding of the exact nature and rate of these upcoming changes. However, lessons can be learned from inspecting past climate states (the study of paleoclimatology). From the past, we can study periods of temperature increase, sea-ice variability, precipitation patterns and more, which can serve as natural analogues to the climate change witnessed today. Climate models can be tested to reproduce these past climate change events, and as such the performance of the Earth System Models can be evaluated.

1.2 The naturally changing climate

The Earth's climate system during the Quaternary period (past 2.58 Ma) is characterized by large variability and fluctuations on a range of different timescales. Naturally, the climate has shifted slowly from cold to warm, and vice versa on orbital timescales, causing the build-up (glacials) and subsequent demise (interglacials) of large continental ice sheets in the Northern Hemisphere. Superimposed over these glacial-interglacial cycles are re-occurring millennial scale climate fluctuations called Dansgaard-Oeschger (DO) events (Figure 1). DO-events apparently occurred during many glacial periods (Jouzel et al., 2007), but are best documented for the Last Glacial period (i.e., 120-11 ka b2k (Rasmussen et al., 2014)). They have a global imprint (Voelker, 2002), but are most prominent in the Greenland ice-core records. There, the DO-events manifested as a series of abrupt warming events (Greenland Interstadials (GI)) over Greenland, followed by a gradual return to cold conditions (Greenland Stadials (GS)) (Dansgaard et al., 1993; NGRIP members et al., 2004). The millennial timescale of DO-events is not consistent with external orbital forcings, and the mechanisms behind the DO-events are still debated and not fully understood. However,

the proposed mechanisms include the combined effects of abrupt shifts in the strength of the Atlantic Meridional Overturning Circulation (AMOC) and wind forcings with sea-ice related feedbacks (Li and Born, 2019), in particular variable sea-ice cover in the Nordic Seas (Dokken et al., 2013; Sadatzki et al., 2019; Sadatzki et al., 2020).

Understanding the mechanisms behind DO-events is crucial as they might be the only past analogue to the rapid sea-ice decline witnessed in the Arctic regions today. However, to disentangle the causes and effects of these events across different climate archives and over larger geographical distances, the records must be robustly linked. The application of tephrochronology offers such a link as the deposition of volcanic ash material can occur near to simultaneously in different climate archives and over a wide geographical area.

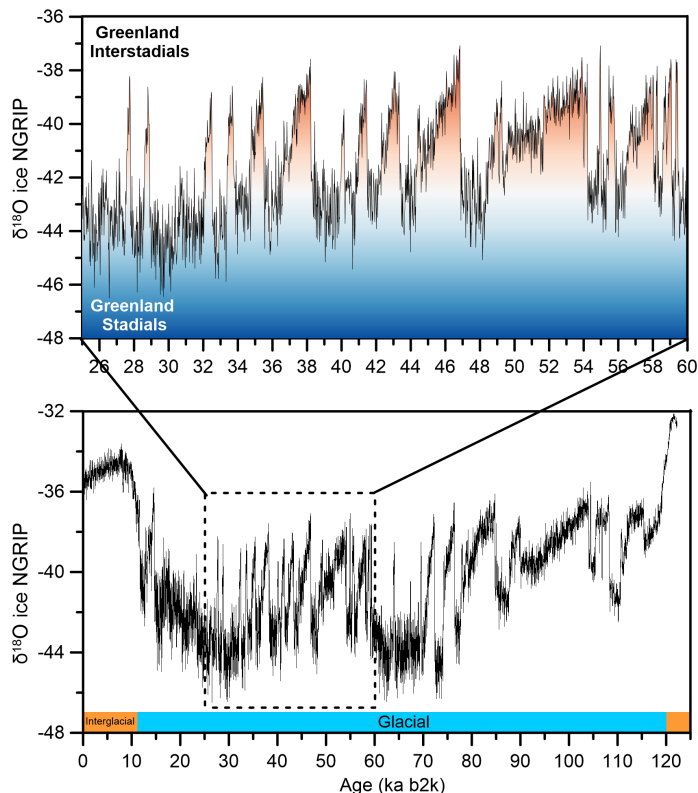


Figure 1: $\delta^{18}\text{O}$ isotope record from the Greenland ice-core NGRIP. Lower panel covers the last 120 ka. Last Glacial period marked in blue, interglacials marked in orange. Top panel covers the period 60–25 ka b2k, noting GI warming events and GS cooling events, collectively known as DO-events (NGRIP members et al., 2004).

Tephrochronology is an event-based dating method that utilizes horizons of volcanic particles (tephra) as time-markers and/or tie-points. When a volcano erupts, large amounts of tephra are ejected up into the atmosphere. Eventually, these tephra particles will fall out of the atmosphere and drop down to the surface of the Earth, such as over an ice sheet, a lake, a bog or the ocean. Over time, the tephra becomes embedded in the climate archive and form an isochron, which represents the same moment in time within the eruption dispersal area. The tephra particles will usually have a unique geochemical fingerprint. Thus, by careful investigation of their geochemical composition, tephra particles can be traced to its source volcano and in some cases to a specific eruption. This allows for tracing the isochron from one geological archive and/or location to another. Eventually, these archives located in different areas of the world can be directly correlated. Once correlated one can study how proxy records (past climate indicators) from these interconnected archives have responded during abrupt climate change events in the past, such as during DO-events.

1.3 A tale of time

The DO-events were rapid, occurred on decadal to millennial timescales and manifested in different climate archives; in lakes, in caves (speleothems), in the ocean and in ice sheets (Voelker, 2002). Thus, precise dating and synchronization of these different archives is critical to understand the rate of change and active transitional mechanisms operating when the climate rapidly shifted. To enable that, many different dating tools are available, with variable degree of precision and accuracy. Tephrochronology is one such tool, which has become increasingly acknowledged in the last decades, in particular after the methodological advances of cryptotephra (tephra invisible to the naked eye) analysis (Davies, 2015). A clear limitation of the tephrochronology method is, however, the necessity of tephra material being present in the archive of investigation. Thus, when such material is not available, other dating tools must be utilized.

In the early twentieth century, the first dating attempts of interglacial-glacial cycles in the Quaternary period involved direct measurements of erosion and weathering rates

and more indirect estimates using the astronomical timescale based on the Milankovitch orbital theory (Walker, 2005). Then some decades later, scientists recognized that layers in lakes called varves represented annual layers that could be counted back in time (Zeuner, 1945). Annual rings in trees were used as a dating tool in a similar manner. Likewise, when the first ice-cores were retrieved, annual layers of winter and summer snow were used for dating. Still today, annual layer counting is considered as one of the most precise dating methods (Walker, 2005).

The perhaps most significant advance in the dating community came with the discovery of the radioactive clock in certain radioactive elements. With the pioneering work of William Libby and colleagues in the late 1940's, the radiocarbon dating method was established. Later, with the advancement of analytical instruments, other radiometric dating methods developed, such as uranium-series, $^{40}\text{K}/^{40}\text{Ar}$ (now largely replaced by $^{40}\text{Ar}/^{39}\text{Ar}$) and fission-track dating (Walker, 2005).

In the mid- to late 1900's, advancement in the coring technology allowed for the recovery of long core sequences from polar ice sheets and ocean sediments, with an increasingly high-resolution on millennial to annual timescales. The high-resolution marine sediment cores revealed shifts in the oxygen isotope signals measured on foraminifera shells between interglacial and glacial stages. The $\delta^{18}\text{O}$ ($^{18}\text{O}/^{16}\text{O}$ ratio) signal is partly controlled by the global ice volume, so that during glacials more ^{16}O is trapped in the ice sheets and the ocean is enriched in ^{18}O , reflected in higher foraminiferal $\delta^{18}\text{O}$ values. During interglacials the opposite pattern occurs. The downcore sequence of the oxygen isotope signal was further divided into a series of isotope stages called marine isotope stages (MIS), numbered from the top down (young to old), with interglacials having odd numbers and glacials having even numbers. This work resulted in over 100 isotope stages through the Quaternary period (Shackleton et al., 1990). The phasing of these large-scale marine $\delta^{18}\text{O}$ minima and maxima events denoting interglacials and glacials, respectively, follow orbital timescales. More specifically, variations in eccentricity ($\sim 100\,000$ and $\sim 413\,000$ years), obliquity ($\sim 41\,000$ years) and precession ($\sim 19\,000$ - $23\,000$ years), commonly referred to as

Milankovitch cycles, which modifies the Northern Hemisphere summer insolation (Milankovitch, 1930; Hays et al., 1976; McIntyre et al., 1989).

The marine and ice-core oxygen isotope record provided a stratigraphic scheme against which records from other archives could compare to. Today, this method is perhaps the most common way of transferring age chronologies from one location to another. The assumption is that the oxygen isotope signal is both continuous and largely geographically consistent (Jansen, 1989). Today, this method of “tuning” or “wigggle-matching” is widely used for not only oxygen isotope series, but also for other time-series such as foraminifera assemblages (e.g. Rasmussen and Thomsen, 2004), tephra markers (e.g. Berben et al., 2020) and magnetic properties of the sediments (e.g. Dokken et al., 2013; Sessford et al., 2018). However, an apparent problem with the “tuning” method is the assumption that events in different archives are synchronous. Although this is plausible, with the “tuning” method the synchronicity or non-synchronicity of these events cannot be assessed, highlighting the need for independent age-models and/or time-markers. A second limitation with this method is that the “tuning” is visually assessed, and thus based on subjective decisions (Blaauw, 2012).

1.4 Tephra as a synchronization tool

The fundamental strength of the tephrochronology method is its correlational power and ability to firmly trace geochemically distinct tephra horizons over a wide range of paleoclimate records. Therefore, tephrochronology is being increasingly utilized as a synchronization tool between marine, ice-core and terrestrial records. This application of tephrochronology is by many considered the key for testing hypotheses regarding the synchronicity of past climate change events on regional to global scales (Lowe, 2011). Although the potential of tephrochronology was raised decades ago (Thorarinsson, 1981; Knox, 1993), it is not until recently that the method has become vital in reaching major milestones when studying past abrupt climate change events.

By using the well-known Vedde Ash horizon deposited in varved sediments from Europe, Lane et al. (2013) established that the climate anomaly during the Younger

Dryas cold period was locally abrupt, but non-synchronous. For example, records from Germany recorded the resumption of the Thermohaline circulation 120 years prior to that recorded in a Norwegian lake record.

Where the records are usually not annually resolved, such as for marine records, tephra layers can be critical tie-points. Austin et al. (2004) used the rhyolitic component of the now well-established North Atlantic Ash Zone (NAAZ) II tephra horizon to compare a marine record from the Barra Fan, northwest of Scotland to the GISP2 ice-core record. The results indicated that the GI-15 climate event (~55 800 - 54 900 b2k (Rasmussen et al., 2014)) was synchronous in peak Atlantic summer sea surface temperature (SST) and warming Greenland air temperature. To further assess the results of Austin et al. (2004), we have as a separate part of this thesis (not included in the three main papers of the thesis) generated additional climate proxy data from two marine sediment cores over the GI-15 climate event (Appendix I). The two cores, retrieved from the Labrador Sea and Norwegian Sea, have been synchronized using the position of the NAAZ II (II-RHY-1) tephra horizon. While Austin et al. (2004) identified a synchronous warming of the surface waters north-west of Scotland (i.e., increased % *N. pachyderma*) and ice-core records over GI-15, our preliminary results identified a cooling of the Norwegian Sea surface waters (i.e., decreasing Mg/Ca based temperatures (*N. pachyderma*) (Figure 2). Simultaneously, the surface waters in the Labrador Sea show a slight warming. Hence, based on these data, coupled with the data by Austin et al. (2004), the North Atlantic surface waters south of the Greenland-Scotland Ridge (GSR) show a synchronous warming response, while the Norwegian Sea north of the GSR show a cooling response to the onset of GI-15. At least partly, these dissimilarities can be explained by variable sea-ice cover in the Norwegian Sea. Deep-water temperatures derived from Mg/Ca measurements of the benthic species *C. neoteretis* show a rapid warming in the Norwegian Sea at the onset of GI-15, coupled with a rapid increase in benthic $\delta^{13}\text{C}$, interpreted to reflect a transition from sea-ice cover to open ocean conditions (e.g. Dokken et al., 2013). Simultaneously, the surface waters are freshened as witnessed in decreasing $\delta^{18}\text{O}$ (*N. pachyderma*) values (Figure 2). Hence, these data indicate that the sea-ice cover in the Norwegian Sea is rapidly diminished due to a warming of the ocean interior. These results are similar to previous

studies of MIS 3 stadial-interstadial transitions from the Denmark Strait and southern Norwegian Sea, also identifying a warming at intermediate depths of the basin at the onset of interstadials (Dokken et al., 2013; Sessford et al., 2018). With the current resolution of the proxy data and the robust chronology, we can estimate that the rapid warming of the intermediate waters and melting of the overlaying sea-ice occurred over a maximum period of 160 years, although with increasing resolution and measurements this time-interval can shorten. Similarly, the peak warming observed in the Greenland ice-cores occurred 160 years prior to peak warming observed in the Norwegian Sea intermediate waters, indicating a non-synchronous response. Furthermore, our preliminary proxy record suggests that the Norwegian Sea was perhaps more sensitive than the Labrador Sea in triggering/responding to the interstadial transition, although more deep-water proxy data from the Labrador Sea is needed to assess this further and will be generated in future studies. These preliminary results are therefore not further discussed in this thesis.

Furthermore, recent cryptotephra work in the Ice2Ice project from a marine sediment core in the southern Norwegian Sea identified four tephra layers that could be correlated to the Greenland ice-core tephra lattice (Berben et al., 2020). This linkage revealed synchronous oceanic and ice sheet changes during DO-events (8-5) but identified an initial change in ocean parameters preceding the peak warming recorded in the ocean and ice sheet temperature proxies (Sadatzki et al., 2019; Berben et al., 2020). More specifically, rapid sea-ice decline in the Nordic Seas amplified ocean-atmosphere processes, ultimately causing the abrupt climate transitions during DO-events (Sadatzki et al., 2020). Moreover, using largely the tephra-based age-model, the interstadial temperature overshoot in the ocean could be estimated to last on average 136 years.

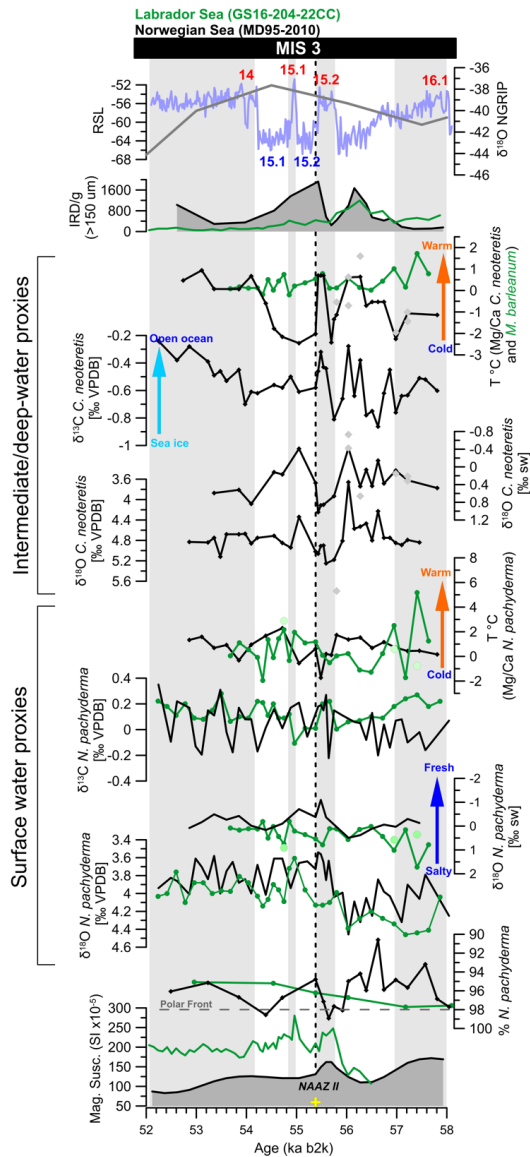


Figure 2: Multi-proxy comparison of marine sediment cores MD95-2010 (Norwegian Sea) and GS16-204-22CC (Labrador Sea) to NGRIP $\delta^{18}\text{O}$ isotope record (NGRIP members et al., 2004). Surface and intermediate/deep-water proxies are highlighted, green and grey circles and squares represent replicated measurements. Interstadials are marked by grey bars. $\delta^{18}\text{O}$ & $\delta^{13}\text{C}$ records, magnetic susceptibility, IRD and % *N. pachyderma* from the Labrador Sea by Griem et al. (2019). $\delta^{18}\text{O}$ & $\delta^{13}\text{C}$ records, magnetic susceptibility, IRD and % *N. pachyderma* from the Norwegian Sea by Dokken and Jansen (1999). Relative Sea Level curve (RSL) by Waelbroeck et al. (2002). Mg/Ca T ($^{\circ}\text{C}$) records by S. Rutledal (Appendix I).

1.5 The North Atlantic marine tephra framework covering the Last Glacial period

Tephra frameworks are a compilation of volcanic glass assemblages (tephra occurrences) identified in both distal and proximal settings. They provide an overview of the spatial dispersion area of a certain volcanic eruption but can also infer the eruption frequency and history of different volcanic systems. The North Atlantic marine tephra framework covering the Last Glacial period (Figure 3) (here defined as 120-11 ka b2k (Rasmussen et al., 2014)) includes several widespread tephra horizons such as the Faroe Marine Ash Zones (FMAZ) II & IV and NAAZ II (Haflidason et al., 2000; Wastegård et al., 2006; Griggs et al., 2014; Abbott et al., 2018a). In addition, with the development of cryptotephra analysis, new tephra horizons have emerged over the past decade, in particular in sites east of Iceland (Brendryen et al., 2010; Griggs et al., 2014; Abbott et al., 2018a; Berben et al., 2020). From the Greenland ice-cores, Bourne et al. (2015) provide an overview covering the period 45-25 ka b2k, identifying over 100 Icelandic eruptions and Abbott et al. (2012) from the period 90-60 ka b2k identifying 15 tephra layers. These results from the Greenland ice-cores indicate a huge potential for ocean-ice synchronization during the Last Glacial period, if these layers can be identified in the ocean.

As mentioned, many new tephra horizons have been identified in marine sediment sequences over the past decade and some are correlative to Greenland ice-core tephra horizons (e.g. Berben et al., 2020). Nevertheless, only the FMAZ-II-1 (26.7 ka b2k) and NAAZ-II (55.3 ka b2k) (Svensson et al., 2008) horizons, have so far been established as clear correlational tie-points between the ocean and ice sheets. Based on the existing work, it is clear that the Icelandic volcanic systems were active during the Last Glacial period, which offers a unique opportunity for high-precision synchronization of paleoclimate records. Therefore, more work is needed to (1) verify the new tephra horizons identified in the eastern North Atlantic in other areas and thus establish marine-marine and/or marine-ice chronological tie-points and (2) investigate the potential to discover new tephra layers using cryptotephra analysis.

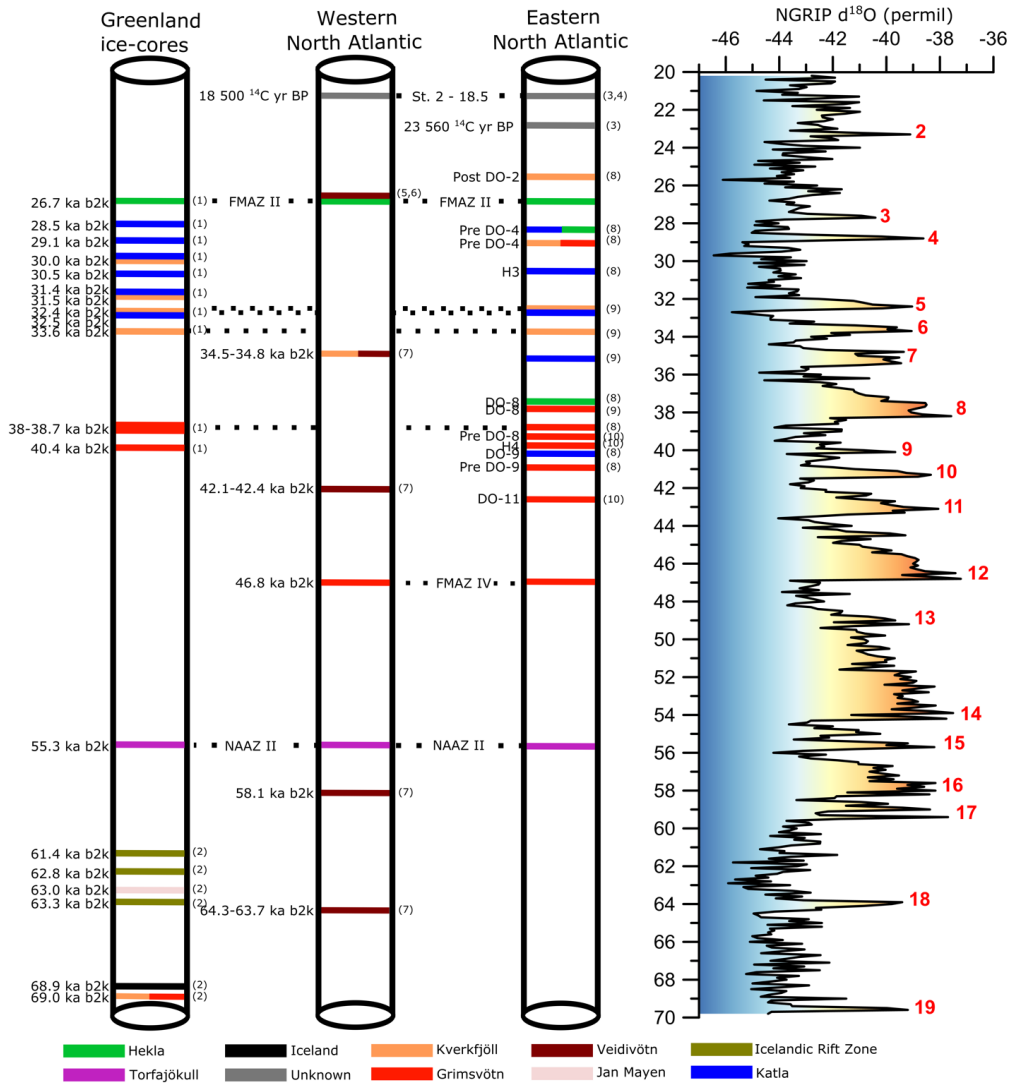


Figure 3: Overview of the North Atlantic marine tephra framework covering parts of the Last Glacial period (70-20 ka b2k). From the marine records, only tephra layers with isochronous characteristics were included. From the Greenland ice-cores, only tephra layers correlative over more than one ice-core were included. We define the western and eastern North Atlantic relative to the Mid-Atlantic ridge. References are as follows: (1) Bourne et al. (2015), (2) Abbott and Davies (2012), (3) Haflidason et al. (2000), (4) Voelker and Haflidason (2015), (5) Rutledal et al. (2020a), (6) Wastegård et al. (2006), (7) Rutledal et al. (2020b) (8) Abbott et al. (2018a), (9) Berben et al. (2020), (10) Abbott et al. (2016). $\delta^{18}\text{O}$ isotope record from NGRIP members et al. (2004), GIs are numbered.

1.5.1 Icelandic volcanism

The North Atlantic marine tephra framework over the Last Glacial period is dominated by tephra layers sourced largely from Icelandic volcanoes, and a few from the volcanic island of Jan Mayen. Iceland is a part of the North Atlantic Igneous Province, located on the Mid-Atlantic Ridge above a mantle hotspot plume (Thordarson and Larsen, 2007). Iceland consists of four major volcanic zones: The Reykjanes Volcanic Zone (RVZ), the Western Volcanic Zone (WVZ), the Eastern Volcanic Zone (EVZ) and the Northern Volcanic Zone (NVZ) (Figure 4). Combined, these volcanic zones host 30 different volcanic systems (Thordarson and Larsen, 2007). Generally, the Icelandic volcanic systems feature a fissure swarm or a central volcano or both. The volcanic material produced by these systems range from basaltic to silicic (dominantly rhyolite) in composition (Figure 5) but are in historical times dominated by basaltic material (Thordarson and Larsen, 2007). The geochemical composition of Icelandic volcanic material group into tholeiitic, transitional alkalic and alkalic (Figure 5). Tholeiitic material will have a lower total alkali content (i.e., $\text{Na}_2\text{O} + \text{K}_2\text{O}$) than alkalic material. In Iceland, the volcanic systems located in the axial rift zones (i.e., NVZ, WVZ and EVZ) generally produce tholeiitic material (Figure 4). The Katla and Hekla systems produce transitional-alkalic material, while the intraplate volcanic belts of Snæfellsnes and Öraefajökull produce alkalic material (Figure 4).

The EVZ axial rift propagates southwest through older crust, and therefore the magma suites produced here show distinct spatial differences. In the north, where Grímsvötn and Bárðarbunga-Veidivötn are located, the magma suites are characterized by tholeiitic composition. In the south, where the volcanic systems of Torfajökull, Tindfjallajökull and Eyjafjallajökull are located, the magma suites characterize an alkalic composition (Figure 4) (Harning et al., 2018). Volcanic material sourced from the Jan Mayen volcanoes can be distinguished from Icelandic volcanic material by higher total alkali content and lower TiO_2 and CaO concentrations (Figure 5).

Explosive eruptions (i.e., Surtseyan, Phreatoplinian and Plinian) producing both dry (i.e., magmatic) and wet (i.e., phreatomagmatic) explosions dominate the Icelandic volcanism (Thordarson and Larsen, 2007). Phreatomagmatic eruptions are typically

related to ice-capped, ice-covered or offshore volcanoes (Larsen, 2002). Eruption frequency estimates suggest that Icelandic explosive silicic eruptions have an eruption frequency of every 200-300 years (Thordarson and Larsen, 2007). Contrarily, effusive eruptions are relatively rare in Iceland, and have only produced small volume ($<0.2 \text{ km}^3$) subaerial block lavas, coulees and domes (Thordarson and Larsen, 2007).

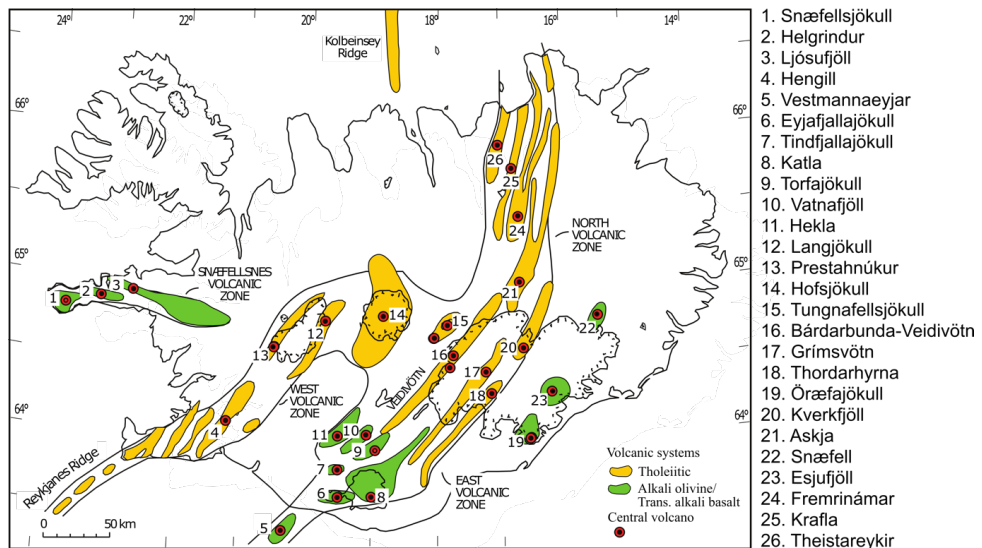


Figure 4: The main volcanic systems of Iceland (modified after Haflidason et al. (2000)).

For the historical period, the Icelandic eruption activity is estimated to be ~ 25 events per century (i.e. every 4 year), with the EVZ being the dominant source (i.e., Grímsvötn, Hekla, Katla and Bárðarbunga-Veidivötn) (Thordarson and Larsen, 2007). However, the volcanic history and eruptive frequency of Icelandic volcanoes during the Last Glacial period is largely unknown. Nevertheless, tephra occurrences in the marine and ice-core archives suggest that the Grímsvötn, Kverkfjöll, Bárðarbunga-Veidivötn, Hekla, Katla and Torfajökull volcanic systems were most active at that time (e.g. Bourne et al., 2015; Voelker and Haflidason, 2015; Abbott et al., 2018a; Rutledal et al., 2020b), at least those producing more explosive eruptions transporting material to distal settings.

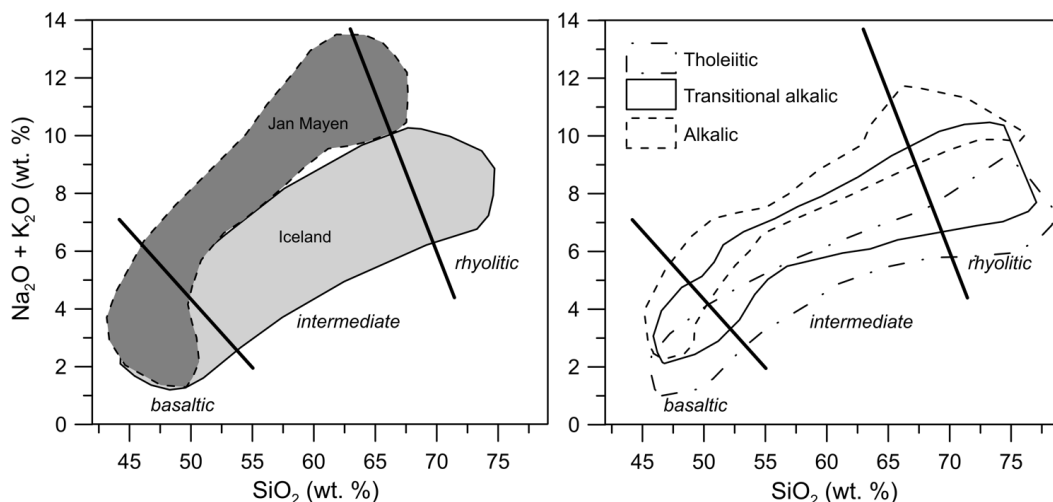


Figure 5: Total-alkali silica plot. Jan Mayen (dark grey) and Icelandic (light grey) fields are based on Voelker and Hafliðason (2015) and references therein. Tholeiitic, transitional alkalic and alkalic Icelandic rock suites (right) are based on Jakobsson et al. (2008). The approximate division lines between basaltic, intermediate and rhyolitic material are shown.

For Icelandic tephra material, pinpointing the source volcano is challenging due to large similarities in the geochemistry of the different volcanic systems. Thus, careful comparison analysis of all ten major element oxides is required. Particularly relevant for this thesis is the challenge in separating the Bárðarbunga-Veidivötn from the Reykjanes system and the Grímsvötn from the Kverkfjöll system. The Bárðarbunga-Veidivötn and Reykjanes systems display extremely similar geochemical characteristics in close to all ten major element oxides. A slight difference can be visually distinguished in the lower TiO₂ (wt. %) and higher MgO (wt. %) of Bárðarbunga-Veidivötn compared to Reykjanes. Similarly, the Grímsvötn geochemical signature is lower in TiO₂ (wt. %) and K₂O (wt. %) and higher in MgO (wt. %) than the Kverkfjöll signature (Figure 6).

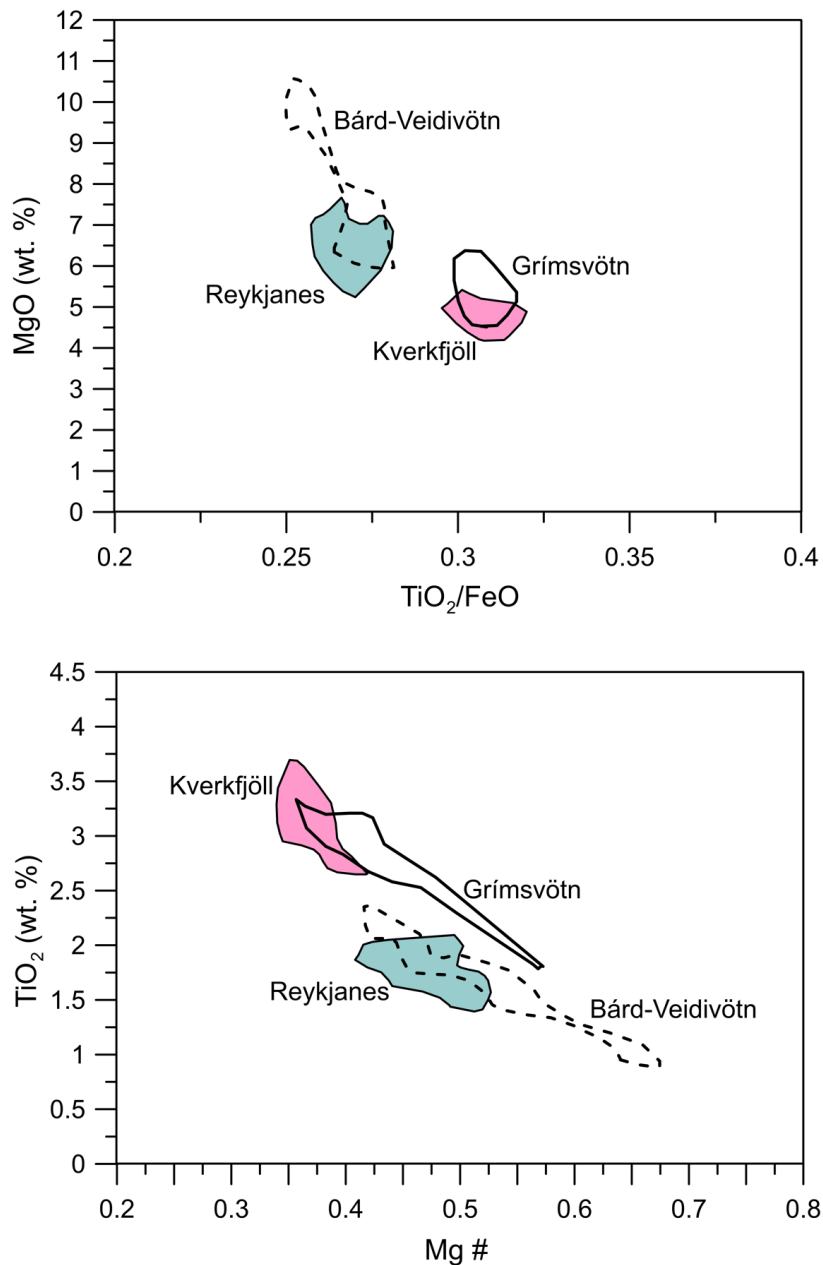


Figure 6: Biplot comparison of the geochemical signatures related to the Bárðarbunga-Veidivötn, Reykjanes, Grímsvötn and Kverkfjöll volcanic systems. $\#Mg = (MgO/40.3)/((FeO/71.8)+MgO/40.3)$ (based on the database of Harning et al. (2018) and references therein).

2. Objectives

This PhD thesis is divided into two main parts: (i) identify new and already established tephra horizons in North Atlantic marine sediment cores covering the Last Glacial period, and (ii) apply the identification of tephra horizons in North Atlantic marine sediment cores to firmly synchronize paleoclimate records.

The main objectives of the first part (i) are: (1) Investigate the newly retrieved Ice2Ice cores (i.e., GS16-204-18CC and GS16-204-22CC) from the Labrador and Irminger Sea for the already established tephra isochrones FMAZ II-1 and NAAZ II. (2) Geochemically confirm the occurrence of FMAZ II-1 in Nordic Seas core MD99-2284. (3) Provide a continuous tephrostratigraphic record from the Labrador Sea covering the Last Glacial period.

The main objectives of the second part (ii) are: (1) Utilize the network of sediment cores with combined FMAZ II-1 horizon and ^{14}C dated foraminiferal material to estimate the marine reservoir ages in the high latitude North Atlantic and (2) investigate the spatial variability in the Atlantic inflow flux at this time.

3. Thesis approach

The methodological approach of this thesis mainly relies on the identification of tephra layers in marine sediment sequences from the North Atlantic (Paper 1 & 3). The identification of established tephra horizons has then further been applied to reconstruct past marine reservoir ages in a transect of marine sediment cores from the high-latitude North Atlantic at the onset of the Last Glacial Maximum (LGM) (Paper 2).

3.1 Tephrochronology

Tephrochronology is an emerging tool being increasingly applied in Quaternary research. Especially, since the need of high-resolution paleoclimate records, and to synchronize those records have become an urgent focus in the recent years. Within the field of geochronology, the tephrochronology method offers a unique precision, which few (if any) dating methods can match.

3.1.1 Principles

The tephrochronology method relies on three principles which must be carefully examined: (a) Stratigraphic signature, (b) Geochemical characterization and (c) Chronology.

(a) Stratigraphic signature

The stratigraphic appearance of a tephra layer changes with increased distance from the volcanic source. Close to the source the tephra layers can be several meters thick and can be traced to more distal settings using physical properties only. With increased distance from the source the tephra grain size decreases, the layers thin out and eventually become invisible to the naked eye (cryptotephra). In these settings, to make a correlation, the stratigraphic signature of the layer must be accompanied by geochemical characterization. For cryptotephra deposits, as there is no visible stratigraphic marker in the sediment sequence, the identification commonly relies on tephra shard concentration methods such as density separation techniques, followed by

optical microscopy to identify and quantify the volcanic glass shards. Usually, the position of peak glass shard concentrations is used as the tephra horizon marker. In the case of no clear main concentration peak, but a sharp base, the first appearance of glass shards can be used to mark the stratigraphic initiation of a volcanic event.

In marine environments, the stratigraphic signature of tephra layers is especially important to determine as the tephra can be transported and deposited in a range of different ways. Therefore, within the marine environment it is distinguished between: (1) primary air-fall tephra, (2) sea-ice rafted tephra, (3) iceberg rafted tephra, and (4) tephra reworked within the ocean environment and at the ocean floor (Figure 7). Tephra deposited by primary air-fall is expected to contain a well-sorted shard size distribution, with decreasing shard size as the distance from the source increases. These deposits are characterized by a homogeneous geochemical composition and are believed to be deposited (on geological timescales) instantaneously following the eruption (Griggs et al., 2014). Sea-ice rafted tephra deposits can be delayed following the eruption by months to years, depending on whether or not the sea-ice was seasonal or perennial. Tephra deposited by seasonal sea-ice is usually interpreted to be near-instantaneous following an eruption. Seasonal sea-ice is short lived, which prevents the accumulation of multiple eruptions, and thus the geochemistry is usually homogeneous. This transport mechanism can in some cases be beneficial in increasing the regional dispersal of tephra shards and is unlikely to affect the isochronous integrity of a tephra horizon. This because the potential temporal delay is far smaller than the average sampling resolution in marine sediment sequences (Griggs et al., 2014). Iceberg rafted tephra pose an apparent problem for tephrochronology covering the Last Glacial period. At that time, large continental ice sheets in the Northern Hemisphere frequently supplied icebergs into the North Atlantic (Ruddiman, 1977). Tephra material deposited by an iceberg can be delayed following the volcanic eruption on decadal to millennial timescales (Brendryen et al., 2010; Brendryen et al., 2011). This significantly delayed deposition allows for the accumulation of multiple eruptions. Therefore, these deposits are characterized by heterogeneous geochemical composition and are not useful as tephra isochrones. After deposition on the ocean floor, tephra material can be reworked by bottom currents and/or bioturbation.

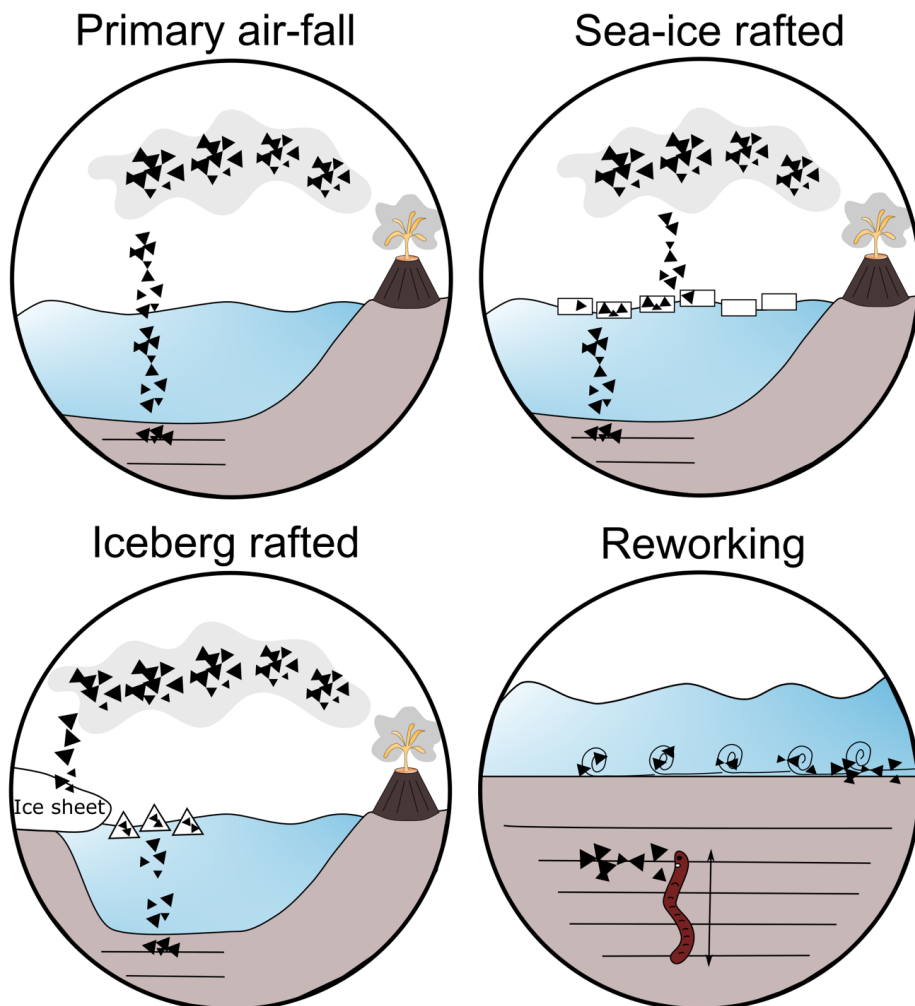


Figure 7: Illustration of how tephra particles can be deposited within the marine environment.
By S. Rutledal.

Characteristic signs of bioturbation are usually upward or downward tailing of shard concentrations, spreading the tephra horizons over several cm. This effect is not likely to affect the position of the main tephra peak but does introduce some additional stratigraphic uncertainties (Griggs et al., 2014). As a part of this thesis, we have used Computed Tomography (CT) imagery to visualize the influence bioturbation might have on tephra horizons. This was in particularly relevant for the NAAZ II (II-RHY-1) layers in the GS16-204-22CC and GS16-204-18CC sediment cores where the tephra

shard concentration profiles revealed a gradational upward tailing (Rutledal et al., 2020a). By the visualization provided by the CT-scan we could determine the tailing to be caused by bioturbation, but not to affect the isochronous nature of the main tephra peak (Figure 8).

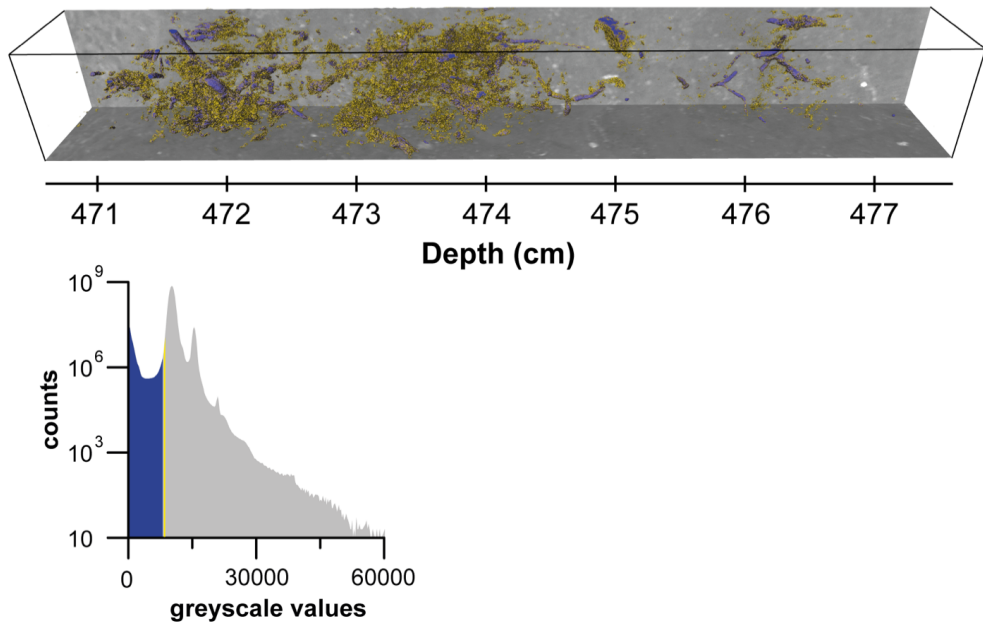


Figure 8: Processed CT-scan of GS16-204-22CC (471-477 cm) with highlighted greyscale values in histograms showing bioturbation (blue) and tephra particles (yellow). Both tephra and bioturbation volume rendered to show the distribution and shape. Detection and visualization of tephra particles using the CT-scanner follow the methodology of van der Bilt et al. (2020). Figure courtesy of JM Cederstrøm.

Furthermore, to tackle these depositional challenges in the marine environment, Abbott et al. (2018b) developed a general deposit type classification scheme, separating between five different deposit types (Figure 9). In this thesis, this classification scheme was used. A Type 1 deposit is classified as a deposit with low tephra shard concentrations (<50 shards/gdw), but a well constrained concentration peak. The geochemical composition is homogeneous, and the deposit likely represents a single depositional event, deposited by primary air-fall. A Type 2 deposit has higher tephra shard concentrations (100s-1000s shards/gdw), and a distinct concentration peak, with

some upward tailing of tephra shards, likely caused by bioturbation. If the deposit has a homogeneous geochemistry it is classified as a Type 2A deposit, whereas if it has a heterogeneous geochemistry it is classified as a Type 2B deposit. The depositional mechanism of a Type 2 deposit can be primary air-fall, sea-ice and/or iceberg rafting, depending on its geochemical characteristics. A Type 3 deposit is characterized by a flat bottomed profile with a gradational upward tailing of tephra shards. The shard concentrations are very high (100.000s-1.000.000s shards/gdw). The geochemical composition of the main concentration peak is homogeneous. Transport mechanisms can be either primary air-fall or sea-ice rafting. A Type 4 deposit typically has a diffuse distribution with multiple tephra shard concentration peaks. Such a deposit likely represents multiple closely spaced eruptions or deposition via iceberg rafting. Type 5 deposits are characterized by a background level of tephra shards and heterogeneous geochemistry. Such deposits are often reworked and remobilized in the oceanic system, which might potentially mask low tephra shard concentration peaks (Abbott et al., 2018b).

(b) Geochemical characterization

The second important principle of tephrochronology is geochemical characterization. Tephra studies rely on the ability to geochemically characterize, i.e., “fingerprint” tephra layers, using geochemical analysis of individual tephra glass shards by methods such as Electron Probe Microanalysis (EPMA). EPMA remains the forefront of tephra shard geochemical analysis due to its good analytical precision, sensitivity and accuracy, and ability to discriminate between different source volcanoes and in some cases individual eruptions using the composition of ten major elements (Hayward, 2012). A Cameca SX100 electron microprobe equipped with five vertical wavelength dispersive spectrometers at the Tephra Analysis Unit (University of Edinburgh) has been used to generate the geochemical data presented in this thesis.

Increasingly, although not utilized in this thesis, Laser Ablation Inductively Coupled Plasma Mass Spectrometry (LA-ICP-MS) has been used to generate trace-element data

of single tephra shards, which can aid in the geochemical characterization of the tephra layers (e.g. Abbott et al., 2011).

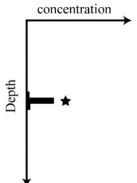
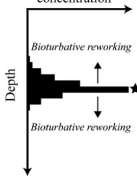
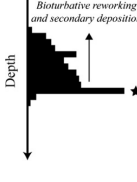
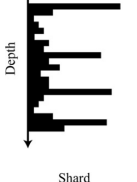
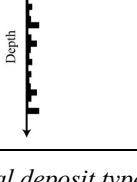
| Deposit type | Typical shard profile | Deposit type characteristics | Transport and deposition processes |
|---|---|---|--|
| TYPE 1 Low concentration peak |  | <ul style="list-style-type: none"> -Well constrained shard concentration peak -Low shard concentrations (< 50 per 0.5 g dws) -Shards generally 25–80 μm in diameter -Homogenous geochemical composition | <ul style="list-style-type: none"> -Single depositional event -Sourced from a single volcanic eruption -Potentially limited post-depositional reworking -Most likely primary airfall deposition |
| TYPE 2 High concentration peak |  | <ul style="list-style-type: none"> -Distinct peak in shard concentration -High shard concentrations (100 s–1000 s per 0.5 g dws) -Upward and downward spanning up to 10 cm -Homogenous (Type 2A) or heterogeneous (Type 2B) geochemical composition | <ul style="list-style-type: none"> -Analysis of geochemistry, shard sizes and IRD required -Bioturbative reworking -Single depositional event -Transport via primary airfall, sea-ice and iceberg rafting possible |
| TYPE 3 High concentration peak; gradational upward tail |  | <ul style="list-style-type: none"> -Flat bottomed profile with a clear gradational upward tail -Very high shard concentrations (100,000 s–1,000,000 per 0.5 g dws) -Deposit spread up to 100 cm -Homogenous composition of shards in peak | <ul style="list-style-type: none"> -Single depositional and volcanic event -Reworking via secondary deposition and bioturbation -Transport via primary airfall or sea-ice rafting -Useful isochron |
| TYPE 4 Diffuse distribution; multiple peaks |  | <ul style="list-style-type: none"> -High shard concentrations (1000 s–1,000,000 s per 0.5 g dws) -Multiple peaks in concentration in a period of elevated shard concentrations -Deposit spread of 10 s of cms -Heterogeneous geochemical composition common between peaks | <ul style="list-style-type: none"> -Deposition of multiple closely spaced eruptions or deposition via iceberg rafting -Comparison to Greenland tephra framework and IRD records required -Potential as regional marine-marine tie-lines |
| TYPE 5 Background of consistent concentration |  | <ul style="list-style-type: none"> -Consistent deposition of shards with limited variability in concentrations between samples -Wide variability of deposit spreads -Heterogeneous or geochemically related to underlying deposits | <ul style="list-style-type: none"> -Background signal of glass shards -Shards reworked and remobilised in the oceanic system -Potential masking of low concentration glass shard deposits |

Figure 9: General deposit type classification scheme by Abbott et al. (2018b).

There are two major challenges when it comes to geochemical characterization of tephra layers. Firstly, volcanoes can erupt successive tephra layers with the same geochemical signature (Lowe, 2011). Secondly, the geochemical composition of the volcanic magma can change over time. Most of the available geochemical data from tephra layers and/or source volcano databases are based on Holocene to modern values, and knowledge about these volcanoes geochemical characteristics in earlier times is sparse.

(c) Chronology

The final important principle is chronology and attaining independent dates of tephra layers. Tephra outcrops can be directly dated using radiometric dating methods, such as $^{40}\text{Ar}/^{39}\text{Ar}$ dating or fission-track dating. Indirectly, tephra in sediment sequences can be dated using nearby organic material such as twigs, plants and shells by the radiocarbon dating method. Due to a half-life of 5730 years (Godwin, 1962), the latter method has an age limit of 55 ka (Reimer et al., 2020). In addition, radiocarbon dating results can be imprecise in the marine environment due to the marine reservoir effect and is thus inadequate when using tephra layers to verify chronologies (see section 3.2.1). Contrarily, if tephra layers are conserved in annually laminated sequences such as in lake or ice-cores, precise calendar ages can be assigned to the layer through annual layer counting.

For cryptotephra layers identified in the marine environment, the age of a tephra layer is usually achieved by transferring the age obtained from a correlating tephra horizon determined by more robust methods, such as annual layer counting in ice-cores.

To avoid misinterpretation and wrongful correlation, it is important that more than one criterion is used when correlating tephra layers, e.g., in addition to geochemical characteristics, its stratigraphic position and/or chronological control must also be evaluated.

3.1.2 Cryptotephra sample preparation

In this thesis (if not stated otherwise), the samples were prepared following the methodology of Abbott et al. (2011); Abbott et al. (2018b). First, approximately 0.5 g of dry and homogenized material was placed in 10 ml centrifuge tubes. To remove carbonate material, 10% HCl was added to the sample and left overnight. Subsequently, the samples were sieved into three size fractions (i.e., $>125\ \mu\text{m}$, $80\text{-}125\ \mu\text{m}$ and $25\text{-}80\ \mu\text{m}$). The fine-grained size fraction, $25\text{-}80\ \mu\text{m}$, was then separated into different density fractions of $<2.3\ \text{g/cm}^3$, $2.3\text{-}2.5\ \text{g/cm}^3$ and $>2.5\ \text{g/cm}^3$ using heavy liquid flotation with sodium polytungstate (SPT). This technique is applied to separate rhyolitic ($2.3\text{-}2.5\ \text{g/cm}^3$) from basaltic ($>2.5\ \text{g/cm}^3$) material, following the thresholds suggested by Turney (1998); Blockley et al. (2005). The density separation step is essential in marine (crypto)tephrochronology, due to large quantities of background material. Following, the $>2.5\ \text{g/cm}^3$ fraction was separated using a Frantz Isodynamic Magnetic Separator to confine basaltic tephra shards, which have paramagnetic properties (Griggs et al., 2014). After the separation procedures, each sample was mounted on microscope slides using Canada Balsam. This resulted in a total of four slides per sample (i.e., $>125\ \mu\text{m}$, $80\text{-}125\ \mu\text{m}$ and $>2.5\ \text{g/cm}^3$, $2.3\text{-}2.5\ \text{g/cm}^3$ from the $25\text{-}80\ \mu\text{m}$ fraction). Tephra shards were then counted using an optical light microscope. Visually, basaltic shards can be distinguished from rhyolitic shards, mainly by their difference in color (Figure 10). If tephra shard concentrations exceeded 10.000 shards/g, the steps described above were repeated and lycopodium spore tablets were added to the $25\text{-}80\ \mu\text{m}$ fraction. This was the case for some tephra layers in Paper 1 and further descriptions of this method are outlined there (see section 2.3 Paper 1). Tephra shard concentration peaks were selected for major element analysis. For this, the described preparation steps were repeated. Then, the samples were embedded in epoxy resin on frosted microprobe slides. To expose the individual tephra shards, the microprobe slide was ground using p1000 silicon carbide paper and polished using $\frac{1}{4}\ \mu\text{m}$ diamond polycrystalline suspension. Finally, individual tephra shards were analyzed using EPMA at the Tephra Analytical Unit, University of Edinburgh.

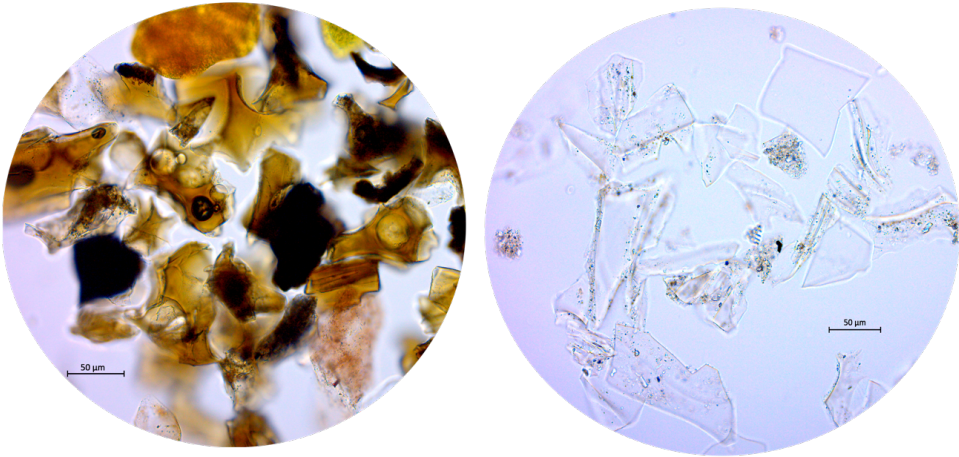


Figure 10: Basaltic shards (left) extracted from MD99-2284 (1408-1409 cm, 25-80 μm) and rhyolitic tephra shards (right) from GS16-204-22CC (474.25 cm, 25-80 μm). Scale bar = 50 μm .

3.1.3 Statistical Analysis

The geochemical signature of each tephra horizon must be validated against already known signatures of selected tephra layers by statistical methods. For that purpose, we have in this thesis calculated the (a) Similarity Coefficient (SC) and (b) Statistical Distance (SD).

(a) Similarity Coefficient

The SC function was used to calculate the similarity between major elements in two datasets. Because the analytical precision on low concentration elements can have large effects on the calculated SC, only major elements with concentrations greater than 1 wt. % were used. Essentially, the closer the calculated SC is to 1, the more similar the datasets are. According to Beget et al. (1992), SC values between 0.95 and 1 indicate identical dataset, values between 0.90 and 0.95 indicate not identical dataset, but likely the same volcanic source, while values <0.90 indicate no relation between the datasets. However, for Icelandic volcanic systems, Abbott et al. (2018a) suggest that only SC values greater than 0.97 represent identical datasets. This due to the great similarity among the Icelandic volcanic systems and their volcanic products. These presented thresholds have been used in this thesis.

SC is calculated using Equation 3.1, where n is the number of elements, $R_k = X_{k1}/X_{k2}$ if $X_{k2} \geq X_{k1}$ or $R_k = X_{k2}/X_{k1}$ if $X_{k1} \geq X_{k2}$. X_{k1} is the concentration of element k in sample 1, while X_{k2} is the concentration of element k in sample 2 (Borchardt et al., 1972).

$$SC = \frac{\sum_{k=1}^n R_k}{n} \quad \text{Equation 3.1}$$

(b) Statistical Distance

The SD function was developed by Perkins et al. (1995) and considers the differences between two datasets. Therefore, the SD values can only be used to determine if two datasets are different, and not that they are the same. The calculated SD values are compared to critical values at the 99% confidence level. The critical values vary depending on the number of elements used in the comparison (i.e., 7 elements for rhyolitic layers give a critical value of 18.48, while 10 elements for basaltic layers give a critical value of 23.21). Only major element oxides with an average concentration greater than 0.1 wt. % are used, therefore the critical values differ between basaltic and rhyolitic material.

If the calculated SD values are greater than the critical values, the two datasets are dissimilar. If the calculated SD values are lower than the critical values, then the samples are considered to *not* be different. However, that does not transfer to identical datasets (Pearce et al., 2008), hence low values suggest that a correlation might exist but is not statistically valid. This because two datasets might have similar mean and standard deviation values, but different trends in the individual data values. This effect can be assessed by visual examination using biplots of elements.

The SD is calculated using Equation 3.2, where n is the number of elements used, x_{k1} and x_{k2} are the mean concentration of element k in sample 1 and 2, respectively.

Whereas σ_{k1} and σ_{k2} are the standard deviations of the values of element k in sample 1 and 2, respectively.

$$SD = \sum_{k=1}^n \frac{(x_{k1} - x_{k2})^2}{(\sigma_{k1}^2 + \sigma_{k2}^2)} \quad \text{Equation 3.2}$$

3.2 Paleoclimate proxies

In addition to the identification of marine tephra deposits, we have in this thesis used the calculation of marine reservoir ages based on AMS ^{14}C dates of foraminiferal material as a proxy for past Atlantic advection (Paper 2).

3.2.1 Radiocarbon Dating and Marine Reservoir Ages

In Paper 2, we combine information of ^{14}C AMS dating and the tephra marker FMAZ II-1 to evaluate the near-surface marine reservoir age in the North Atlantic and use this as a proxy for past Atlantic advection. For this, we retrieved ^{14}C AMS dates from the shell of the planktonic species *N. pachyderma* (formerly known as *N. pachyderma* sinistral (Darling et al., 2006)) picked from two marine North Atlantic sediment cores with an already identified FMAZ II-1 horizon (i.e., GS16-204-18CC and MD99-2284).

In the atmosphere, ^{14}C is continuously produced by cosmic ray neutrons colliding with nitrogen. Through CO_2 , ^{14}C enters the carbon cycle and is absorbed by living organisms. When the organism is alive, and in contact with the atmosphere, it continuously absorbs ^{14}C . However, when it dies the input of ^{14}C stops, and since ^{14}C is an unstable isotope, it will start to decay and the amount of ^{14}C decreases with a half-life of 5730 years (Godwin, 1962). Thus, by measuring the quantity of ^{14}C in a dead organism, one can calculate the amount of time passed since the organism was alive. However, the method is limited by a relatively short half-life, and thus has an age limit of 55 ka (Reimer et al., 2020).

The ^{14}C method comes with limitations. First, studies have shown that the level of ^{14}C in the atmosphere is not constant over time (de Vries, 1958). To correct for this and obtain more accurate age estimates, ^{14}C calibration curves have been developed and are continuously improved, resulting in the recent publication of the IntCal20 and Marine20 calibration curves (Heaton et al., 2020; Reimer et al., 2020), which have been used in this thesis.

In the marine environment, the *marine reservoir effect* adds additional uncertainty to the radiocarbon dating method. The marine reservoir effect refers to an offset between the ^{14}C age of marine and terrestrial living organisms. While the terrestrial organisms

remain in a continuous equilibrium with the contemporaneous atmosphere, the marine organisms are affected by the water mass surrounding them. A body of water can only take up atmospheric ^{14}C while at the surface and in contact with the atmosphere. As this water sinks to form deep-water in the polar regions, the contact with the surface is cut off and ^{14}C starts to decay. Thus, marine organisms will be depleted in ^{14}C relative to terrestrial organisms (e.g. Ascough et al., 2005). This offset in the ^{14}C age between marine and terrestrial samples is corrected for by estimating the marine reservoir age for the given sample. Today, the global marine reservoir age is estimated to be ~ 400 ^{14}C years (Bard, 1988), still local variations deviate from this standard correction. In addition, studies have shown that the marine reservoir age is both spatially and temporally specific (e.g. Waelbroeck et al., 2001; Mangerud et al., 2006; Muschitiello et al., 2019; Brendryen et al., 2020) as it is influenced by factors that are largely climatically controlled, such as the presence of sea-ice and ocean circulation patterns (i.e. upwelling and deep-water formation regions) (Alves et al., 2018).

In general, warmer surface currents are associated with lower marine reservoir ages, whereas in regions where deep-waters are upwelled to the surface higher marine reservoir ages are recorded (Ascough et al., 2006). Furthermore, sea-ice cover significantly reduces the ocean-atmosphere exchange flux, resulting in higher marine reservoir ages. Additionally, higher marine reservoir ages in deep-waters can be largely attributed to a slowed down overturning circulation (Ritz et al., 2008). The marine reservoir ages for the Last Glacial period are expected to be higher than modern. This both due to these climatically controlled factors, but also due to a lower atmospheric CO_2 partial pressure at that time, slowing the ocean-atmosphere radiocarbon equilibration rate and producing higher marine reservoir ages (Galbraith et al., 2015).

4. Summary of papers

Paper 1: Extending the North Atlantic marine tephra framework during the Last Glacial period

In Paper 1, we investigated the occurrence of two well-known tephra layers, the Faroe Marine Ash Zone II (FMAZ II-1) and the North Atlantic Ash Zone II (NAAZ II (II-RHY-1)) in three North Atlantic marine sediment cores. We found FMAZ II-1 as a visible basaltic layer in core MD99-2284 from the Nordic Seas and as a cryptotephra layer in core GS16-204-18CC from the Irminger Sea. With these results we extended the known distribution of this particular tephra layer in a north-western direction, as previous studies have focused on areas east of Iceland. In addition, we found a new tephra layer with geochemical affinities to either the Bárðarbunga-Veidivötn or the Reykjanes Volcanic system, associated with the FMAZ II-1 layer in the Irminger Sea. Potentially this layer can be linked to a layer with similar geochemistry identified in the Labrador Sea (Wastegård et al., 2006). In addition, we identified the NAAZ II (II-RHY-1) horizon in the sediment cores from the Labrador and Irminger Sea, which is the first tangible evidence of this layer in that area. Lastly, we utilize high-resolution CT imagery to quantify the effect of bioturbation on the NAAZ II (II-RHY-1) horizons.

The main implication of the study was the identification of cryptotephra layers in the western North Atlantic region. Due to the prevailing eastward wind direction from Iceland, past cryptotephra studies had mainly focused on the eastern North Atlantic region. However, our results demonstrate unique and rather unexplored tephrochronological opportunities in the western sector, allowing for a wider marine-marine cross-correlation of paleorecords.

Paper 2: Sustained Atlantic inflow into the Nordic Seas at the onset of the LGM revealed by near-surface marine reservoir ages

In Paper 2, we utilized the identification of the FMAZ II-1 tephra horizon in the sediment cores from the Nordic Seas and Irminger Sea from Paper 1. We obtained ^{14}C AMS dates measured on the planktonic foraminifera *N. pachyderma* sampled from the exact same depth as the position of the tephra layer. Moreover, we obtained a ^{14}C date measured on a mix of benthic species from the Nordic Seas core MD99-2284. In addition, we added already published ^{14}C dates from eight North Atlantic marine sediment cores, where FMAZ II-1 had been identified. The absolute age of the tephra horizon retrieved from the Greenland ice-cores (i.e., $26\,740 \pm 390$ years b2k) allowed us to estimate the near-surface marine reservoir ages in all ten sediment cores, and the benthic-planktonic (B-P) offsets in two of the sediment cores.

The tephra horizon is perfectly positioned to constrain the onset of the Last Glacial Maximum (LGM), and thus we could estimate the spatial configuration of the Atlantic surface inflow branches at that time. This because higher than modern near-surface marine reservoir ages (i.e., >400 ^{14}C), representing a vigorous Atlantic inflow, can be interpreted to reflect a reduced inflow of Atlantic water. The results revealed overall higher than modern near-surface marine reservoir ages in the North Atlantic, but large spatial variability. Most notably, in the area around the Faroe-Shetland Channel, younger ages were found along the path of the western Atlantic current (WNAC), compared to the eastern current (ENAC). Moreover, we detected upwelling of old carbon rich waters (no B-P offsets) in the eastern Nordic Seas, likely due to strong katabatic winds from the continental ice sheets. In total, coupled mechanisms related to sea-ice variability, subpolar gyre strength, and continental ice sheet extent may have caused the observed pattern. Most importantly, we provide evidence for continued inflow of Atlantic waters into the Nordic Seas at the onset of the LGM. As a result, the region was most likely seasonally sea-ice free, and thus could have acted as an important moisture source in the build-up of the LGM ice sheets.

Paper 3: A continuous tephrostratigraphic record from the Labrador Sea spanning the last 65 ka

In Paper 3, we build on the lessons from Paper 1 indicating the presence of isochronous tephra horizons in the western North Atlantic sector. Thus, we focused on creating a continuous tephra record from the Labrador Sea (core GS16-204-22CC), covering the time period ca. 65-5 ka b2k, an area and time period that has, so far, not been investigated in detail within the established North Atlantic marine tephra framework. The results were eight tephra layers, where five can be used as tephra isochrones and independent tie-points. Four of these layers can be traced to the Icelandic volcanic system Bárðarbunga-Veidivötn, and one to the Grímsvötn system. None of the newly identified tephra isochrones could be geochemically matched to already established tephra horizons. The main transport mechanism of tephra shards to the core site in the Labrador Sea was most likely near-instantaneous by drifting sea-ice along the East Greenland Current. This mode of transportation might confine the deposition of these volcanic eruptives to the Labrador Sea region, with no or little contemporaneous deposition in sites east of Iceland, explaining why these layers have not been reported elsewhere.

Based on the tephrostratigraphic record generated in the study, we draw assumptions on the activity of different Icelandic volcanic systems during the Last Glacial period. We find that the Bárðarbunga-Veidivötn system was most active during the early parts of the record (i.e., MIS 4 and early MIS 3). The activity and/or transport mechanisms of this material reveal a cyclicity of 3-5 ka. This cyclicity might represent variability in the Icelandic ice volume and/or changes in the effectiveness of the transport mechanism to the Labrador Sea.

5. Synthesis and outlook

The research leading up to this thesis is a significant contribution to both the tephrochronological and paleoclimate community. The findings increase our understanding on dispersal patterns of past volcanic eruptions from the Last Glacial period by the new and detailed identifications in the high-latitude North Atlantic (Paper 1 & 3). These findings will act as crucial tie-points in future studies and will enable much improved constraints on the understanding of the spatial pattern and phasing of climate signals in the North Atlantic domain. Furthermore, the results presented in this thesis clearly highlight the potential of applying tephrochronology in paleoclimate studies by the use of tephra constrained marine reservoir ages as a proxy for past Atlantic surface water flux (Paper 2).

In **Paper 1** we identified the presence of two well-established tephra horizons (FMAZ II-1 and NAAZ II (II-RHY-1), in marine sediment cores located in the Labrador, Irminger and Nordic Seas. As such, we reveal the previously unknown potential of tephra horizons with isochronous features in a region with formerly sparse cryptotephra evidence. Previous cryptotephra studies have focused on regions east of Iceland, due to the inherent wind direction transporting the majority of Icelandic volcanic material to these sites. However, our findings reveal that, at least for large and explosive eruptions, material rapidly settled at sites southwest of Iceland. This opens for new and important marine-marine and marine-ice sheet tie-points in future studies aiming for synchronization of paleoclimate records over a wider geographical area.

Furthermore, in **Paper 3** we add to our recently obtained knowledge from **Paper 1** of Last Glacial isochronous tephra horizons in the western North Atlantic by producing a continuous tephrostratigraphic record from the Labrador Sea. Similar records have never before been generated from this area and time period, and as such we add crucial information regarding the tephrochronological potential of this region, which is a key region for high-latitude climate change through its influence on ocean circulation and water mass conversion. We identified five near-instantaneously deposited tephra horizons of Icelandic origin, with potential to serve as future chronological tie-points

in connecting marine records from the western North Atlantic to those from the eastern sector and the Greenland ice-cores. None of the identified isochrones could be tied to previously reported tephra horizons, which highlights potential different transport mechanisms at play in the various North Atlantic sectors. Based on our results, it is clear that the flux of the East Greenland Current, transporting sea-ice along the east Greenland margin played a likely role in limiting the dispersal of certain volcanic eruptions to areas southwest of Iceland.

Finally, in **Paper 2** we demonstrate the huge potential of applying tephrochronological findings in paleoclimate research. By the use of the FMAZ II-1 tephra layer identified in **Paper 1**, combined with previous reports, we reconstruct the near-surface marine reservoir ages in ten marine sediment cores spread across the North Atlantic Basin. If assuming that higher than modern marine reservoir ages indicate reduced northward flux of warm and saline Atlantic water, we can map out the likely surface current configuration at the onset of the LGM. Indeed, the inflow of Atlantic surface waters into the Nordic Seas at this time is highly debated and largely unknown. However, with the unprecedented age-constraint of the FMAZ II-1 horizon, we are able to pinpoint the entry pathways of Atlantic advection to sites west of the Faroe-Shetland Channel. The results form a significant advance in understanding the ocean's role as a potential moisture source for the rapid growth of the NW European ice sheets at the onset of the LGM. In addition, we show the potential of marine reservoir ages as not only an important chronological correction tool, but also as a valuable climate proxy on their own.

5.1 Future outlook

Based on the findings presented in this thesis, there are still largely unexplored tephrochronological potential in sites southwest of Iceland, which should be a research focus in future studies. **Paper 3** marks the beginning of hopefully many tephrochronology based publications from sites in the Labrador Sea and surrounding basins. Still, many questions regarding tephra deposits in this region remain unanswered. In particular, in **Paper 3** we only investigated the fine fraction (i.e., <150

μm) for tephra occurrences at selected intervals, and not continuous. Hence, this region's full tephrochronological potential remains unresolved. Furthermore, none of the isochronous tephra horizons identified in **Paper 3** could be linked to already established tephra horizons. We hypothesize that this might be due to sea-ice transport along the East Greenland Current, confining the tephra dispersal to site southwest of Iceland, an area with very limited published tephrochronological records. Thus, additional continuous tephrostratigraphic investigations in the Labrador Sea and/or Irminger Sea regions are needed to verify our tephra findings from the Labrador Sea.

In addition, it remains a challenge to link tephra deposits from the period ca. 60-45 ka b2k to the Greenland ice-cores. This largely due to a limited number of studies covering this period and lack of ice-core tephra studies from the southern parts of the Greenland ice-sheet. Detailed tephrochronological studies from the ice-cores during this time are essential to correlate the new North Atlantic tephra findings to the Greenland ice-core tephra framework and should be a priority in the future.

Furthermore, we highlight the potential to use marine reservoir ages constrained by tephra horizons as tracers of past Atlantic advection. This fairly new and uncommon approach with successful results, should be attempted both at spatially larger scales, including more sites, and for other wide-spread isochronous tephra horizons.

6. References

- Abbott, P. M., Davies, S. M., Austin, W. E. N., Pearce, N. J. G. & Hibbert, F. D. 2011. Identification of cryptotephra horizons in a North East Atlantic marine record spanning marine isotope stages 4 and 5a (~60,000–82,000 a b2k). *Quaternary International*, 246, 1-2, 177-189.
- Abbott, P. M. & Davies, S. M. 2012. Volcanism and the Greenland ice-cores: the tephra record. *Earth-Science Reviews*, 115, 3, 173-191.
- Abbott, P. M., Davies, S. M., Steffensen, J. P., Pearce, N. J. G., Bigler, M., Johnsen, S. J., Seierstad, I. K., Svensson, A. & Wastegard, S. 2012. A detailed framework of Marine Isotope Stages 4 and 5 volcanic events recorded in two Greenland ice-cores. *Quaternary Science Reviews*, 36, 59-77.
- Abbott, P. M., Bourne, A. J., Purcell, C. S., Davies, S. M., Scourse, J. D. & Pearce, N. J. G. 2016. Last glacial period cryptotephra deposits in an eastern North Atlantic marine sequence: Exploring linkages to the Greenland ice-cores. *Quaternary Geochronology*, 31, 62-76.
- Abbott, P. M., Griggs, A. J., Bourne, A. J., Chapman, M. R. & Davies, S. M. 2018a. Tracing marine cryptotephra in the North Atlantic during the last glacial period: Improving the North Atlantic marine tephrostratigraphic framework. *Quaternary Science Reviews*, 189, 169-186.
- Abbott, P. M., Griggs, A. J., Bourne, A. J. & Davies, S. M. 2018b. Tracing marine cryptotephra in the North Atlantic during the last glacial period: Protocols for identification, characterisation and evaluating depositional controls. *Marine Geology*, 401, 81-97.
- Alves, E. Q., Macario, K., Ascough, P. & Bronkramsey, C. 2018. The Worldwide Marine Radiocarbon Reservoir Effect: Definitions, Mechanisms, and Prospects. *Reviews of Geophysics*, 56, 1, 278-305.
- Ascough, P., Cook, G. & Dugmore, A. 2005. Methodological approaches to determining the marine radiocarbon reservoir effect. *Progress in Physical Geography-Earth and Environment*, 29, 4, 532-547.
- Ascough, P. L., Cook, G. T., Church, M. J., Dugmore, A. J., Arge, S. V. & Mcgovern, T. H. 2006. Variability in North Atlantic marine radiocarbon reservoir effects at c. AD 1000. *The Holocene*, 16, 1, 131-136.
- Austin, W. E. N., Wilson, L. J. & Hunt, J. B. 2004. The age and chronostratigraphical significance of North Atlantic Ash Zone II. *Journal of Quaternary Science*, 19, 2, 137-146.
- Bard, E. 1988. Correction of accelerator mass spectrometry ¹⁴C ages measured in planktonic foraminifera: Paleooceanographic implications. *Paleoceanography*, 3, 6, 635-645.
- Beget, J., Mason, O. & Anderson, P. 1992. Age, extent and climatic significance of the c. 3400 BP Aniakchak tephra, western Alaska, USA. *Holocene*, 2, 1, 51-56.
- Berben, S. M. P., Dokken, T. M., Abbott, P. M., Cook, E., Sadatzki, H., Simon, M. H. & Jansen, E. 2020. Independent tephrochronological evidence for rapid and synchronous oceanic and atmospheric temperature rises over the Greenland

- stadial-interstadial transitions between ca. 32 and 40 ka b2k. *Quaternary Science Reviews*, 236, 106277.
- Blockley, S. P. E., Pyne-O'donnell, S. D. F., Lowe, J. J., Matthews, I. P., Stone, A., Pollard, A. M., Turney, C. S. M. & Molyneux, E. G. 2005. A new and less destructive laboratory procedure for the physical separation of distal glass tephra shards from sediments. *Quaternary Science Reviews*, 24, 1952-1960.
- Blaauw, M. 2012. Out of tune: the dangers of aligning proxy archives. *Quaternary Science Reviews*, 36, 38-49.
- Borchardt, G. A., Aruscava, P. J. & Millard, H. T. 1972. Correlation of the Bishop Ash, a Pleistocene Marker Bed, Using Instrumental Neutron Activation Analysis. *Journal of Sedimentary Research*, 42, 2, 301-306.
- Bourne, A. J., Cook, E., Abbott, P. M., Seierstad, I. K., Steffensen, J. P., Svensson, A., Fischer, H., Schupbach, S. & Davies, S. M. 2015. A tephra lattice for Greenland and a reconstruction of volcanic events spanning 25-45 ka b2k. *Quaternary Science Reviews*, 118, 122-141.
- Brendryen, J., Hafliðason, H. & Sejrup, H. P. 2010. Norwegian Sea tephrostratigraphy of marine isotope stages 4 and 5: Prospects and problems for tephrochronology in the North Atlantic region. *Quaternary Science Reviews*, 29, 847-864.
- Brendryen, J., Hafliðason, H. & Sejrup, H. P. 2011. Non-synchronous deposition of North Atlantic Ash Zone II in Greenland ice cores, and North Atlantic and Norwegian Sea sediments: an example of complex glacial-stage tephra transport. *Journal of Quaternary Science*, 26, 7, 739-745.
- Brendryen, J., Hafliðason, H., Yokoyama, Y., Haaga, K. A. & Hannisdal, B. 2020. Eurasian Ice Sheet collapse was a major source of Meltwater Pulse 1A 14,600 years ago. *Nature Geoscience*, 13, 363-368.
- Dansgaard, W., Johnsen, S. J., Clausen, H. B., Dahl-Jensen, D., Gundestrup, N. S., Hammer, C. U., Hvidberg, C. S., Steffensen, J. P., Sveinbjörnsdóttir, A. E., Jouzel, J. & Bond, G. C. 1993. Evidence for general instability of past climate from a 250-kyr ice-core record. *Nature*, 364, 6434, 218-220.
- Darling, K., F., Kucera, M., Kroon, D. & Wade, C., M. 2006. A resolution for the coiling direction paradox in *Neogloboquadrina pachyderma*. *Paleoceanography*, 21, 2.
- Davies, S. M. 2015. Cryptotephra: the revolution in correlation and precision dating. *Journal of Quaternary Science*, 30, 2, 114-130.
- De Vries, H. 1958. Variation in concentration of radiocarbon with time and location on Earth. *Proceedings of the Koninklijke Nederlandse Akademie van Wetenschappen Series B*, 61, 94-102.
- Dokken, T. M. & Jansen, E. 1999. Rapid changes in the mechanism of ocean convection during the last glacial period. *Nature*, 401, 458-461.
- Dokken, T. M., Nisancioglu, K. H., Li, C., Battisti, D. S. & Kissel, C. 2013. Dansgaard-Oeschger cycles: Interactions between ocean and sea ice intrinsic to the Nordic seas. *Paleoceanography*, 28, 3, 491-502.
- Galbraith, E. D., Kwon, E. Y., Bianchi, D., Hain, M. P. & Sarmiento, J. L. 2015. The impact of atmospheric pCO₂ on carbon isotope ratios of the atmosphere and ocean. *Global Biogeochemical Cycles*, 29, 3, 307-324.

- Godwin, H. 1962. Radiocarbon Dating: Fifth International Conference. *Nature*, 195, 943-945.
- Griem, L., Voelker, A. H. L., Berben, S. M. P., Dokken, T. M. & Jansen, E. 2019. Insolation and Glacial Meltwater Influence on Sea-Ice and Circulation Variability in the Northeastern Labrador Sea During the Last Glacial Period. *Paleoceanography and Paleoclimatology*, 34, 11, 1689-1709.
- Griggs, A. J., Davies, S. M., Abbott, P. M., Rasmussen, T. L. & Palmer, A. P. 2014. Optimising the use of marine tephrochronology in the North Atlantic: a detailed investigation of the Faroe Marine Ash Zones II, III and IV. *Quaternary Science Reviews*, 106, 122-139.
- Haflidason, H., Eiriksson, J. & Van Kreveld, S. 2000. The tephrochronology of Iceland and the North Atlantic region during the Middle and Late Quaternary: a review. *Journal of Quaternary Science*, 15, 1, 3-22.
- Harning, D. J., Thordarson, T., Geirsdóttir, Á., Zalzal, K. & Miller, G. H. 2018. Provenance, stratigraphy and chronology of Holocene tephra from Vestfirðir, Iceland. *Quaternary Geochronology*, 46, 59-76.
- Hays, J. D., Imbrie, J. & Shackleton, N. J. 1976. Variations in the Earth's Orbit: Pacemaker of the Ice Ages. *Science*, 194, 4270, 1121-1132.
- Hayward, C. 2012. High spatial resolution electron probe microanalysis of tephra and melt inclusions without beam-induced chemical modification. *Holocene*, 22, 1, 119-125.
- Heaton, T. J., Kohler, P., Butzin, M., Bard, E., Reimer, R. W., Austin, W. E. N., Ramsey, C. B., Grootes, P. M., Hughen, K. A., Kromer, B., Reimer, P. J., Adkins, J., Burke, A., Cook, M. S., Olsen, J. & Skinner, L. C. 2020. Marine20-the Marine Radiocarbon Age Calibration Curve (0-55,000 Cal BP). *Radiocarbon*, 62, 4, 779-820.
- Jakobsson, S. P., Jónasson, K. & Sigurdsson, I. A. 2008. The three igneous rock suites of Iceland. *Jökull*, 58, 117-138.
- Jansen, E. 1989. The use of stable oxygen and carbon isotope stratigraphy as a dating tool. *Quaternary International*, 1, 151-166.
- Jouzel, J., Masson-Delmotte, V., Cattani, O., Dreyfus, G., Falourd, S., Hoffmann, G., Minster, B., Nouet, J., Barnola, J. M., Chappellaz, J., Fischer, H., Gallet, J. C., Johnsen, S., Leuenberger, M., Loulergue, L., Luethi, D., Oerter, H., Parrenin, F., Raisbeck, G., Raynaud, D., Schilt, A., Schwander, J., Selmo, E., Souchez, R., Spahni, R., Stauffer, B., Steffensen, J. P., Stenni, B., Stocker, T. F., Tison, J. L., Werner, M. & Wolff, E. W. 2007. Orbital and millennial Antarctic climate variability over the past 800,000 years. *Science*, 317, 5839, 793-796.
- Knox, R. W. O. B. 1993. Tephra layers as precise chronostratigraphical markers. *Geological Society, London, Special Publications*, 70, 1, 169-186.
- Lane, C. S., Brauer, A., Blockley, S. P. E. & Dulski, P. 2013. Volcanic ash reveals time-transgressive abrupt climate change during the Younger Dryas. *Geology*, 41, 12, 1251-1254.
- Larsen, G. 2002. A brief overview of eruptions from ice-covered and ice-capped volcanic systems in Iceland during the past 11 centuries: frequency, periodicity and implications. *Geological Society, London, Special Publications*, 202, 1, 81-90.

-
- Li, C. & Born, A. 2019. Coupled atmosphere-ice-ocean dynamics in Dansgaard-Oeschger events. *Quaternary Science Reviews*, 203, 1-20.
- Lowe, D. J. 2011. Tephrochronology and its application: A review. *Quaternary Geochronology*, 6, 2, 107-153.
- Mangerud, J., Bondevik, S., Gulliksen, S., Karin Hufthammer, A. & Høisæter, T. 2006. Marine 14C reservoir ages for 19th century whales and molluscs from the North Atlantic. *Quaternary Science Reviews*, 25, 23-24, 3228-3245.
- Mcintyre, A., Ruddiman, W. F., Karlin, K. & Mix, A. C. 1989. Surface water response of the equatorial Atlantic Ocean to orbital forcing. *Paleoceanography*, 4, 1, 19-55.
- Milankovitch, M. 1930. Mathematische klimalehre und astronomische theorie der Klimaschwankungen. In: KÖPPEN, W. & GEIGER, R. (eds.) *Handbuch der Klimatologie, I*. Berlin: Gebrüder Borntraeger.
- Muschitiello, F., D'andrea, W. J., Schmittner, A., Heaton, T. J., Balascio, N. L., Deroberts, N., Caffee, M. W., Woodruff, T. E., Welten, K. C., Skinner, L. C., Simon, M. H. & Dokken, T. M. 2019. Deep-water circulation changes lead North Atlantic climate during deglaciation. *Nature Communications*, 10, 1272.
- Ngrip Members, Andersen, K. K., Azuma, N., Barnola, J. M., Bigler, M., Biscaye, P., Caillon, N., Chappellaz, J., Clausen, H. B., Dahl-Jensen, D., Fischer, H., Fluckiger, J., Fritzsche, D., Fujii, Y., Goto-Azuma, K., Gronvold, K., Gundestrup, N. S., Hansson, M., Huber, C., Hvidberg, C. S., Johnsen, S. J., Jonsell, U., Jouzel, J., Kipfstuhl, S., Landais, A., Leuenberger, M., Lorrain, R., Masson-Delmotte, V., Miller, H., Motoyama, H., Narita, H., Popp, T., Rasmussen, S. O., Raynaud, D., Rothlisberger, R., Ruth, U., Samyn, D., Schwander, J., Shoji, H., Siggard-Andersen, M. L., Steffensen, J. P., Stocker, T., Sveinbjornsdottir, A. E., Svensson, A., Takata, M., Tison, J. L., Thorsteinsson, T., Watanabe, O., Wilhelms, F. & White, J. W. 2004. High-resolution record of Northern Hemisphere climate extending into the last interglacial period. *Nature*, 431, 147-151.
- Pearce, N. J. G., Alloway, B. V. & Westgate, J. A. 2008. Mid-Pleistocene silicic tephra beds in the Auckland region, New Zealand: Their correlation and origins based on the trace element analyses of single glass shards. *Quaternary International*, 178, 1, 16-43.
- Perkins, M. E., Nash, W. P., Brown, F. H. & Fleck, R. J. 1995. Fallout Tuffs of Trapper-Creek, Idaho - a Record of Miocene Explosive Volcanism in the Snake River Plain Volcanic Province. *Geological Society of America Bulletin*, 107, 12, 1484-1506.
- Rasmussen, S. O., Bigler, M., Blockley, S. P., Blunier, T., Buchardt, S. L., Clausen, H. B., Cvijanovic, I., Dahl-Jensen, D., Johnsen, S. J., Fischer, H., Gkinis, V., Guillevic, M., Hoek, W. Z., Lowe, J. J., Pedro, J. B., Popp, T., Seierstad, I. K., Steffensen, J. P., Svensson, A. M., Vallelonga, P., Vinther, B. M., Walker, M. J. C., Wheatley, J. J. & Winstrup, M. 2014. A stratigraphic framework for abrupt climatic changes during the Last Glacial period based on three synchronized Greenland ice-core records: refining and extending the INTIMATE event stratigraphy. *Quaternary Science Reviews*, 106, 14-28.

- Rasmussen, T. L. & Thomsen, E. 2004. The role of the North Atlantic Drift in the millennial timescale glacial climate fluctuations. *Palaeogeography, Palaeoclimatology, Palaeoecology*, 210, 1, 101-116.
- Reimer, P. J., Austin, W. E. N., Bard, E., Bayliss, A., Blackwell, P. G., Ramsey, C. B., Butzin, M., Cheng, H., Edwards, R. L., Friedrich, M., Grootes, P. M., Guilderson, T. P., Hajdas, I., Heaton, T. J., Hogg, A. G., Hughen, K. A., Kromer, B., Manning, S. W., Muscheler, R., Palmer, J. G., Pearson, C., Van Der Plicht, J., Reimer, R. W., Richards, D. A., Scott, E. M., Southon, J. R., Turney, C. S. M., Wacker, L., Adolphi, F., Buntgen, U., Capano, M., Fahrni, S. M., Fogtmann-Schulz, A., Friedrich, R., Kohler, P., Kudsk, S., Miyake, F., Olsen, J., Reinig, F., Sakamoto, M., Sookdeo, A. & Talamo, S. 2020. The Intcal20 Northern Hemisphere Radiocarbon Age Calibration Curve (0-55 Cal k BP). *Radiocarbon*, 62, 4, 725-757.
- Ritz, S. P., Stocker, T. F. & Müller, S. A. 2008. Modeling the effect of abrupt ocean circulation change on marine reservoir age. *Earth and Planetary Science Letters*, 268, 1, 202-211.
- Ruddiman, W. F. 1977. Late Quaternary deposition of ice-rafted sand in the subpolar North Atlantic (lat 40° to 65°N). *Geological Society of America Bulletin*, 88, 12, 1813.
- Rutledal, S., Berben, S. M. P., Dokken, T. M., Van Der Bilt, W. G. M., Cederstrom, J. M. & Jansen, E. 2020a. Tephra horizons identified in the western North Atlantic and Nordic Seas during the Last Glacial Period: Extending the marine tephra framework. *Quaternary Science Reviews*, 240, 106247.
- Rutledal, S., Hafliðason, H., Berben, S. M. P., Griem, L. & Jansen, E. 2020b. A continuous tephrostratigraphic record from the Labrador Sea spanning the last 65 ka. *Journal of Quaternary Science*, 35, 7, 855-868.
- Sadatzi, H., Dokken, T. M., Berben, S. M. P., Muschitiello, F., Stein, R., Fahl, K., Menviel, L., Timmermann, A. & Jansen, E. 2019. Sea ice variability in the southern Norwegian Sea during glacial Dansgaard-Oeschger climate cycles. *Science Advances*, 5, 3, eaau6174.
- Sadatzi, H., Maffezzoli, N., Dokken, T. M., Simon, M. H., Berben, S. M. P., Fahl, K., Kjaer, H. A., Spolaor, A., Stein, R., Vallelonga, P., Vinther, B. M. & Jansen, E. 2020. Rapid reductions and millennial-scale variability in Nordic Seas sea ice cover during abrupt glacial climate changes. *Proceedings of the National Academy of Sciences - PNAS*, 117, 47, 29478-29486.
- Sessford, E. G., Tisserand, A. A., Risebrobakken, B., Andersson, C., Dokken, T. & Jansen, E. 2018. High-Resolution Benthic Mg/Ca Temperature Record of the Intermediate Water in the Denmark Strait Across D-O Stadial-Interstadial Cycles. *Paleoceanography and Paleoclimatology*, 33, 11, 1169-1185.
- Shackleton, N. J., Berger, A. & Peltier, W. R. 1990. An Alternative Astronomical Calibration of the Lower Pleistocene Timescale Based on ODP Site 677. *Transactions of the Royal Society of Edinburgh-Earth Sciences*, 81, 4, 251-261.
- Svensson, A., Andersen, K. K., Bigler, M., Clausen, H. B., Dahl-Jensen, D., Davies, S. M., Johnsen, S. J., Muscheler, R., Parrenin, F., Rasmussen, S. O., Rothlisberger, R., Seierstad, I. K., Steffensen, J. P. & Vinther, B. M. 2008. A 60 000 year Greenland stratigraphic ice core chronology. *Climate of the Past*, 1, 47-57.

-
- Thorarinsson, S. 1981. The application of tephrochronology in Iceland. *In: SHELF, S. & SPARKS, R. S. J. (eds.) Tephra Studies*. Dordrecht: D. Reidel Publishing Company.
- Thordarson, T. & Larsen, G. 2007. Volcanism in Iceland in historical time: Volcano types, eruption styles and eruptive history. *Journal of Geodynamics*, 43, 1, 118-152.
- Tierney, J. E., Poulsen, C. J., Montanez, I. P., Bhattacharya, T., Feng, R., Ford, H. L., Honisch, B., Inglis, G. N., Petersen, S. V., Sagoo, N., Tabor, C. R., Thirumalai, K., Zhu, J., Burls, N. J., Foster, G. L., Godderis, Y., Huber, B. T., Ivany, L. C., Kirtland Turner, S., Lunt, D. J., McElwain, J. C., Mills, B. J. W., Otto-Bliesner, B. L., Ridgwell, A. & Zhang, Y. G. 2020. Past climates inform our future. *Science*, 370, eaay3701.
- Turney, C. S. M. 1998. Extraction of rhyolitic component of Vedde microtephra from minerogenic lake sediments. *Journal of Paleolimnology*, 19, 2, 199-206.
- Van Der Bilt, W. G., Cederstrøm, J. M., Støren, E. W., Berben, S. M. P. & Rutledal, S. 2020. Rapid tephra identification in geological archives with Computed Tomography (CT): experimental results and natural applications. *Frontiers of Earth Science*.
- Voelker, A. H. L. 2002. Global distribution of centennial-scale records for Marine Isotope Stage (MIS) 3: a database. *Quaternary Science Reviews*, 21, 10, 1185-1212.
- Voelker, A. H. L. & Hafliðason, H. 2015. Refining the Icelandic tephrochronology of the last glacial period – The deep-sea core PS2644 record from the southern Greenland Sea. *Global and Planetary Change*, 131, 35-62.
- Waelbroeck, C., Duplessy, J. C., Michel, E., Labeyrie, L., Paillard, D. & Duprat, J. 2001. The timing of the last deglaciation in North Atlantic climate records. *Nature*, 412, 724-727.
- Waelbroeck, C., Labeyrie, L., Michel, E., Duplessy, J. C., McManus, J. F., Lambeck, K., Balbon, E. & Labracherie, M. 2002. Sea-level and deep water temperature changes derived from benthic foraminifera isotopic records. *Quaternary Science Reviews*, 21, 1-3, 295-305.
- Walker, M. J. C. 2005. *Quaternary dating methods*, Chichester, John Wiley.
- Wastegård, S., Rasmussen, T. L., Kuijpers, A., Nielsen, T. & Van Weering, T. C. E. 2006. Composition and origin of ash zones from Marine Isotope Stages 3 and 2 in the North Atlantic. *Quaternary Science Reviews*, 25, 17-18, 2409-2419.
- Zeuner, F. E. 1945. *The Pleistocene period : its climate, chronology and faunal successions*, London, Bernard Quaritch.

7. Scientific Results

I**Paper I**

Tephra horizons identified in the western North Atlantic and Nordic Seas during the Last Glacial Period: Extending the marine tephra framework.

Rutledal, S., Berben, S. M. P., Dokken, T. M., van der Bilt, W. G. M., Cederstrøm, J. M., and Jansen, E.

(2020)

Published in *Quaternary Science Reviews*



Contents lists available at ScienceDirect

Quaternary Science Reviews

journal homepage: www.elsevier.com/locate/quascirev

Tephra horizons identified in the western North Atlantic and Nordic Seas during the Last Glacial Period: Extending the marine tephra framework

Sunniva Rutledal ^{a, b, *}, Sarah M.P. Berben ^{a, b}, Trond M. Dokken ^{b, c},
Willem G.M. van der Bilt ^{a, b}, Jan Magne Cederstrøm ^{a, b}, Eystein Jansen ^{a, b, c}

^a Department of Earth Science, University of Bergen, Allégaten 41, 5007, Bergen, Norway

^b Bjerknes Centre for Climate Research, Jahnebakken 5, 5007, Bergen, Norway

^c Norwegian Research Centre (NORCE), Jahnebakken 5, 5007, Bergen, Norway

ARTICLE INFO

Article history:

Received 6 November 2019

Received in revised form

25 February 2020

Accepted 25 February 2020

Available online 17 March 2020

Keywords:

Tephrochronology
Cryptotephra
Tephrostratigraphy
Tephra isochrons
FMAZ II
NAAZ II
Geochemistry
Paleoceanography
Marine sediment cores
Quaternary
North Atlantic Ocean

ABSTRACT

Geochemically distinct volcanic ash (tephra) deposits are increasingly acknowledged as a key geochronological tool to synchronize independent paleoclimate archives. Recent advances in the detection of invisible (crypto) tephra have led to the ongoing establishment, development and integration of regional tephra lattices. These frameworks offer an overview of the spatial extent of geochemically characterized tephra from dated eruptions – a valuable tool for precise correlation of paleorecords within these areas. Here, we harness cryptotephra analysis to investigate the occurrence of two well-known tephra markers from the Last Glacial Period (i.e. FMAZ II-1 (26.7 ka b2k) and NAAZ II (II-RHY-1) (55.3 ka b2k)), in marine sediment cores from the Nordic, Irminger and Labrador Seas. In addition, we assess the imprint of bioturbation on two of these tephra deposits using Computed Tomography (CT) imagery. We have successfully identified FMAZ II-1 in the Nordic and Irminger Seas. The tephra deposit is a visible deposit in the Nordic Seas, whereas it appears as a single high concentration peak within the fine-grained shard size fraction (i.e. 25–80 μm) in the Irminger Sea. Both horizons are primary airfall deposits, and this study is the first to identify a FMAZ II-1 deposit of isochronous nature in the Irminger Sea region. In addition, we have identified a new tephra horizon in the Irminger Sea, which is stratigraphically associated with FMAZ II-1, and geochemically similar to the known 2-JPC-192-1 population. We discuss its potential to serve as a new reference tie-point for correlations in the region. Lastly, we have successfully identified NAAZ II (II-RHY-1) of isochronous nature in both the Irminger and Labrador Sea. The layers are interpreted to be deposited by either direct airfall or by sea-ice drifting past the sites. Compared to the existing frameworks, which previously mainly focused on sites east of Iceland, our findings expand the knowledge and utility of the FMAZ II-1 and NAAZ II (II-RHY-1) horizons.

© 2020 The Authors. Published by Elsevier Ltd. This is an open access article under the CC BY license (<http://creativecommons.org/licenses/by/4.0/>).

1. Introduction

Tephrochronology, the use of synchronously deposited and geochemically fingerprinted ash horizons as time markers across geological archives, has become an increasingly recognized tool for correlating Late Quaternary climate records. Fundamentally, the detection of well-dated and geochemically distinct tephra horizons within disparate and/or distant records allows for an assessment of

the synchronicity of change during abrupt climate transitions in the past (Austin et al., 2012). Recent advances in cryptotephra (invisible to the naked eye) analysis (Davies, 2015), have resulted in the discovery of new chronological tie-points at more distal localities, further promoting the development of more detailed tephra frameworks (Bourne et al., 2015; Abbott et al., 2018a).

Tephra frameworks are a compilation of both visible and cryptotephra occurrences in distal and proximal settings. In addition, they provide an overview of the dispersal area of certain volcanic eruptions and of the past eruptive frequency of volcanoes in the region. Several tephra frameworks from the North Atlantic region already exist, such as the overview of tephra horizons identified in

* Corresponding author. Department of Earth Science, University of Bergen, Allégaten 41, 5007, Bergen, Norway
E-mail address: Sunniva.Rutledal@uib.no (S. Rutledal).

sites further to the west is required. Additionally, the latter would provide a more comprehensive picture of the ash dispersal across the broader northern North Atlantic Ocean during the Last Glacial Period.

The objective of this study is to further develop the existing North Atlantic tephra framework between 60 and 25 ka b2k previously presented by Abbott et al. (2018a). This objective is aimed for by examining the occurrence of FMAZ II-1 and NAAZ II (II-RHY-1) in marine sediment cores from the eastern (Nordic Seas) and western (Irminger and Labrador Sea) North Atlantic Ocean. In addition, we will assess the isochronous nature of these tephra layers and, as such, investigate whether they can act as independent time-markers (isochrons) for future correlation to other records.

2. Materials and methods

2.1. Marine sediment cores

In this study, we carried out tephra investigations on three marine sediment cores from the North Atlantic Ocean (i.e. MD99-2284, GS16-204-18CC and GS16-204-22CC) (Fig. 1). Core MD99-2284, was retrieved with the R/V *Marion Dufresne* in the eastern part of the Nordic Seas, north of the Faroe-Shetland Channel, at a water depth of 1500 m (62° 22,48 N; 00° 58,81 W) (Dokken et al., 2013; Sadatzki et al., 2019). Marine sediment cores GS16-204-18CC and GS16-204-22CC were collected during the ice2ice-2016 cruise aboard R/V *G.O. Sars* within the western part of the North Atlantic Ocean, south of Greenland. GS16-204-18CC was retrieved within the Irminger Sea at 2220 m water depth along the southeast Greenland margin (60° 01,84 N; 40° 33,45 W), whereas GS16-204-22CC was collected in the Labrador Sea at 3160 m water depth on the southern flank of the Eirik Drift (58° 02,83 N; 47° 02,36 W).

2.2. Selection of marine core depth-intervals

Previously developed chronologies for all investigated cores allowed us to target the time intervals, and thus core depths, where we expect FMAZ II-1 and NAAZ II (II-RHY-1) to be deposited.

2.2.1. MD99-2284

The position of a black tephra layer between 1404 and 1409 cm in MD99-2284, stratigraphically possibly correlating to FMAZ II-1, was first visually identified and reported by Dokken et al. (2013). Nonetheless, its geochemical composition has, so far, never been analyzed. The first visual appearance of ash at the base of the layer was used as the tephra marker horizon (i.e. 1408–1409 cm).

2.2.2. GS16-204-18CC

Samples with the potential of containing FMAZ II-1 and NAAZ II (II-RHY-1) material in GS16-204-18CC were carefully selected using the magnetic susceptibility record (Dokken and Cruise-Members, 2016) which records cycles of Greenland Interstadials (GI) and Greenland Stadials (GS) (Voelker and Hafidason, 2015). To further support the sampling interval selection, we analyzed concentrations of ice rafted debris (IRD) and planktic foraminifera $\delta^{18}\text{O}$ values (Lisa Griem pers. commun 20.08.2018). Subsequently, light isotope events that mark the stratigraphic position of Heinrich events were used, supporting a preliminary age model. Based on this evidence, we selected the intervals 210–250 cm and 505–525 cm, stratigraphically located between GI-3 and GI-2, after Heinrich event 3 and GI-15, respectively, for tephra analysis.

2.2.3. GS16-204-22CC

The existing age model for GS16-204-22CC, presented by Griem

et al. (2019) was constructed by tuning GS16-204-22CC to marine sediment core PS2644, previously collected within the Denmark Strait (Voelker et al., 1998) using planktic $\delta^{18}\text{O}$ and $\delta^{13}\text{C}$ isotopes. Based on that age model, the depth-intervals 191–210 cm (23.4–27.5 ka b2k (FMAZ II-1)) and 463–479 cm (54.3–55.8 ka b2k (NAAZ II (II-RHY-1))) were selected for tephra analysis.

2.3. Tephra analysis

Sediment samples from depth-intervals that fall within the age range of the targeted tephra deposits were sampled as 0.5 cm (GS16-204-18/22CC) and 1 cm (MD99-2284) slices at 1 cm intervals. An exception was made for core GS16-204-18CC (250–210 cm) that initially was sampled at 2 cm intervals, and in the case of increased tephra shard concentrations at 1 cm. The samples were first freeze-dried and homogenized. Subsequently, ca 0.5 g dry weight of material from each sample was prepared for tephra analysis following the methodology for marine tephra deposits (Abbott et al., 2011, 2018b). To remove carbonate material, dilute (10%) hydrochloric acid (HCl) was added to each sample and left overnight (~12 h). Samples were subsequently sieved into three size fractions (i.e. >125 μm , 80–125 μm and 25–80 μm). The fine-grained size fraction (25–80 μm) was then separated into different density fractions (i.e. >2.5 g/cm^3 , 2.3–2.5 g/cm^3 and <2.3 g/cm^3) using heavy liquid flotation with sodium polytungstate (SPT). This technique is applied to separate rhyolitic (2.3–2.5 g/cm^3) from basaltic (>2.5 g/cm^3) glass shards (Turney, 1998; Blockley et al., 2005). Using the methodology from Griggs et al. (2014), the >2.5 g/cm^3 fraction was magnetically separated using a Frantz Isodynamic Magnetic Separator in an effort to separate the paramagnetic basaltic shards from the non-magnetic minerogenic material. Finally, each sample was mounted on glass slides using Canada Balsam. If tephra shard concentrations exceeded 10,000 shards/g, the preparation steps described previously were repeated and lycopodium spore tablet(s) were added to the 25–80 μm fraction after the final density separation step. The required number of tablets varied (1–2 tablets) but the aim was to ensure that >300 spores were represented on each microscope slide. Then, to allow total dissolution of the spore tablet(s) the sample was soaked in ca. 5 ml HCl, where after it was washed and rinsed three times to ensure that the remaining HCl was completely removed. To ensure a representative range of the sample, three drops of the sample, with the material in suspension, were mounted on a microscope slide. Eventually, all tephra shards and lycopodium spores on the microscope slide were counted after Gehrels et al. (2006). The relative amount of tephra shards was calculated using equation (2.1), where l is the number of lycopodium spores in each tablet ($n = 18\,584 \pm 354$, batch no. 177745).

Concentration = l

$$\times \left(\frac{\text{glass shard count}}{\text{Lycopodium spore count} \times \text{sample dry weight}} \right) \quad (2.1)$$

For each analyzed depth interval, peaks in the tephra shard concentration profiles were selected for major element analysis. After repeating the previously described preparation steps, the samples were embedded in epoxy resin on frosted microprobe slides. To expose the surface of the glass tephra shards, the mounted material was ground using p1000 silicon carbide paper and polished using $\frac{1}{4}$ μm diamond polycrystalline suspension. Individual tephra shards were analyzed using Electron-probe microanalysis (EPMA). These measurements were performed at the Tephrochronological Analytical Unit at the University of Edinburgh using a Cameca SX100 electron microprobe with five vertical wavelength dispersive spectrometers, providing oxide values (wt.

%) for 10 major elements (see supplementary information). Approximately 20–40 individual shards per sample were analyzed following the protocols outlined by Hayward (2012). Based on the sample's shard size, a 3 μm or 5 μm beam diameter was used (see supplementary information). To monitor analytical precision, glass standards (Lipari Obsidian (rhyolitic) and BCR2g (basaltic)) were measured regularly. For geochemical data comparison, the data was normalized to 100% total oxides. All raw data values are given in the supplementary information. Totals below 94% and 97% for rhyolitic and basaltic material, respectively, were rejected.

The major element data (oxides expressed as wt. %) was statistically compared to previously published geochemical populations using statistical distance (SD) and similarity coefficient (SC) tests following the methods outlined in Perkins et al. (1995) and Borchardt et al. (1972), respectively. In addition, graphical examination using bi-plots was carried out. When calculating the SC's, we only included elements with concentrations >1 wt.%. Traditionally, values between 0.95 and 1 have been interpreted as identical dataset; whereas values between 0.90 and 0.95 as not identical dataset, but most likely originate from the same volcanic source (Davis, 1985; Beget et al., 1992). However, it should be noted that for Icelandic Volcanic systems, Abbott et al. (2018a) only accept SC's higher than 0.97 as identical geochemical compositions. The SD function considers the differences between two datasets and can only be used to assess if two populations are different and thus, not that they are the same. The calculated values are compared to critical values (=18.48 (rhyolitic) and = 23.21 (basaltic)) at a 99% confidence level. The difference in the critical values between rhyolitic and basaltic material is a result of comparing major element oxides with an average value higher than 0.1 wt.% (10 elements for basaltic and 7 elements for rhyolitic material). If the statistical distance value is higher than the critical value, the datasets are considered to be different. If the value is lower than the critical value the datasets are not considered to be different, but not necessarily identical (Pearce et al., 2008). In addition to statistical tests, the stratigraphic position of the tephra horizons in the different marine sequences were also considered when correlating deposits.

2.4. Ice rafted debris

In ice-proximal areas like the studied region, icebergs provide a possible transport pathway for tephra shards that eventually hamper the isochronous nature of a tephra horizon. Therefore, to evaluate the influence of tephra transported to the region by icebergs, we generated IRD records for the same depth intervals as investigated for the tephra analysis. This combination of IRD and tephra shard concentration profiles will offer insight to whether or not a tephra peak results from ice-rafting transport to the study sites (represented by increased IRD) (Griggs et al., 2014; Abbott et al., 2018b). For GS16-204-18CC we constructed a new IRD record (lithic grains between 150 and 500 μm) using the standard method of split counting (Heinrich, 1988; Bond and Lotti, 1995). For GS16-204-22CC, we used the IRD record presented in Griem et al. (2019).

2.5. Computed Tomography (CT) scanning

We visualize the imprint of bioturbation and IRD on parts of the cores GS16-204-18CC (510–529.5 cm) and GS16-204-22CC (452.5–488.5 cm), using Computed Tomography (CT) after e.g. Griggs et al. (2015). To do so, we employed a ProCon X-Ray CT-ALPHA scanner, operated at 100 kV and 850 μA and using a 267 ms exposure time. To capture sub-millimeter scale features, we minimized the distance between the detector and source by

scanning 2 cm wide u-channels. Reconstructed 16 bit scans were processed with the Thermo Scientific™ Avizo™ 9.1.1 software suite. First, we selected specific CT grayscale ranges with the *threshold* tool to highlight the density of hollow burrows (air) and ice rafted debris (clastic). For this purpose, we relied on the grayscale intensity histograms of our scans after Griggs et al. (2015): the lightest (low grayscale) peak corresponds to air, while the densest (high grayscale) peak reflects clastic material. To warrant correct interpretation, the outcome of this iterative process was compared to visual evidence of hollows and rock particles in the scanned core segments. Next, we created 3-D visualizations of thresholded (highlighted) CT grayscale ranges (features) using the *volume rendering* tool. Finally, we used the sieving tool to remove isolated voxels with a diameter smaller than 400 μm to reduce cluttering (noise), before visualizing highlighted features using a combination of 2-D ortho slices and 3-D visualizations after Van der bilt et al. (2018).

2.6. Evaluating the isochronous nature of tephra deposits

Tephra shards can be transported to the marine realm by a range of different pathways and during the Last Glacial Period, in our study areas, this was predominantly via direct aerial ash fall-out, by icebergs or sea-ice (Griggs et al., 2014). However, tephra layers are also susceptible to secondary depositional mechanisms such as remobilization of material by bioturbation and/or strong bottom currents. To be able to use tephra layers as time-markers, they need to be deposited and incorporated in the sediment sequence near-instantaneously following an eruption. In this study, we evaluate tephra layers with respect to their potential primary and secondary depositional mechanisms following the newly introduced classification scheme on deposit types outlined by Abbott et al. (2018b). They classified tephra deposits into five different types common in North Atlantic marine sequences. The five deposit types are summarized in Table 1. A type 1 deposit is defined as a well-constrained, low concentration shard peak with homogeneous composition, representing one single depositional event most likely deposited by primary airfall. A type 2 deposits reveals a distinct high concentration peak in shard concentration with an upward or downward spanning of shards and is either geochemically homogeneous (2A) or heterogeneous (2B). The deposit represents one single depositional event, but can be subjected to secondary reworking. The transport mechanism of this deposit type must be evaluated based on the geochemical composition as primary airfall, sea-ice rafting and iceberg rafting is possible. A type 3 deposit typically shows a flat bottom profile with an upward tailing of shards, a very high shard concentration and a geochemically homogeneous composition. Secondary reworking and/or bioturbation cause the gradational upward tailing and the most likely transport mechanism is either primary airfall or sea-ice rafting. A type 4 deposit has high shard concentrations and reveals multiple peaks over a large spread (10s of cm). Such a deposit type likely represents either several closely spaced eruptions or deposition by icebergs. A type 5 deposit has a wide spread of consistent shard concentrations, which typically represents a background signal. These shards are most likely reworked and remobilized within the ocean system, which could mask low concentration peaks representing single volcanic events.

3. Results

The tephra deposits identified in this study are summarized in Table 2.

Table 1Overview of the tephra deposit type classification scheme used in this study after [Abbott et al. \(2018b\)](#).

| Deposit type | Characteristics and transport/deposition | Useful isochron? |
|--------------|---|---|
| Type 1 | <ul style="list-style-type: none"> Well constrained, low concentration shard peak Homogeneous geochemical composition Most likely deposited by primary airfall | Yes |
| Type 2 | <ul style="list-style-type: none"> Clear high concentration shard peak Upward and downward tailing of shards Geochemically homogeneous (2A) or heterogeneous (2B) Could be transported and deposited by sea-ice rafting, iceberg rafting or primary airfall | Yes, if homogeneous geochemistry |
| Type 3 | <ul style="list-style-type: none"> High concentration of shards. Flat bottom with upward tailing. Geochemically homogeneous Most likely transported by primary airfall or sea-ice rafting. No IRD peaks | Yes |
| Type 4 | <ul style="list-style-type: none"> Distribution of multiple high concentration peaks Large deposit spread Either several closely spaced eruptions or iceberg rafted tephra. | Yes, if peaks can be tied to the Greenland tephra framework. The tephra peaks also have potential as regional marine tie-lines. |
| Type 5 | <ul style="list-style-type: none"> Background signal of consistent low shard concentration. Geochemically heterogeneous Reworking and remobilization within the ocean system. | No, but potential isochrons could be masked by the background signal. |

Table 2

Summary of tephra deposits investigated in this study with respect to their isochronous integrity, deposit type, climatic event, correlative isochrons and volcanic source. GS = Greenland stadial, GI = Greenland interstadial, H=Heinrich event. References are as follows: (1) this study; (2) [Wastegård et al. \(2006\)](#); (3) [Davies et al. \(2008\)](#); (4) [Griggs et al. \(2014\)](#); (5) [Brendryen et al. \(2011\)](#); (6) [Abbott et al. \(2018a\)](#); (7) [Abbott et al. \(2016\)](#); (8) [Austin et al. \(2004\)](#); (9) [Grönvold et al. \(1995\)](#).

| Tephra deposit | Climatic event | Deposit Type | Useful isochron? | Correlative isochron | Volcanic source | Reference (s) |
|--|----------------|----------------|------------------|----------------------|------------------------------------|---------------|
| MD99-2284 (1408–1409 cm) | GS-3 | Visible/Type 3 | Yes | FMAZ II-1 | Hekla/Vatnafjöll | 1,2,3,4 |
| GS16-204-18CC (228.5–229 cm, 25–80 µm) | GS-3 | Type 2A | Yes | FMAZ II-1 | Hekla/Vatnafjöll | 1,2,3,4 |
| GS16-204-18CC (225.5–226 cm, >125 µm) | GS-3 | Type 2A | Yes | 2-JPC-192-1 (?) | Bárdarbunga-Veidivötn or Reykjanes | 1,2 |
| GS16-204-22CC (191–210 cm) | Post H3 | Type 5 | No | | | 1 |
| GS16-204-18CC (512.5–513 cm) | GI-15 | Type 2A | Yes | NAAZ II (II-RHY-1) | Torfajökull | 1,2,5,6,7,8,9 |
| GS16-204-22CC (474–474.5 cm) | GI-15 | Type 3 | Yes | NAAZ II (II-RHY-1) | Torfajökull | 1,2,5,6,7,8,9 |

3.1. FMAZ II-1

3.1.1. MD99-2284

The tephra deposit in core MD99-2284 has a sharp visual boundary between the tephra layer and the underlying sediments as well as a visible upward tailing of decreasing tephra shards ([Fig. 2B](#)). Tephra shards from the base (1408–1409 cm) of the visible layer have been geochemically analyzed for major elements.

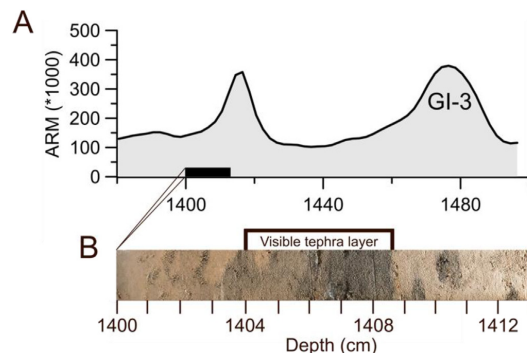


Fig. 2. A: Anhyseretic remanent magnetization (ARM) (log scale/unit 10^{-6} A/m) in MD99-2284 (1380–1500m) from [Dokken et al. \(2013\)](#) plotted against depth (cm). GI-3 = Greenland Interstadial 3. B: Image of the visual tephra layer in MD99-2284 (1404–1409 cm).

The tephra shard geochemistry reveals a basaltic homogeneous composition in the three different grain size fractions analyzed (i.e. >125 µm, 80–125 µm, 25–80 µm) ([Fig. 3](#)). Characteristic features of selected oxides (expressed as wt. %) include contents of ca. 49–51 wt. % SiO₂, ca. 3.4–3.8 wt. % TiO₂, ca. 4.2–5.6 wt. % MgO, ca. 8.5–9.8 wt. % CaO, ca. 0.3–0.7 wt. % K₂O and FeO/MgO ratios between 2.6 and 3.6. This geochemical signature exhibits strong affinities with the Hekla-Vatnafjöll volcanic system in the Eastern Volcanic Zone (EVZ), SW Iceland ([Jakobsson, 1979](#); [Larsen, 1981](#)). Using the similarity coefficient (SC) and statistical distance (SD) function we evaluate (1) how well the MD99-2284 (1408–1409 cm) tephra shard geochemistry correlates to the FMAZ II-1 suite reported in previous studies and (2) if the MD99-2284 (1408–1409 cm) basaltic horizon can be considered identical to previous reports of the FMAZ II-1 tephra shard geochemistry (i.e. SC between 0.95 and 1 and SD < 23.21; see section 2.3). The statistical results show SC's ranging from 0.94 to 0.98 and SD's ranging from 6.78 to 14.84 ([Table 3](#)). Hence, the tephra shard geochemistry from MD99-2284 (1408–1409 cm) correlates with the FMAZ II-1 suite reported from both a Greenland ice-core ([Davies et al., 2008](#)) and several North Atlantic marine records ([Wastegård et al., 2006](#); [Griggs et al., 2014](#)). This correlation can also visually be observed in the geochemical biplots ([Fig. 3B](#)) where selected major element oxides from MD99-2284 (1408–1409 cm) plot within the FMAZ II-1 geochemical field.

The stratigraphic and geochemical features of the MD99-2284 (1408–1409 cm) deposit are consistent with a deposit type 3 ([Table 1](#)), which is most likely transported via primary airfall or sea-ice rafting. The visibility of the layer and thus the immense

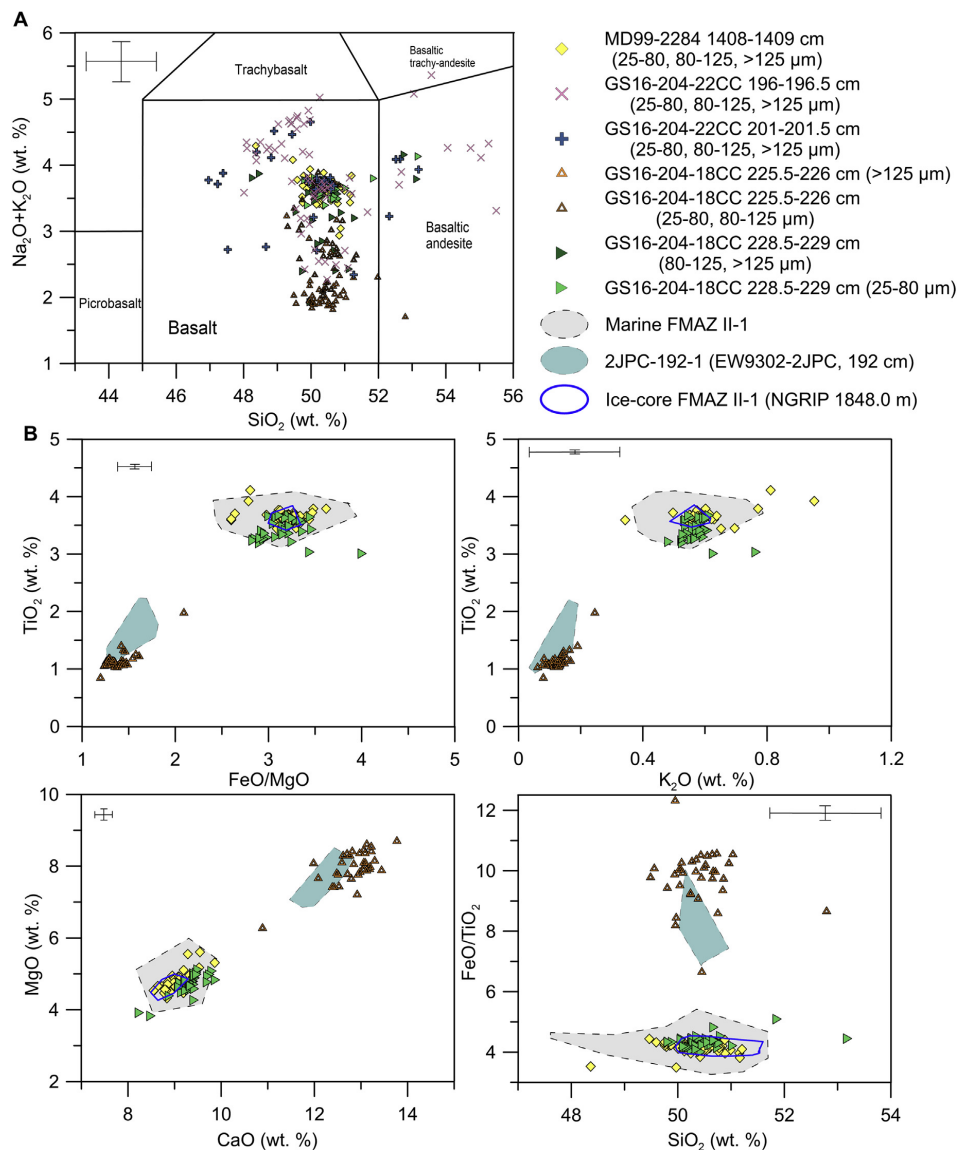


Fig. 3. Tephra shard geochemistry from cores MD99-2284 (1408–1409 cm), GS16-204-18CC (225.5–226 cm and 228.5–229 cm) and GS16-204-22CC (196–196.5 cm and 201–201.5 cm). A: Total alkali silica (TAS) plot of the chemical composition of tephra shards from MD99-2284 (1408–1409 cm), GS16-204-18CC (225.5–226 cm and 228.5–229 cm) and GS16-204-22CC (196–196.5 cm and 201–201.5 cm). Chemical classification and nomenclature from [Le Maitre and Bateman \(1989\)](#). B: Visual biplot comparison of tephra shard analyses (major element oxides) from GS16-204-18CC (228.5–229 cm) and MD99-2284 (1408–1409 cm) to the FMAZ II-1 geochemical data from the North Atlantic marine tephra framework (grey shaded area) ([Wastegård et al., 2006](#); [Griggs et al., 2014](#)) and from the Greenland ice core NGRIP (blue circle), ([Davies et al., 2008](#)). In addition, the tephra shard geochemistry from GS16-204-18CC (225.5–226 cm, >125 μm) is compared to the 2-JPC-192-1 geochemical data (blue area) from [Wastegård et al., \(2006\)](#). Error bars represent 2 standard deviations of replicate analyses of BC2rg reference glass. (For interpretation of the references to colour in this figure legend, the reader is referred to the Web version of this article.)

concentration of shards argue for a primary airfall deposition although sea-ice rafting cannot be fully excluded. Nonetheless, as the potential temporal delay by sea-ice rafting (months to years) is shorter than the chronological resolution within marine sequences

([Brendryen et al., 2010](#)), neither of these potential transport processes are considered to cause a significant temporal delay. Thus, this deposit contains all the required characteristics to be defined as an isochron.

Table 3

Statistical comparison of the geochemical compositions from the basaltic layers of MD99-2284 (1408–1409 cm) and GS16-204-18CC (228.5–229 cm, 25–80 μm) with the FMAZ II-1 population in North Atlantic marine records and the Greenland ice-core record. In addition, statistical comparison of the geochemical compositions of the rhyolitic layers in GS16-204-18CC (512.5–513 cm) and GS16-204-22CC (474–475 cm) with the NAAZ II (II-RHY-1) population in North Atlantic marine records and the Greenland ice-core record.

| | FMAZ II-1 | | | | NAAZ II (II-RHY-1) | | | |
|--|--------------------------|-------|--|-------|------------------------------|-------|------------------------------|-------|
| | MD99-2284 (1408–1409 cm) | | GS16-204-18CC (228.5–229 cm, 25–80 μm) | | GS16-204-18CC (512.5–513 cm) | | GS16-204-22CC (474–474.5 cm) | |
| | SC | SD | SC | SD | SC | SD | SC | SD |
| NGRIP (1848 m) (Davies et al., 2008) | 0.96 | 8.57 | 0.96 | 8.81 | – | – | – | – |
| JM11-19 PC (Griggs et al., 2014) | 0.98 | 6.96 | 0.97 | 22.31 | 0.97 | 4.12 | 0.98 | 9.72 |
| ENAM 93-20 (Wastegård et al., 2006) | 0.97 | 9.99 | 0.97 | 5.27 | 0.94 | 21.47 | 0.93 | 23.72 |
| ENAM 93-21 (Wastegård et al., 2006) | 0.97 | 14.84 | 0.97 | 8.96 | – | – | – | – |
| ENAM 33 (Wastegård et al., 2006) | 0.94 | 6.78 | 0.94 | 7.33 | 0.94 | 19.87 | 0.93 | 20.85 |
| LINK 17 (Wastegård et al., 2006) | 0.98 | 8.30 | 0.96 | 12.20 | – | – | – | – |
| LINK 04 (Wastegård et al., 2006) | 0.98 | 11.65 | 0.98 | 5.92 | – | – | – | – |
| EW 9302-2JPC (Wastegård et al., 2006) | 0.96 | 12.28 | 0.96 | 7.74 | 0.92 | 15.78 | 0.91 | 17.11 |
| MD95-2006 (Austin et al., 2004) | – | – | – | – | 0.95 | 14.59 | 0.94 | 16.01 |
| SO82-05/B-3 (Brendryen et al., 2011) | – | – | – | – | 0.94 | 3.77 | 0.92 | 7.12 |
| SO82-05/A-1 (Brendryen et al., 2011) | – | – | – | – | 0.97 | 6.09 | 0.96 | 11.29 |
| SO82-05/B-2 (Brendryen et al., 2011) | – | – | – | – | 0.98 | 1.98 | 0.96 | 7.92 |
| SO82-05/A-4 (Brendryen et al., 2011) | – | – | – | – | 0.98 | 2.03 | 0.96 | 6.37 |
| MD99-2289 (Brendryen et al., 2011) | – | – | – | – | 0.98 | 5.19 | 0.96 | 4.20 |
| MD04-2820CQ (Abbott et al., 2016) | – | – | – | – | 0.98 | 1.26 | 0.98 | 2.77 |
| MD04-2822 (Abbott et al., 2018a) | – | – | – | – | 0.97 | 0.48 | 0.95 | 2.81 |
| MD95-2024 (Abbott et al., 2018a) | – | – | – | – | 0.98 | 0.99 | 0.96 | 3.55 |
| MD99-2251 (Abbott et al., 2018a) | – | – | – | – | 0.98 | 1.19 | 0.98 | 3.41 |
| M23485-1 (Abbott et al., 2018a) | – | – | – | – | 0.98 | 0.34 | 0.99 | 2.74 |
| MD01-2461 (Abbott et al., 2018a) | – | – | – | – | 0.98 | 0.46 | 0.98 | 3.22 |
| MD95-2010 (Abbott et al., 2018a) | – | – | – | – | 0.98 | 2.55 | 0.99 | 1.40 |
| GIR23415-9 (Abbott et al., 2018a) | – | – | – | – | 0.99 | 0.84 | 0.98 | 2.64 |
| GRIP (2430.95 m) (Grönvold et al., 1995) | – | – | – | – | 0.94 | 1.84 | 0.96 | 1.78 |

3.1.2. GS16-204-18CC

The tephrostratigraphy for GS16-204-18CC (210–250 cm) is presented in Fig. 4. Between 225.5 cm and 229 cm a basaltic tephra horizon is observed in all size fractions. However, within the fine-grained size fraction (i.e. 25–80 μm), the basaltic tephra concentration peak occurs between 228.5 and 229 cm. In contrast, within the coarser-grained size fractions (i.e. >125 μm and 80–125 μm), both concentration peaks appear 3 cm upwards, between 225.5 and 226 cm. Tephra shards from all size fractions from the depth intervals that capture a concentration peak were geochemically analyzed for major elements.

3.1.2.1. GS16-204-18CC: 228.5–229 cm. The geochemical composition of the tephra shards from the fine-grained size fraction (i.e. 25–80 μm) of GS16-204-18CC (228.5–229 cm) shows, with the exception of two outliers, a homogeneous basaltic geochemistry (Fig. 3B). Distinct geochemical characteristics of the analyzed tephra layer are FeO/MgO ratios of ca. 2.8–3.4, ca. 49–51 wt. % SiO₂, ca. 3.1–3.7 wt. % TiO₂, ca. 4.2–5.1 wt. % MgO, ca. 8.8–9.8 wt. % CaO, and ca. 0.5–0.6 wt. % K₂O. These characteristics are comparable to the signature of the Hekla-Vatnafjöll volcanic system (Jakobsson, 1979; Larsen, 1981). The calculated SC's and SD's from the comparison between the tephra shard geochemistry of GS16-204-18CC (228.5–229 cm, 25–80 μm) and of FMAZ II-1 from both a Greenland ice-core (Davies et al., 2008) and several North Atlantic marine records (Wastegård et al., 2006; Griggs et al., 2014) are 0.94–0.97 and 5.2–22, respectively (Table 3). These values are indicative of a correlation between the deposits. This correlation is also observed in the geochemical biplots (Fig. 3B), which reveals a strong visual correlation between selected major element oxides and the FMAZ II-1 geochemical field. The tephra shard

geochemistry from the coarser-grained size fractions (i.e. >125 and 80–125 μm) of GS16-204-18CC (228.5–229 cm) shows a heterogeneous basaltic geochemistry with SiO₂ values between 47.6 and 52.33 wt % (Fig. 3A). Although, we note that half (14/28) of these shards have a similar geochemistry as the fine-fraction (i.e. FMAZ II-1) (see supplementary).

One single high concentration peak with a homogeneous geochemistry and no up- or downward tailing of shards characterizes the fine-grained (i.e. 25–80 μm) tephra deposit from 228.5 to 229 cm. In addition, the concentration peak does not co-occur with any peaks in the IRD record (Fig. 4). This evidence is most consistent with a type 2A deposit (Table 1). Such a deposit is most likely transported and deposited by primary airfall or sea-ice rafting, which cause no significant temporal delay after the eruption. Therefore, this deposit is defined as an isochron.

3.1.2.2. GS16-204-18CC: 225.5–226 cm. Concerning the tephra deposit found 3 cm upwards between 225.5 and 226 cm, the tephra shard geochemistry from the two smallest size fractions (i.e. 80–125 μm and 25–80 μm) is basaltic and heterogeneous. For instance, SiO₂ values range from 48 to 51.3 wt % (Fig. 3A). Of these shards, six (of 39) have a geochemistry similar to FMAZ II-1, which is recorded 3 cm earlier. These FMAZ II-1 shards are likely deposited as a result of secondary transport mechanisms such as reworking and/or iceberg rafting. On the other hand, the geochemistry from the coarser-grained shards (i.e. GS16-204-18CC, 225.5–226 cm; >125 μm) shows, with the exception of two outliers, a fairly homogeneous basaltic composition. Representative features are normalized values of ca. 49.5–51 wt. % SiO₂, ca. 1–1.4 wt. % TiO₂, ca. 7.4–8.6 wt. % MgO, ca. 12–13.7 wt. % CaO, ca. 0.06–0.16 wt. % K₂O and FeO/MgO ratios between 1.2 and 1.6 (Fig. 3B). This geochemical

GS16-204-18CC (Irminger Sea)

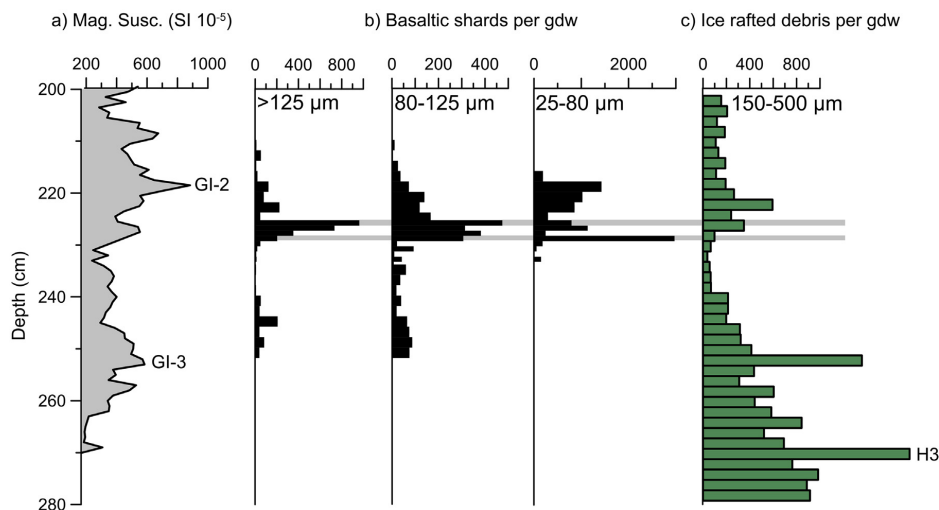


Fig. 4. Summary of marine sediment core GS16-204-18CC from the Irminger Sea. a) Magnetic susceptibility (10^{-5} Si units) of GS16-204-18CC (200–270 cm) (Dokken and Cruise-Members, 2016). GI = Greenland Interstadial. b) Tephrostratigraphy of GS16-204-18CC (210–250 cm, 2 cm resolution and 224.5–234.5 cm, 1 cm resolution) plotted versus depth (cm). The concentration of basaltic shards per gdw (gram dry weight) is quantified in three different size fractions (i.e. $>125 \mu\text{m}$, $80\text{--}125 \mu\text{m}$ and $25\text{--}80 \mu\text{m}$ ($>2.5 \text{ g/cm}^3$)). c) Ice rafted debris per gdw from the $150\text{--}500 \mu\text{m}$ size fraction of GS16-204-18CC (200–280 cm, every 2 cm). H3 refers to Heinrich event 3. Grey horizontal line marks the position of the two tephra horizons at 225.5–226 cm and at 228.5–229 cm that were geochemically analyzed.

composition is distinctly different from the FMAZ II-1 population identified 3 cm lower in the core, respectively at 228.5–229 cm. This geochemical signature suggests an origin from either the Bardarbunga-Veidivötn volcanic system in the Eastern Volcanic Zone (EVZ) (Jakobsson, 1979; Óladóttir et al., 2011) or the Reykjanes volcanic system in the Western Volcanic Zone (WVZ) (Jakobsson et al., 1978) (see supplementary figures). The only report of a tephra deposit that is stratigraphically related to the FMAZ II-1 isochron, but has a distinctly different geochemistry is the 2-JPC-192-1 deposit from the Labrador Sea (core EW9302-2JPC) (Wastegård et al., 2006). Statistical comparison between this deposit and the GS16-204-18CC (225.5–226 cm, $>125 \mu\text{m}$) geochemical population reveals a SC of 0.90 and a SD of 7.02. The low SC value of 0.90 indicates that the geochemical signatures are not similar. The small number of measurements ($n = 7$) from the 2-JPC-192-1 layer (Wastegård et al., 2006) offers a limited dataset for statistical comparison which might explain the low SC. Nonetheless, the 2-JPC-192-1 and GS16-204-18CC (225.5–226 cm, $>125 \mu\text{m}$) populations could also represent different, but closely spaced eruptions from the same volcanic center. The tephra shard concentration profile of this deposit shows a high concentration peak with tailing of shards a few centimeters downwards (Fig. 4). In addition, the deposit co-occurs with increased peaks in IRD concentration, which is indicative of iceberg transport to the site. However, geochemical data from the $>125 \mu\text{m}$ fraction reveals a fairly homogeneous population. This particular deposit was most likely not deposited by icebergs as iceberg-rafted deposits often exhibit a heterogeneous geochemistry. These results argue for a type 2A deposit (Table 1), which most likely is transported to the site by primary airfall or sea-ice rafting. These are transport and depositional mechanisms that do not affect the isochronous integrity of the deposit and therefore, the deposit is defined as an isochron.

3.1.3. GS16-204-22CC

The tephra shard concentration profile from GS16-204-22CC (191–210 cm) reveals in all size fractions a continuous background signal of basaltic tephra shards (<500 shards/g) (Fig. 5b). A minor tephra shard concentration peak was observed between 196 and 196.5 cm in all size fractions and therefore, shard material from this depth was prepared for geochemical analysis. In addition, based on increasing concentrations in the $>125 \mu\text{m}$ size fraction, tephra shards from the 201–201.5 cm interval was geochemically analyzed.

3.1.3.1. GS16-204-22CC: 201–201.5 cm. The tephra shard geochemistry from the fine-grained size fraction (i.e. $25\text{--}80 \mu\text{m}$) from GS16-204-22CC (201–201.5 cm) shows a heterogeneous geochemistry (Fig. 3A). For instance, normalized SiO_2 values vary between 47.5 wt. % and 53.1 wt. %. However, 11 out of 17 measurements of the geochemical analyses form a tight homogeneous sub-population with values of ca. 49.9–50.6 wt. % SiO_2 , ca. 3.5–3.7 wt. % TiO_2 , ca. 4.37–4.84 wt. % MgO , ca. 8.74–9.20 wt. % CaO , ca. 0.52–0.64 wt. % K_2O and FeO/MgO ratios between 3.12 and 3.46. This suggests similarities to the Hekla-Vatnafjöll volcanic system (Larsen, 1981; Jakobsson, 1979). A statistical comparison between this homogeneous sub-population and the FMAZ II-1 geochemistry from a Greenland ice-core (Davies et al., 2008) and several North Atlantic marine records (Wastegård et al., 2006; Griggs et al., 2014) reveals SC's between 0.93 and 0.98 and SD's between 0.25 and 1.15, which are indicative of a correlation (Table 3). Geochemical analyses of shards from the two coarser-grained size fractions (i.e. $>125 \mu\text{m}$ and $80\text{--}125 \mu\text{m}$) of GS16-204-22CC (201–201.5 cm) reveal a basaltic heterogeneous geochemistry (Fig. 3A). Five (of 15) of these shards correlate to the FMAZ II-1 geochemical suite and are likely deposited as a product of secondary transport mechanisms.

GS16-204-22CC (Labrador Sea)

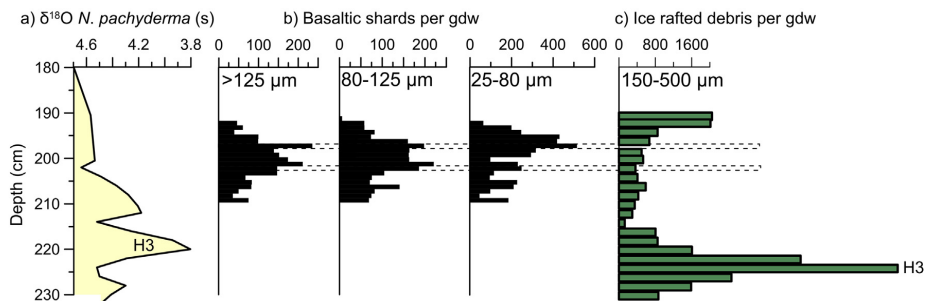


Fig. 5. Summary of marine sediment core GS16-204-22CC from the Labrador Sea. a) $\delta^{18}\text{O}$ record of the planktic foraminifera *Neogloboquadrina pachyderma sinistral* (*N. pachyderma* (s)) for GS16-204-22CC from (Griem et al., 2019). H3 = Heinrich event 3. b) Tephrostratigraphy of GS16-204-22CC (191–210 cm, 1 cm resolution) plotted versus depth (cm). The concentration of basaltic shards per gdw (gram dry weight) is quantified in three different size fractions (i.e. >125 μm , 80–125 μm and 25–80 μm (>2.5 g/cm^3)). c) Ice rafted debris per gdw from the 150–500 μm size fraction of GS16-204-18CC (200–280 cm, every 2 cm). Dotted horizontal lines mark the position of the two depth intervals, 196–196.5 cm and 201–201.5 cm, that were geochemically analyzed.

3.1.3.2. *GS16-204-22CC: 196–196.5 cm.* The geochemical composition of GS16-204-22CC (196–196.5 cm) is basaltic and heterogeneous across all size fractions (i.e. 25–80 μm , 80–125 μm and >125 μm). For example, SiO_2 values range between 48 and 55 wt. % and thus, this heterogeneous geochemistry represents tephra material derived from a mix of volcanic sources (Fig. 3A). One dominant source is the FMAZ II-1 eruption as 19 (of 67) shards correlate to this isochron.

The GS16-204-22CC (191–210 cm) tephrostratigraphy is characterized by a consistent background concentration of tephra shards with no clear concentration peak. In addition, the tephra shard concentration is low (<500 shards/g) and generally the geochemistry of the measured intervals is heterogeneous. The upper part of the deposit (191–196 cm) coincides with increased levels of IRD concentrations. This evidence argues for a type 5 deposit (Table 1), which has most likely been influenced by post-depositional reworking and remobilization, potentially masking smaller tephra shard concentration peaks. Possibly, the analyzed tephra shards from the fine-grained size fraction between 201 and 201.5 cm that correlate to the FMAZ II-1 horizon are such a masked deposit. However, due to the remobilization of this material, the deposit cannot be convincingly correlated to the FMAZ II-1 isochron.

3.2. NAAZ II

3.2.1. GS16-204-18CC

The tephra shard concentration profile of GS16-204-18CC (505–525 cm) reveals a rhyolitic deposit in the 25–80 μm and >125 μm size fractions between 511 and 518 cm (Fig. 6). We find a distinct high concentration peak between 512.5 cm and 513 cm (Fig. 6) and analyzed tephra shards from this high concentration peak as well as from the base of the deposit between 517.5 cm and 518 cm. Due to the immense shard concentrations the size fraction 80–125 μm was not counted.

The shard geochemistry from GS16-204-18CC (512.5–513 cm) and GS16-204-18CC (517.5–518 cm) both reveal a similar rhyolitic homogeneous composition with characterizing major element values of ca. 74.8–76.3 wt. % SiO_2 , ca. 2.4–2.9 wt. % FeO, ca. 0.3–0.45 wt. % CaO and ca. 4.5–5.7 wt. % Na_2O (Fig. 7). These characteristics are similar to the geochemical signature of the Thórsmörk Ignimbrite, from which the NAAZ II (II-RHY-1) suite likely derives (Sigurdsson, 1982; Lacasse et al., 1996) and now is

attributed to the Torfajökull volcano in the Eastern Volcanic Zone (EVZ) (Moles et al., 2019). The geochemistry of the rhyolitic tephra of GS16-204-18CC (512.5–513 cm) was statistically compared to the geochemical data from the NAAZ II (II-RHY-1) population in a Greenland ice-core (Grönvold et al., 1995) and several North Atlantic marine records (Austin et al., 2004; Wastegård et al., 2006; Brendryen et al., 2011; Abbott et al., 2018a). The results yield SC's of 0.92–0.99 and SD's ranging between 0.3 and 21.4 supporting a correlation between the GS16-204-18CC (512.5–513 cm) tephra layer and the NAAZ II (II-RHY-1) isochron (Table 3). There are some offsets between the geochemical analyses of this study and older analyses like those presented in Wastegård et al. (2006). The latter contributes to similarity coefficients lower than 0.95 and statistical distance values over 18.48. In particular, the analyses from GS16-204-18CC (512.5–513 cm) display lower Al_2O_3 and SiO_2 values as well as higher Na_2O concentrations. Some of these differences are most likely caused by the sodium (Na) loss effect during older analyses (Hunt and Hill, 2001; Hayward, 2012). These results corresponds to previous reports by Abbott et al. (2016). Therefore, comparisons with more recent analyses should be prioritized.

On either side of the main concentration peak we identify a high number of rhyolitic tephra shards (Fig. 6). Evidence from the high-resolution CT-scan between 510 and 529.5 cm, which identified 0.5–1 cm elongated burrows positioned just below the main concentration peak between 512.5 and 513 cm, indicate that bioturbation has been an active process in this section of the core and the downward tailing of shards could be a product of this activity (Fig. 8A). The geochemistry of the deposit is homogeneous, and there is no IRD peak coinciding with the concentration peak. These results are indicative of a type 2A deposit (Table 1) hinting at two possible transport mechanisms: (1) the tephra was transported to the site directly by airfall or (2) the tephra was transported by primary airfall onto sea-ice that most likely drifted to the site along the East Greenland Current (EGC) (Fig. 1). Although the proximity to the Icelandic source and the presence of a relatively high concentration of coarse shards (>125 μm) argue stronger for sea-ice rafting, deciphering between the two transport mechanisms is at this point not possible. However, in either scenario, there is no significant temporal delay of deposition after the eruption that would affect the integrity of the isochron.

3.2.2. GS16-204-22CC

The GS16-204-22CC (455–479 cm, >125 μm and 25–80 μm)

GS16-204-18CC (Irminger Sea)

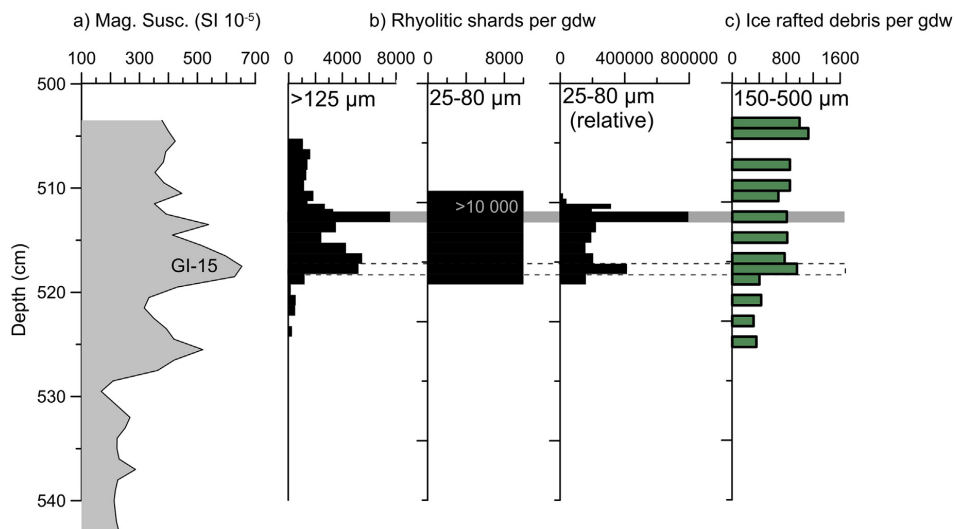


Fig. 6. Summary of marine sediment core GS16-204-18CC from the Irminger Sea. a) Magnetic susceptibility (10^{-5} Si units) from GS16-204-18CC (500–540 cm) (Dokken and Cruise-Members, 2016). GI = Greenland Interstadial. b) Tephrostratigraphy from GS16-204-18CC (505–525 cm) plotted versus depth (cm). The concentration of rhyolitic shards per gdw (gram dry weight) is quantified in two different size fractions (i.e. $>125 \mu\text{m}$ and $25\text{--}80 \mu\text{m}$ ($2.3\text{--}2.5 \text{g/cm}^3$)). Note that the middle panel refers to the level of shard counts $>10,000/\text{g}$, which were treated with lycopodium to achieve the panel on the right. c) Ice rafted debris per gdw from the $150\text{--}500 \mu\text{m}$ size fraction from GS16-204-18CC (502–522 cm). Grey horizontal line marks the position of the tephra isochron. The dotted horizontal line marks the position of peaks geochemically analyzed in addition to the main peak.

tephrostratigraphy shows a relatively flat-bottomed profile with an upward tailing of tephra shards starting from a high concentration peak between 474 cm and 474.5 cm. The deposit is positioned between 469 and 474.5 cm (Fig. 9b) and the main rhyolitic shard maximum is observed between 474 cm and 474.5 cm in both size fractions (i.e. $>125 \mu\text{m}$ and $25\text{--}80 \mu\text{m}$). Due to the extensive shard concentrations, the size fraction $80\text{--}125 \mu\text{m}$ was not counted. Tephra shards from the main concentration peak (474–474.5 cm) and from neighbouring samples (473–473.5 cm and 470–470.5 cm) were geochemically analyzed for major elements in order to assess the relationship to the main concentration peak.

Geochemical analysis reveals a similar homogenous rhyolitic geochemistry for all analyzed depth intervals. Characteristic geochemical features from the main concentration peak between 474 and 474.5 cm are values of ca. 75–76 wt. % SiO_2 , ca. 2.4–2.9 wt. % FeO, ca. 0.3–0.5 wt. % CaO and ca. 4.9–5.8 wt. % Na_2O (Fig. 9). This geochemical signature can be linked to the Thórsrörk Ignimbrite from the Torfajökull volcano in the Eastern Volcanic Zone (EVZ) (Sigurdsson, 1982; Lacasse et al., 1996; Moles et al., 2019). To determine whether the GS16-204-22CC (474–474.5 cm) rhyolitic layer can indeed be correlated to the NAAZ II (II-RHY-1) population, we compared its geochemistry to the geochemical signature of NAAZ II (II-RHY-1) from a Greenland ice-core (Grönvold et al., 1995) and several North Atlantic marine records (Austin et al., 2004; Wastegård et al., 2006; Brendryen et al., 2011; Abbott et al., 2018a). Similar as for NAAZ II (II-RHY-1) in GS16-204-18CC, high SD numbers for two of the comparisons can be attributed to sodium (Na) loss in the older analyses. We calculate SC's between 0.91 and 0.99 and SD's between 1.4 and 23.72, which indicate a correlation between the GS16-204-22CC (474–474.5 cm) rhyolitic tephra layer and the NAAZ II (II-RHY-1) isochron (Table 3).

The high resolution CT-scan of GS16-204-22CC (452.5–488.5 cm) reveals 1–2 cm elongated burrows upwards

from 474 to 474.5 cm (Fig. 8B). The presence of burrows at this level in the core verifies bioturbation as an active process that could cause the upward tailing of tephra shards identified in the tephra shard concentration profile. In addition, there are no IRD peaks coinciding with the tephra deposit. These characteristics indicate a type 3 deposit (Table 1), which was most likely deposited by primary airfall or sea-ice rafting. Subsequently, the tephra deposit is useful as an isochron.

4. Discussion

4.1. Expanding the North Atlantic tephra framework covering the Last Glacial Period

4.1.1. FMAZ II-1

Both the visible tephra layer recorded in MD99-2284 (1408–1409 cm) from the Nordic Seas and the fine-grained fraction ($25\text{--}80 \mu\text{m}$) in GS16-204-18CC (228.5–229 cm) are of isochronous nature and can be correlated to the established geochemistry of the FMAZ II-1 horizon in the literature. Similar to our results in MD99-2284 (1408–1409 cm), FMAZ II-1 appears as a thick and visible layer in many records from the Nordic Seas and Faroe region (Kuijpers et al., 1998; Rasmussen et al., 2003; Wastegård et al., 2006; Griggs et al., 2014). In fact, previous marine investigations of airfall deposited FMAZ II-1 have mainly focused on the latter region, and this study is the first to observe primary airfall deposited FMAZ II-1 in the Irminger Sea (GS16-204-18CC). With the new data presented, we expand the known dispersal range of the FMAZ II-1 tephra towards the west (Fig. 1).

Close in depth to the FMAZ II-1 isochron in GS16-204-18CC we find a coarse-grained homogenous basaltic tephra layer with geochemical characteristics similar to the 2-JPC-1-192 layer, previously reported mixed with the FMAZ II-1 horizon in the Labrador

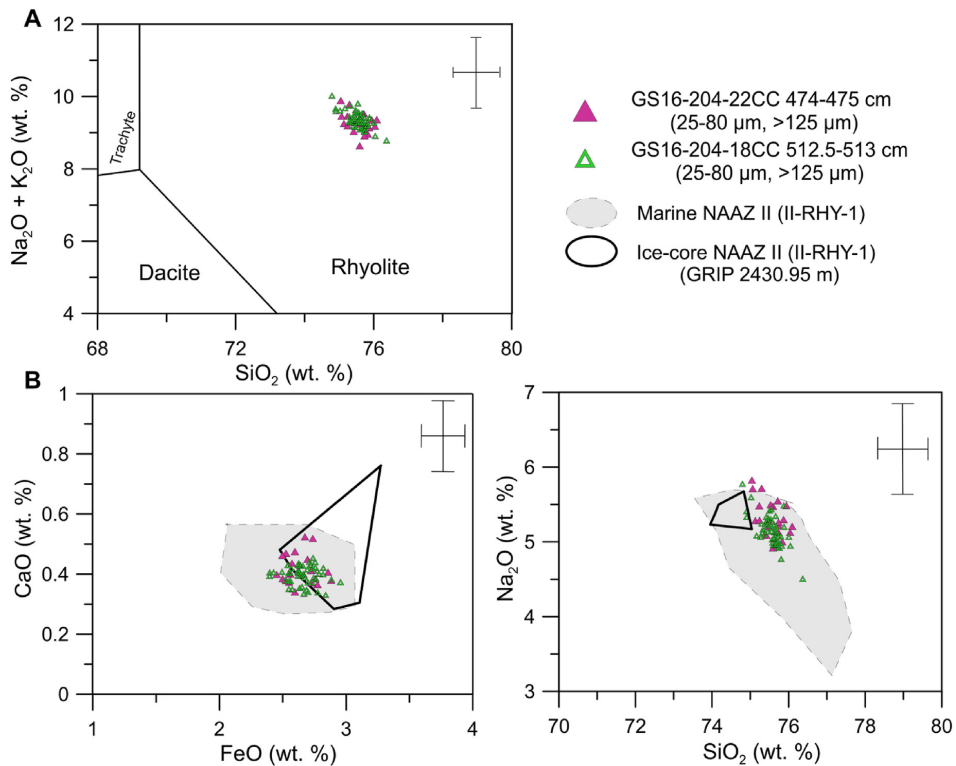


Fig. 7. Tephra shard geochemistry from cores GS16-204-18CC (474–4 cm) and GS16-204-22CC (512.5–513 cm). A: Total alkali silica (TAS) plot of the chemical composition of tephra shards from cores GS16-204-18CC (474–4 cm) and GS16-204-22CC (512.5–513 cm). Chemical classification and nomenclature from [Le Maitre and Bateman \(1989\)](#). B: Visual biplot comparison of tephra shard analyses (major element oxides) GS16-204-18CC (474–4 cm) and GS16-204-22CC (512.5–513 cm) to the NAAZ II (II-RHY-1) geochemical data from the North Atlantic marine tephra framework (grey shaded area) ([Austin et al., 2004](#); [Wastegård et al., 2006](#); [Brendryen et al., 2011](#); [Abbott et al., 2016, 2018a](#)) and from the Greenland ice core GRIP (black line) ([Grönvold et al., 1995](#)). Error bars represents 2 standard deviations of replicate analyses of Lipari Obsidian reference glass.

Sea ([Wastegård et al., 2006](#)). However, a clear statistical correlation between the 2-JPC-1-192 layer and 225.5–226 cm (>125 μm) layer in GS16-204-18CC cannot be ascertained. Still, with additional geochemical data from these horizons, they may be linked in the future. The tephra from these two horizons appears only as coarser tephra grains (>125/150 μm) and is restricted to the areas south/southwest of Iceland (i.e. Irminger and Labrador Sea). Nonetheless, attempts have been made to discover the horizon in cores from the Faroe Island region and the Reykjanes ridge ([Griggs et al., 2014](#)). The occurrence of coarser grains and the, so far, exclusive recordings southwest of Iceland argue for more local eruption(s) and a regional transport mechanism that transported the tephra material from Iceland and solely to the southwesterly sites. We suggest that the tephra material was predominantly carried westwards by winds and deposited on sea-ice that drifted along the EGC ([Fig. 1](#)). In this manner, the material would only be distributed to the south-southwestern parts of the North Atlantic Ocean. Indeed, it has been suggested that in Greenland Stadials, during which FMAZ II-1 is deposited, a southward shift of the polar front allowed for the EGC to expand and divert southwards, carrying drifting sea-ice to more southerly sites than today (e.g. to core EW 9302-2JPC in the Labrador Sea) ([Van Kreveland et al., 2000](#)).

The investigations of FMAZ II-1 in core GS16-204-22CC (191–201 cm) from the Labrador Sea were inconclusive. Although

FMAZ II-1 material was present, the core depth-interval that recorded tephra showed evidence for remobilization and reworking of material, and no isochron could be determined. Either the lack of FMAZ II-1 material in GS16-204-22CC (191–201 cm) is a result of local remobilization of sediments or the core site is located outside the western limit of the primary FMAZ II-1 tephra distribution. However, in order to further investigate the FMAZ II-1 air-dispersal limits in a southwesterly direction, new efforts might be able to identify primary airfall deposited FMAZ II-1 layers southwest of our findings in the Irminger Sea in marine sediment cores that show no evidence of remobilization.

The largest and most updated MIS 3 and 2 North Atlantic tephra framework was presented by [Abbott et al. \(2018a\)](#) in which they investigated ten North Atlantic marine sediment cores. Within this framework, the FMAZ II-1 horizon is reported in one core from the southeastern Nordic Seas (JM11-19 PC) ([Griggs et al., 2014](#)). In the North Atlantic tephra framework by [Wastegård et al. \(2006\)](#), the FMAZ II-1 horizon (>150 μm) is reported in six cores. Five of the six cores within that framework are located in the region around the Faroe Islands whereas only one of them is located in the Labrador Sea. Hence, based on the existing tephra frameworks, there is no comprehensive understanding of the air dispersal pattern of FMAZ II-1 in a southwesterly direction from Iceland. In this study, we show that cryptotephra analysis allows the detection of the FMAZ

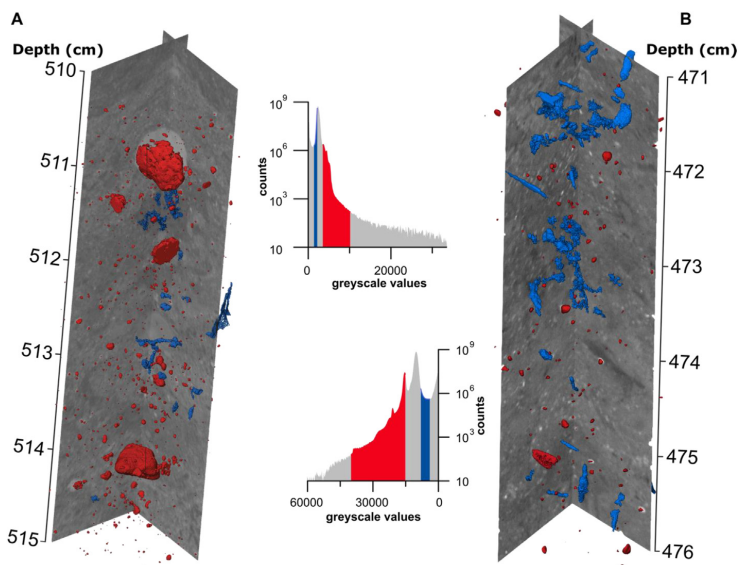


Fig. 8. Processed CT scan orthoslices of A: GS16-204-18CC (510–515 cm) and B: GS16-204-22CC (471–476 cm), with highlighted grayscale values in histograms showing IRD (red) and bioturbation (blue). Both IRD and bioturbation have been volume rendered to show the distribution and shape. (For interpretation of the references to colour in this figure legend, the reader is referred to the Web version of this article.)

GS16-204-22CC (Labrador Sea)

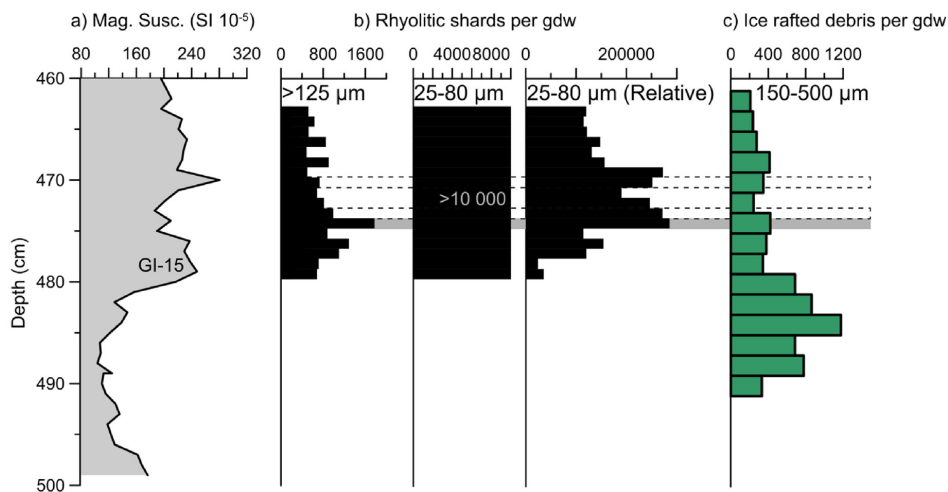


Fig. 9. Summary of marine sediment core GS16-204-22CC from the Labrador Sea. a) Magnetic susceptibility (10^{-5} SI units) from GS16-204-22CC (460–500 cm) (Dokken and Cruise-Members, 2016). GI = Greenland Interstadial. b) Tephrostratigraphy from GS16-204-22CC (463–479 cm) plotted versus depth (cm). The concentration of rhyolitic shards per gdw (gram dry weight) is quantified in two different size fractions (i.e. $>125 \mu\text{m}$ and $25\text{--}80 \mu\text{m}$ ($2.3\text{--}2.5 \text{ g/cm}^3$)). Note that the middle panel refers to the level of shard counts $>10,000/\text{g}$, which were treated with lycopodium to achieve the right panel. c) Ice rafted debris per gdw from the $150\text{--}500 \mu\text{m}$ size fraction of GS16-204-22CC (460–490 cm). Grey horizontal line marks the position of the tephra isochron. The dotted horizontal lines mark the position of peaks geochemically analyzed in addition to the main peak.

II-1 horizon at sites on the western side of the North Atlantic Ocean. These results expand the tephra framework westwards and allow to link both sides of the North Atlantic Ocean (Fig. 10). Future investigations of FMAZ II-1 should preferentially focus on the

western side of the North Atlantic, as existing frameworks by Abbott et al. (2018a) and Wastegård et al. (2006) already cover most of the eastern side. In addition, we cautiously add a new tephra horizon to the framework that is associated with the FMAZ II-1

south-southwestern core sites. This is consistent with the lack of a basaltic NAAZ II component in our sites in the Labrador and Irminger Sea.

Abbott et al. (2018a) report nine recordings of NAAZ II (II-RHY-1) within the North Atlantic marine tephra framework; five of these are from cores located west of the British Isles, two are from cores north and northeast of Iceland, and two are from sites south of Iceland (Gardar Drift and Labrador Sea). Within the North Atlantic tephra framework by Wastegård et al. (2006), the NAAZ II (II-RHY-1) isochron was identified in four cores; three of these cores are located in the Faroe Island region and one is from the Labrador Sea. In addition, Brendryen et al. (2011) contributes to the framework with NAAZ II (II-RHY-1) data from a site on the Reykjanes ridge, south of Iceland, as well as one site in the Nordic Seas (Fig. 10). A NAAZ II (II-RHY-1) horizon has also been inferred in the Irminger Sea (Elliot et al., 1998; Stoner et al., 1998); this reporting is, however, not substantiated with geochemical data. Our results therefore contribute to the North Atlantic tephra framework with new and updated geochemical data of the NAAZ II (II-RHY-1) horizon at localities that either fall outside the existing framework or are sparsely covered (Fig. 10). In addition, through the use of high-resolution CT-imagery, we determine that bioturbation most likely attributed to the tailing of shard concentrations in both deposits; this has not convincingly been shown in cores from the existing framework.

5. Conclusions

We have successfully identified the FMAZ II-1 isochron in MD99-2284 (1408–1409 cm) from the Nordic Seas and in GS16-204-18CC (228.5–229 cm, 25–80 µm) from the Irminger Sea. In contrast with sites in the Nordic Seas and Faroe Islands, where the FMAZ II-1 is recorded as a visible layer, the FMAZ II-1 is observed as a fine-fraction layer in the Irminger Sea (GS16-204-18CC, 228.5–229 cm, 25–80 µm). The discovery of FMAZ II-1 in the Irminger Sea is the first in the region and expands the previously known dispersal of the FMAZ II-1 tephra in a more northwesterly direction than showed by previous studies (Fig. 10A). This result broadens the North Atlantic tephra framework westwards and offers a new strategically located tie-point between the eastern and western side of the North Atlantic Ocean. Close in depth to our discovery of the FMAZ II-1 tephra in the Irminger Sea, a tephra deposit was recorded in the >125 µm size fraction (GS16-204-18CC, 225.5–226 cm). The geochemical composition of this coarser layer shows characteristics similar to 2-JPC-192-1 from the Labrador Sea. This horizon, found in stratigraphic proximity to FMAZ-II-1, has so far only been found southwest of Iceland. We suggest that tephra shards from these horizons were distributed from Iceland on sea-ice via the EGC, limiting the dispersal in a southwestward direction. Potentially, this new horizon can act as a reference horizon for correlation of records if more occurrences are fingerprinted in the region. We have also successfully identified the NAAZ II (II-RHY-1) in GS16-204-18CC (512.5–513 cm) from the Irminger Sea and in GS16-204-22CC (474–474.5 cm) from the Labrador Sea. These findings contribute to the North Atlantic tephra framework with new and updated geochemical data from the NAAZ II (II-RHY-1) isochron in the region. In addition, in order to better understand secondary reworking processes, we show how high-resolution CT-imagery can be used to visualize small-scale bioturbation above and below tephra isochrons.

In total, we report three different tephra horizons in three North Atlantic marine sediment cores that all possess an isochronous nature. All of these layers have potential to be used as time-markers or correlational tie-points in future studies and will aid in unraveling the synchronicity of rapid climatic transitions in different

climate archives during the Last Glacial Period.

Declaration of interests

The authors declare that they have no known competing financial interests or personal relationships that could have appeared to influence the work reported in this paper.

CRedit authorship contribution statement

Sunniva Rutledal: Conceptualization, Investigation, Visualization, Writing - original draft. **Sarah M.P. Berben:** Conceptualization, Writing - review & editing, Supervision. **Trond M. Dokken:** Supervision, Funding acquisition. **Willem G.M. van der Bilt:** Investigation, Visualization, Writing - review & editing. **Jan Magne Cederstrøm:** Investigation, Visualization, Writing - review & editing. **Eystein Jansen:** Writing - review & editing, Supervision, Project administration, Funding acquisition.

Acknowledgement

The research leading to these results has received funding from the European Research Council under the European Community's Seventh Framework Program (FP7/2007–2013)/ERC grant agreement 610055 as part of the ice2ice project. We thank Dr. Chris Hayward for his assistance with the use of the electron microprobe at the Tephra Analysis Unit, University of Edinburgh. We thank Dr. Eivind Støren from EARTHLAB, Department of Earth Science, University of Bergen for his guidance in using the CT scanner. We would also like to thank Nontje Marie Rücker for help in sample preparation and the R/V G.O. Sars and the ice2ice GS16-204 cruise crew members for retrieving the material used in this study. We also thank the IMAGES program and the R/V Marion Dufresne crew on leg MD114 for retrieving the MD99-2284 material. Siwan Davies and a second reviewer are thanked for their constructive feedback that greatly improved this manuscript.

Appendix A. Supplementary data

Supplementary data to this article can be found online at <https://doi.org/10.1016/j.quascirev.2020.106247>.

References

- Abbott, P.M., Bourne, A.J., Purcell, C.S., Davies, S.M., Scourse, J.D., Pearce, N.J.G., 2016. Last glacial period cryptotephra deposits in an eastern North Atlantic marine sequence: exploring linkages to the Greenland ice-cores. *Quat. Geochronol.* 31, 62–76.
- Abbott, P.M., Davies, S.M., Austin, W.E.N., Pearce, N.J.G., Hibbert, F.D., 2011. Identification of cryptotephra horizons in a North East Atlantic marine record spanning marine isotope stages 4 and 5a (–60,000–82,000 ka b2k). *Quat. Int.* 246, 177–189.
- Abbott, P.M., Griggs, A.J., Bourne, A.J., Chapman, M.R., Davies, S.M., 2018a. Tracing marine cryptotephra horizons in the North Atlantic during the last glacial period: improving the North Atlantic marine tephrostratigraphic framework. *Quat. Sci. Rev.* 189, 169–186.
- Abbott, P.M., Griggs, A.J., Bourne, A.J., Davies, S.M., 2018b. Tracing marine cryptotephra horizons in the North Atlantic during the last glacial period: protocols for identification, characterisation and evaluating depositional controls. *Mar. Geol.* 401, 81–97.
- Austin, W.E.N., Hibbert, F.D., Rasmussen, S.O., Peters, C., Abbott, P.M., Bryant, C.L., Blockley, S.P.E., Lane, C.S., Bronk Ramsey, C., Turney, C.S.M., 2012. The synchronization of palaeoclimatic events in the North Atlantic region during Greenland Stadial 3 (ca 27.5 to 23.3 kyr b2k). *Quat. Sci. Rev.* 36, 154–163.
- Austin, W.E.N., Wilson, L.J., Hunt, J.B., Hedges, R., Rhodes, E.J., 2004. The age and chronostratigraphical significance of North Atlantic Ash zone II. *J. Quat. Sci.* 19, 137–146.
- Beget, J., Mason, O., Anderson, P., 1992. Age, extent and climatic significance of the c. 3400 BP Aniakchak tephra, western Alaska, USA. *Holocene* 2, 51–56.
- Blockley, S.P.E., Bourne, A.J., Brauer, A., Davies, S.M., Hardiman, M., Harding, P.R., Lane, C.S., Macleod, A., Matthews, I.P., Pyne-O'Donnell, S.D.F., Rasmussen, S.O.,

- Wulf, S., Zanchetta, G., 2014. Tephrochronology and the extended intimate (integration of ice-core, marine and terrestrial records) event stratigraphy 8–128 ka b2k. *Quat. Sci. Rev.* 106, 88–100.
- Blockley, S.P.E., Pyne-O'donnell, S.D.F., Lowe, J.J., Matthews, I.P., Stone, A., Pollard, A.M., Turney, C.S.M., Molyneux, E.G., 2005. A new and less destructive laboratory procedure for the physical separation of distal glass tephra shards from sediments. *Quat. Sci. Rev.* 24, 1952–1960.
- Bond, G.C., Lotti, R., 1995. Iceberg discharges into the North Atlantic on millennial time scales during the last glacial. *Science* 267, 1005–1010.
- Borchardt, G.A., Aruscavage, P.J., Millard Jr., H.T., 1972. Correlation of the Bishop Ash, a Pleistocene marker bed, using instrumental neutron activation analysis. *J. Sediment. Petrol.* 42, 301–306.
- Bourne, A.J., Cook, E., Abbott, P.M., Seierstad, I.K., Steffensen, J.P., Svensson, A., Fischer, H., Schupbach, S., Davies, S.M., 2015. A tephra lattice for Greenland and a reconstruction of volcanic events spanning 25–45 ka b2k. *Quat. Sci. Rev.* 118, 122–141.
- Bramlette, M.N., Bradley, W.H., 1941. Geology and biology of North Atlantic deep-sea cores between Newfoundland and Ireland: 1. Lithology and geologic interpretation. *U. S. Geol. Surv. Prof. Pap.* 196-A, 1–34.
- Brendryen, J., Hafliðason, H., Sejrup, H.P., 2010. Norwegian Sea tephrostratigraphy of marine isotope stages 4 and 5: prospects and problems for tephrochronology in the North Atlantic region. *Quat. Sci. Rev.* 29, 847–864.
- Brendryen, J., Hafliðason, H., Sejrup, H.P., 2011. Non-synchronous deposition of North Atlantic Ash Zone II in Greenland ice cores, and North Atlantic and Norwegian Sea sediments: an example of complex glacial-stage tephra transport. *J. Quat. Sci.* 26, 739–745.
- Davies, S.M., 2015. Cryptotephra: the revolution in correlation and precision dating. *J. Quat. Sci.* 30, 114–130.
- Davies, S.M., Wastegård, S., Rasmussen, T.L., Svensson, A., Johnsen, S.J., Steffensen, J.P., Andersen, K.K., 2008. Identification of the Fugloyabanki tephra in the NGRIP ice core: a key tie-point for marine and ice-core sequences during the last glacial period. *J. Quat. Sci.* 23, 409–414.
- Davis, J.O., 1985. Correlation of late Quaternary tephra layers in a long pluvial sequence near Summer Lake, Oregon. *Quat. Res.* 23, 38–53.
- Dokken, T.M., Cruise-Members, 2016. Ice2Ice cruise GS16-204. In: Trond, M.D. (Ed.), *Bjerknes Climate Data Centre*.
- Dokken, T.M., Nisançioğlu, K.H., Li, C., Battisti, D.S., Kissel, C., 2013. Dansgaard-Oeschger cycles: interactions between ocean and sea ice intrinsic to the Nordic seas. *Paleoceanography* 28, 491–502.
- Elliot, M., Labeyrie, L., Bond, G., Cortijo, E., Turon, J.-L., Tisnerat, N., Duplessy, J.-C., 1998. Millennial-scale iceberg discharges in the Irminger basin during the last Glacial Period: relationship with the Heinrich events and environmental settings. *Paleoceanography* 13, 433–446.
- Gehrels, M.J., Lowe, D.J., Hazell, Z.J., Newnham, R.M., 2006. A continuous 5300-yr Holocene cryptotephrostratigraphic record from northern New Zealand and implications for tephrochronology and volcanic hazard assessment. *Holocene* 16, 173–187.
- Griem, L., Voelker, A.H.L., Berben, S.M.P., Dokken, T.M., Jansen, E., 2019. Insolation and glacial meltwater influence on sea-ice and circulation variability in the northeastern Labrador Sea during the last Glacial Period. *Paleoceanography and Paleoclimatology* 34, 1689–1709. <https://doi.org/10.1029/2019PA003605>.
- Griggs, A.J., Davies, S.M., Abbott, P.M., Coleman, M., Palmer, A.P., Rasmussen, T.L., Johnston, R., 2015. Visualizing tephra deposits and sedimentary processes in the marine environment: the potential of X-ray microtomography. *G-cubed* 16, 4329–4343.
- Griggs, A.J., Davies, S.M., Abbott, P.M., Rasmussen, T.L., Palmer, A.P., 2014. Optimising the use of marine tephrochronology in the North Atlantic: a detailed investigation of the Faeroe marine ash zones II, III and IV. *Quat. Sci. Rev.* 106, 122–139.
- Grönvold, K., Oskarsson, N., Johnsen, S.J., Clausen, H.B., Hammer, C.U., Bond, G., Bard, E., 1995. Ash layers from Iceland in the Greenland GRIP ice core correlated with oceanic and land sediments. *Earth Planet Sci. Lett.* 135, 149–155.
- Hafliðason, H., Eiriksson, J., Kreveld, S.V., 2000. The tephrochronology of Iceland and the North Atlantic region during the middle and late quaternary: a review. *J. Quat. Sci.* 15, 3–22.
- Hayward, C., 2012. High spatial resolution electron probe microanalysis of tephra and melt inclusions without beam-induced chemical modification. *Holocene* 22, 119–125.
- Heinrich, H., 1988. Origin and consequences of cyclic ice rafting in the Northeast Atlantic Ocean during the past 130,000 years. *Quat. Res.* 29, 142–152.
- Hunt, J., Hill, P.G., 2001. Tephrological implications of beam size-sample-size effects in electron microprobe analysis of glass shards. *J. Quat. Sci.* 16, 105–117.
- Jakobsson, S.P., 1979. Petrology of Recent Basalts of the Eastern Volcanic Zone, Iceland. Reykjavík.
- Jakobsson, S.P., Jonsson, J., Shido, F., 1978. Petrology of the western Reykjanes peninsula, Iceland. *J. Petrol.* 19, 669–705.
- Kuijpers, A., Andersen, M.S., Kenyon, N.H., Kunzendorf, H., Van Weering, T.C.E., 1998. Quaternary sedimentation and Norwegian sea overflow pathways around bill bailey bank, northeastern Atlantic. *Mar. Geol.* 152, 101–127.
- Kvamme, T., Mangerud, J., Furnes, H., Ruddiman, W.F., 1989. Geochemistry of pleistocene ash zones in cores from the North Atlantic. *Nor. Geol. Tidsskr.* 69, 251–272.
- Lacasse, C., Sigurdsson, H., Carey, S., Paterne, M., Guichard, F., 1996. North Atlantic deep-sea sedimentation of Late Quaternary tephra from the Iceland hotspot. *Mar. Geol.* 129, 207–235.
- Lacasse, C., Werner, R., Paterne, M., Sigurdsson, H., Carey, S., Pinte, G., Saunders, A.D., Larsen, H.C., Clift, P.D., Ali, J.R., Beget, J., Cambray, H., Demant, A., Fitton, J.G., Fram, M.S., Fukuma, K., Gieskes, J.M., Holmes, M.A., Hunt, J.M., Lacasse, C., Larsen, L.M., Lykke-Andersen, H., Meltzer, A., Morrison, M.L., Nemoto, N., Okay, N., Saito, S., Sinton, C.W., Spezzaferri, S., Stax, R., Vallier, T.L., Vandamme, D., Wei, W., Werner, R., Wise Jr., S.W., 1998. Long-range transport of Icelandic tephra to the Irminger basin, site 919. *Proc. Ocean Drill. Progr. Sci. Results* 152, 51–65.
- Lackschewitz, K.S., Wallrabe-Adams, H.-J., 1997. Composition and origin of volcanic ash zones in Late Quaternary sediments from the Reykjanes Ridge: evidence for ash fallout and ice-rafting. *Mar. Geol.* 136, 209–224.
- Larsen, G., 1981. Tephrochronology by microprobe glass analysis. In: Self, S., Sparks, R.S.J. (Eds.), *Tephra Studies*. NATO Advanced Study Institutes Series (Series C — Mathematical and Physical Sciences). Springer, Dordrecht.
- Le Maitre, R.W., Bateman, P., 1989. A Classification of Igneous Rocks and Glossary of Terms: Recommendations of the International Union of Geological Sciences Subcommittee on the Systematics of Igneous Rocks. Blackwell, Oxford.
- Moles, J.D., Mcgarvie, D., Stevenson, J.A., Sherlock, S.C., Abbott, P.M., Jenner, F.E., Halton, A.M., 2019. Widespread tephra dispersal and ignimbrite emplacement from a subglacial volcano (Torfajökull, Iceland). *Geology* 47, 577–580.
- Óladóttir, B.A., Sigmarrsson, O., Larsen, G., Devidal, J.-L., 2011. Provenance of basaltic tephra from Vatnajökull subglacial volcanoes, Iceland, as determined by major- and trace-element analyses. *Holocene* 21, 1037–1048.
- Pearce, N.J.G., Alloway, B.V., Westgate, J.A., 2008. Mid-Pleistocene silicic tephra beds in the Auckland region, New Zealand: their correlation and origins based on the trace element analyses of single glass shards. *Quat. Int.* 178, 16–43.
- Perkins, M., Nash, W., Brown, F., Fleck, R., Perkins, M., 1995. Fallout tuffs of trapper creek, Idaho-A record of miocene explosive volcanism in the snake river plain volcanic province. *Bull. Geol. Soc. Am.* 107, 1484–1506.
- Ram, M., Donarummo, J., Sheridan, M., 1996. Volcanic ash from Icelandic -57,300 Yr BP eruption found in GISP2 (Greenland) Ice Core. *Geophys. Res. Lett.* 23, 3167–3169.
- Ram, M.I., Gayley, R.I., 1991. Long-range transport of volcanic ash to the Greenland ice sheet. *Nature* 349, 401–404.
- Rasmussen, T.L., Wastegård, S., Kuijpers, A., Van Weering, T.C.E., Heinemeier, J., Thomsen, E., 2003. Stratigraphy and distribution of tephra layers in marine sediment cores from the Faeroe Islands, North Atlantic. *Mar. Geol.* 199, 263–277.
- Ruddiman, W.F., Glover, L.K., 1972. Vertical mixing of ice-rafted volcanic ash in North Atlantic sediments. *Geol. Soc. Am. Bull.* 83, 2817–2835.
- Sadatki, H., Dokken, T.M., Berben, S.M.P., Muschiello, F., Stein, R., Fahl, K., Menviel, L., Timmermann, A., Jansen, E., 2019. Sea ice variability in the southern Norwegian Sea during glacial Dansgaard-Oeschger climate cycles. *Sci. Adv.* 5.
- Sigurdsson, H., 1982. Útbreiðsla íslenskra góskulaga á botni Atlantshafs. In: THORARINSDÓTTIR, H. (Ed.), *Eldur er í Nordri*. Reykjavík: Sögufélag.
- Stoner, J.S., Channell, J.E.T., Hillaire-Marcel, C., 1998. A 200 ka geomagnetic chronostratigraphy for the Labrador Sea: indirect correlation of the sediment record to SPECMAP. *Earth Planet Sci. Lett.* 159, 165–181.
- Svensson, A., Andersen, K.K., Bigler, M., Clausen, H.B., Dahl-Jensen, D., Davies, S.M., Johnsen, S.J., Muscheler, R., Parrenin, F., Rasmussen, S.O., Röthlisberger, R., Seierstad, I.K., Steffensen, J.P., Vinther, B.M., 2008. A 60 000 year Greenland stratigraphic ice core chronology. *Clim. Past* 4, 47–57.
- Svensson, A., Andersen, K.K., Bigler, M., Clausen, H.B., Dahl-Jensen, D., Davies, S.M., Johnsen, S.J., Muscheler, R., Rasmussen, S.O., Röthlisberger, R., Peder Steffensen, J., Vinther, B.M., 2006. The Greenland Ice Core Chronology 2005, 15–42 ka. Part 2: comparison to other records. *Quat. Sci. Rev.* 25, 3258–3267.
- Turney, C., 1998. Extraction of rhyolitic component of Vedde microtephra from minerogenic lake sediments. *J. Paleolimnol.* 19, 199–206.
- Van der bilt, W.G.M., Rea, B., Spagnolo, M., Roerdink, D.L., Jørgensen, S.L., Bakke, J., 2018. NOVEL sedimentological fingerprints link shifting depositional processes to Holocene climate transitions in East Greenland. *Global Planet. Change* 164, 52–64.
- Van Kreveld, S., Sarnthein, M., Erlenkeuser, H., Grootes, P., Jung, S., Nadeau, M.J., Pflaumann, U., Voelker, A., 2000. Potential links between surging ice sheets, circulation changes, and the Dansgaard-Oeschger Cycles in the Irminger Sea, 60–18 Kyr. *Paleoceanography* 15, 425–442.
- Voelker, A.H.L., Hafliðason, H., 2015. Refining the Icelandic tephrochronology of the last glacial period — the deep-sea core PS2644 record from the southern Greenland Sea. *Global Planet. Change* 131, 35–62.
- Voelker, A.H.L., Sarnthein, M., Grootes, P.M., Erlenkeuser, H., Laj, C., Mazaud, A., Nadeau, M.-J., Schleicher, M., Mook, W.G., Van Der Plicht, J., 1998. Correlation of marine (super 14) C ages from the Nordic Seas with the GISP2 isotope record; implications for (super 14) C calibration beyond 25 ka BP. *Radiocarbon* 40, 517–534.
- Wastegård, S., Rasmussen, T.L., Kuijpers, A., Nielsen, T., Van Weering, T.C.E., 2006. Composition and origin of ash zones from marine isotope stages 3 and 2 in the North Atlantic. *Quat. Sci. Rev.* 25, 2409–2419.

Supplementary Information

“Tephra horizons identified in the western North Atlantic and Nordic Seas during the Last Glacial Period: Extending the marine tephra framework”

Rutledal, S., Berben, S. M. P., Dokken, T. M., van der Bilt W. G. M., Cederstrøm, J. M., and Jansen, E.

2020, *Quaternary Science Reviews*, 240, 106247.

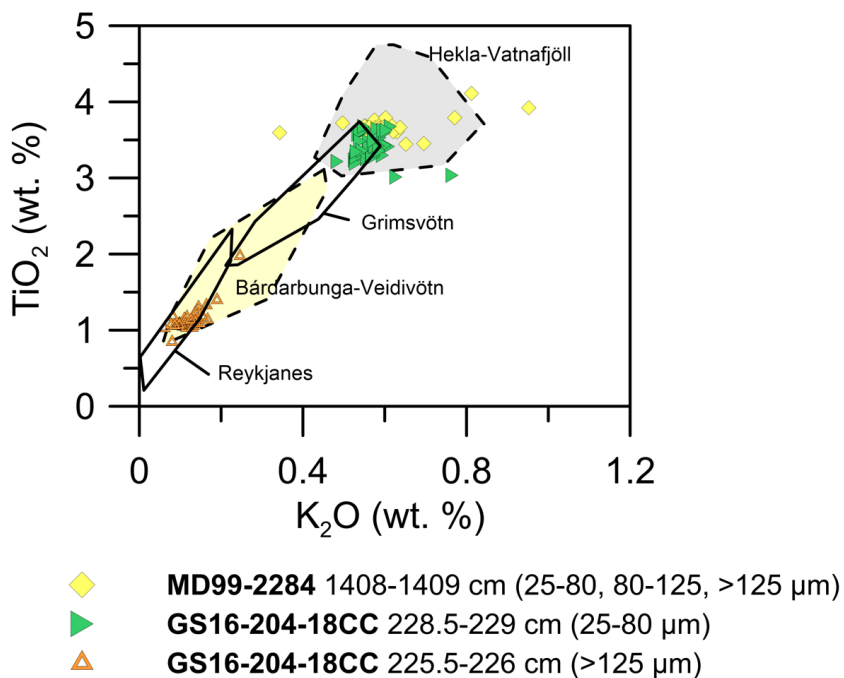


Figure A1: Geochemical data from the FMAZ II-1 horizon in GS16-204-18CC and MD99-2284 and the GS16-204-18CC (225.5-226 cm) horizon compared to the geochemical envelopes of Hekla-Vatnafjöll (Jakobsson, 1979), Grímsvötn (Jakobsson, 1979; Óladóttir et al., 2008), Bárðarbunga-Veivötn (Jakobsson, 1979; Óladóttir et al., 2008) and Reykjanes volcanic systems (Jakobsson et al., 1978).

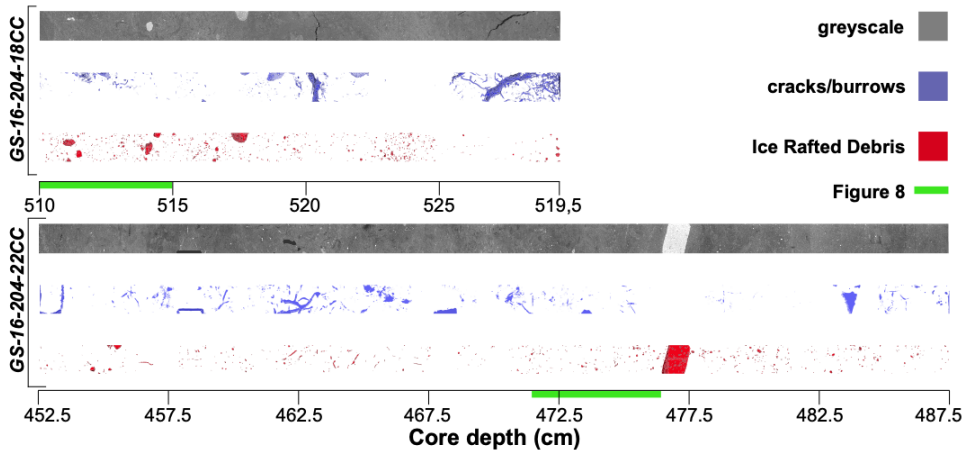


Figure A3: Overview of the complete CT-scanned sections of GS16-204-18CC and GS16-204-22CC. Grayscale image shows a single slice of the scan with all the components. Red is the extracted IRD and blue is the extracted cracks/burrows, both volume rendered prior.

References:

- Jakobsson, S. P. 1979. *Petrology of recent basalts of the eastern volcanic zone, Iceland*, Reykjavík.
- Jakobsson, S. P., Jonsson, J. & Shido, F. 1978. Petrology of the western Reykjanes Peninsula, Iceland. *Journal of Petrology*, 19, 4, 669-705.
- Lacasse, C., Sigurdsson, H., Carey, S., Johannesson, H., Thomas, L. & Rogers, N. 2007. Bimodal volcanism at the Katla subglacial caldera, Iceland: insight into the geochemistry and petrogenesis of rhyolitic magmas. *Bulletin of Volcanology*, 69, 4, 373-399.
- Moles, J. D., Mcgarvie, D., Stevenson, J. A., Sherlock, S. C., Abbott, P. M., Jenner, F. E. & Halton, A. M. 2019. Widespread tephra dispersal and ignimbrite emplacement from a subglacial volcano (Torfajökull, Iceland). *Geology*, 47, 6, 577-580.
- Óladóttir, B., Sigmarsson, O., Larsen, G. & Thordarson, T. 2008. Katla volcano, Iceland: magma composition, dynamics and eruption frequency as recorded by Holocene tephra layers. *Official Journal of the International Association of Volcanology and Chemistry of the Earth's Interior (IAVCEI)*, 70, 4, 475-493.

Paper II

Sustained Atlantic inflow into the Nordic Seas at the onset of the LGM revealed by
near-surface marine reservoir ages.

Rutledal, S., Simon, M. H., Hafliðason, H., Berben, S. M. P., and Dokken, T. M.

Manuscript in review

Paper III

A continuous tephrostratigraphic record from the Labrador Sea spanning the last 65
ka

Rutledal, S., Hafliðason, H., Berben, S. M. P., Griem, L., and Jansen E.

(2020)

Published in *Journal of Quaternary Science*

A continuous tephrostratigraphic record from the Labrador Sea spanning the last 65 ka

SUNNIVA RUTLEDAL,^{1*} HAFLIDI HAFLIDASON,¹ SARAH M. P. BERBEN,¹ LISA GRIEM^{1,2} and EYSTEIN JANSEN^{1,2}

¹Department of Earth Science, University of Bergen and Bjerknes Centre for Climate Research, Bergen, Norway

²Norwegian Research Centre (NORCE), Bergen and Bjerknes Centre for Climate Research, Bergen, Norway

Received 2 April 2020; Revised 10 August 2020; Accepted 13 August 2020

ABSTRACT: Volcanic ash preserved in marine sediment sequences is key for independent synchronization of palaeoclimate records within and across different climate archives. Here we present a continuous tephrostratigraphic record from the Labrador Sea, spanning the last 65–5 ka, an area and time period that has not been investigated in detail within the established North Atlantic tephra framework. We investigated marine sediment core GS16-204-22CC for increased tephra occurrences and geochemically analysed the major element composition of tephra shards to identify their source volcano(es). In total we observed eight tephra zones, of which five concentration peaks show isochronous features that can be used as independent tie-points in future studies. The main transport mechanism of tephra shards to the site was near-instantaneous deposition by drifting of sea ice along the East Greenland Current. Our results show that the Icelandic Veidivötn volcanic system was the dominant source of tephra material, especially between late Marine Isotope Stage (MIS) 4 and early MIS 3. The Veidivötn system generated volcanic eruptions in cycles of ca. 3–5 ka. We speculate that the quantity of tephra delivered to the Labrador Sea was a result of variable Icelandic ice volume and/or changes in the transportation pathway towards the Labrador Sea.

© 2020 The Authors. *Journal of Quaternary Science* Published by John Wiley & Sons Ltd.

KEYWORDS: marine tephra; North Atlantic; Quaternary; tephra isochrons; tephrochronology

Introduction

Tephra (volcanic ash) shards ejected from volcanoes are deposited over large geographical areas in different sedimentary settings and can act as regional time-parallel marker horizons. The often geochemically distinct signature of tephra shards allows tracing of the source volcanic system and, in some cases, the specific eruption event from which the shards originate. Geochemically distinctive tephra shards embedded in marine sediment sequences have potential to be utilized as a reliable correlational tool in dating and synchronization of palaeoclimatic events within the marine realm, but also across different climate archives (e.g. Haflidason *et al.*, 2000; Lowe, 2011; Berben *et al.*, 2020). Marine tephrochronology is especially useful as marine sediment sequences are long and continuous and record clear climate signals simultaneously, both regionally and globally.

The established North Atlantic marine tephra framework spanning the Last Glacial period (LGP) [hereafter defined as Marine Isotope Stage (MIS) 5–2 (Rasmussen *et al.*, 2014)] includes significant widespread tephra horizons such as Faroe Marine Ash Zones (FMAZ) II–IV and North Atlantic Ash Zone (NAAZ) II (Haflidason *et al.*, 2000; Wastegård *et al.*, 2006; Griggs *et al.*, 2014; Abbott *et al.*, 2018a). In addition, with the recent advances in cryptotephra (tephra invisible to the naked eye) analysis (Davies, 2015), new tephra horizons, particularly from sites in the eastern North Atlantic (Abbott *et al.*, 2016, 2018a) and Nordic Seas (Griggs *et al.*, 2014; Berben *et al.*, 2020) have been reported. These recently discovered tephra deposits are predominantly of Icelandic origin and occur stratigraphically between Heinrich events (H) 4 and 3 (ca. 40 and 31 ka,

respectively). They indicate an increase in Icelandic volcanic activity during this time interval. Spanning a longer time period, from ca. 86 to 12 ka, at least 78 tephra deposits have been identified in the northern Denmark Strait, with increased volcanic activity during the periods ca. 40–37 ka and ca. 56–50 ka (Voelker and Haflidason, 2015). Hence, there is an enormous potential to uncover tephra deposits in marine regions both distal and proximal to Iceland.

Due to the predominant strong westerlies, the prevailing direction for windblown ash from Iceland is eastwards (Haflidason *et al.*, 2000; Lacasse, 2001). Therefore, previous marine tephrochronological studies have mainly focused on these downwind regions east of Iceland. The synchronization of marine records across the wider North Atlantic requires the exploration of marine sediments in the western sector, which was the motive for investigation of the tephrochronological potential of the Labrador Sea reported here. This locality is key for monitoring palaeoclimatic shifts between the Nordic Seas, the east North Atlantic and the west North Atlantic (Griem *et al.*, 2019). Tephra deposits from this region dating to the LGP have been reported previously (Kvamme *et al.*, 1989; Wastegård *et al.*, 2006; Hesse and Khodabakhsh, 2016), but here we report the first continuous tephrostratigraphic record with comprehensive geochemical fingerprinting, an essential step for aligning marine records from the Labrador Sea to other North Atlantic marine records and the Greenland ice-core records.

The objective of this study is to provide a continuous tephra record from the Labrador Sea spanning the period 65–5 ka, and particularly the time interval ca. 65–30 ka. This objective has been achieved by using geochemical characteristics to link tephra layers to Icelandic volcanic systems and to already established tephra isochrons within the North Atlantic marine

*Correspondence: S. Rutledal, as above.
E-mail: sunniva.rutledal@uib.no

tephra framework and the Greenland ice-core tephra lattice (Bourne *et al.*, 2013, 2015; Griggs *et al.*, 2014; Wastegård and Rasmussen, 2014; Voelker and Hafliðason, 2015; Abbott *et al.*, 2016, 2018a).

Materials and methods

Marine sediment core

In this study, marine sediment core GS16-204-22CC, retrieved during the ice2ice-2016 cruise aboard R/V *G. O. Sars*, was investigated for potential existence of tephra deposits. This calypso sediment core was taken from the eastern Labrador Sea, south of Greenland (58°02.83'N, 47°02.36'W) at 3160 m water depth (Fig. 1A). The marine sediment core is 1964 cm long and spans the early Holocene to approximately late MIS 6 (Griem *et al.*, 2019). The general lithology varies between grey silty clay and sandy silt (Dokken and Cruise-members, 2016). Previously, Griem *et al.* (2019) reported high-resolution stable

isotope records measured on planktonic foraminifera *Neogloboquadrina pachyderma* (*N. pachyderma*) and ice-rafted debris (IRD) from this core (Fig. 2).

Chronology

An age model for core GS16-204-22CC has been presented by Griem *et al.* (2019). This age model is based on the tuning of planktonic $\delta^{18}\text{O}$ and $\delta^{13}\text{C}$ time series between core GS16-204-22CC and core PS2644-5 from the northern Denmark Strait (Voelker *et al.*, 1998). In addition, the identified rhyolitic component of Vedde Ash [12 171 ± 57 b2k (Svensson *et al.*, 2008)] (this study, Supporting information Fig. S1) and NAAZ II (II-RHY-1) [55 380 ± 1184 b2k (Svensson *et al.*, 2008)] (Griem *et al.*, 2019; Rutledal *et al.*, 2020) were used as independent time-markers. In total, the chronology is based on 10 tuning points, two accelerator mass spectrometry (AMS) ^{14}C dates and two tephra markers (Supporting Information Table S1). For the time period 65–25 ka, the average sedimentation

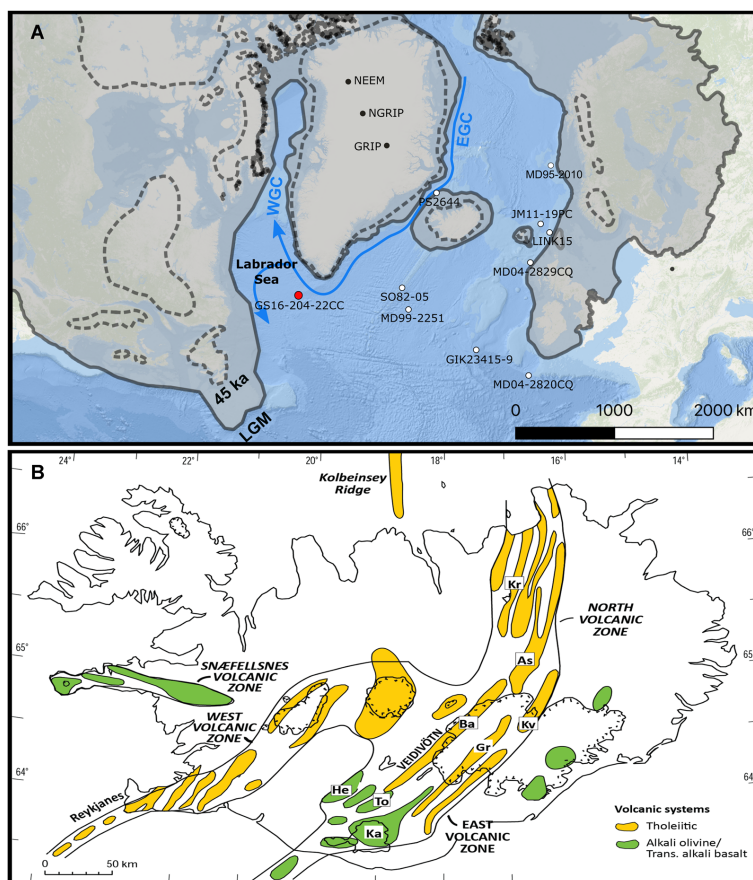


Figure 1. A: Map of the study region. The location of the marine sediment core GS16-204-22CC is marked by a red dot. The ice sheet extents of northern hemisphere ice sheets during the Last Glacial Maximum (LGM) (solid line) and ca. 45 ka b2k (dotted line) are shown by grey shading after Batchelor *et al.* (2019). The locations of marine sediment and ice cores referenced in the text are marked by white and black dots. WGC = West Greenland Current, EGC = East Greenland Current, JM = Jan Mayen. Basemap by ESRI Ocean. B: The main volcanic systems on Iceland (modified from Hafliðason *et al.*, 2000). As = Askja, Ba = Bárðarbunga-Veidivötn, Gr = Grimsvötn, He = Hekla, Ka = Katla, Kr = Krafla, Kv = Kverkfjöll, To = Torfajökull. [Color figure can be viewed at wileyonlinelibrary.com]

rate is 8.5 cm ka^{-1} . Hence, ~ 230 years separate each analysis when analysed with a 2-cm spacing. In addition, with a sample width of 0.5 cm, each sample represents ~ 50 years. Here, the age model established for core GS16-204-22CC is predominantly used as a tool to provide a chronological context for the identified tephra deposits, and thus aid in their potential geochemical correlation to established tephra deposits in the literature. For a more detailed description of the GS16-204-22CC chronology, we refer the reader to Griem *et al.* (2019).

Tephra analysis

The sediment core sequence between 0 and 540 cm was investigated for tephra occurrences. First the section between 0 and 190 cm was continuously investigated every 5 cm and the section between 190 and 540 cm every 2 cm, in the grain size fraction 150–500 μm . Intervals of elevated tephra shard concentrations were further investigated in the grain size fractions 106–150 and 63–106 μm . These specific size fractions are the result of previously published IRD and foraminiferal concentration records (Griem *et al.*, 2019). Tephra shards were counted using the same technique as for IRD counting. Here the sample is divided into equal parts using a sample splitter (Feyling-Hanssen, 1971), until a minimum of 300 grains are left for counting under an optical microscope. Depth intervals with elevated tephra shard concentrations were chosen for geochemical analysis. From the selected depth intervals, tephra shards were carefully extracted and placed onto frosted microscope slides and eventually embedded in epoxy resin following previously published methodologies (Abbott *et al.*, 2011, 2018b; Griggs *et al.*, 2014). To expose the glass shards, the mounted tephra material was carefully ground on p1000 silicon carbide paper and polished using $\frac{1}{4}$ diamond polycrystalline suspension. Single tephra shards were analysed using electron-probe microanalysis (EPMA) at the Tephrochronological Analysis unit, University of Edinburgh. A Cameca SX100 with five vertical wavelength dispersive spectrometers provided oxide values (wt.%) of 10 major elements from each measured tephra shard. Following the protocols outlined in Hayward (2012), ~ 10 –40 shards were analysed for each sample. Totals <97 wt.% were rejected. We used a beam size of 5 μm for all analyses. In addition, to ensure analytical precision, secondary standards [BCR2g (Basalt) and Lipari Obsidian (Rhyolitic)] were measured at the start and end of each run.

The major element data obtained from each tephra deposit were graphically examined and statistically compared to previously published marine and ice-core tephra horizons dating to the same time period using similarity coefficient (SC) and statistical distance (SD) tools (Borchardt *et al.*, 1972; Perkins *et al.*, 1995). Davis (1985) suggests that SC values between 0.95 and 1 indicate identical datasets. However, due to great similarity among the Icelandic volcanic systems and the products of individual volcanic systems, Abbott *et al.* (2018a) suggest that only SCs >0.97 represent identical datasets. While the SC considers how similar two datasets are, the SD function estimates the differences between datasets. The SD values are compared to critical values at a 99% confidence interval, which is 18.48 for rhyolitic material and 23.21 for basaltic material. The rhyolitic and basaltic values differ because major element comparisons are based only on those elements recording (averaged) values >0.1 wt.% (10 elements for basaltic material and seven elements for rhyolitic material). SD values larger than the critical value at a 99% confidence interval [i.e. 18.48 (rhyolitic) and 23.21

(basaltic)] suggest two different datasets, but lower values do not indicate identical datasets (Pearce *et al.*, 2008).

Volcanic source identification

Iceland consists of four volcanic zones: the North, East, West and Reykjanes volcanic zones (NVZ, EVZ, WVZ and RVZ) (Fig. 1B) (Thordarson and Larsen, 2007). These volcanic zones are further separated into 30 volcanic systems. Based on occurrences of tephra shards in Greenland ice-cores and marine sediment cores, the volcanic systems Katla, Hekla, Bárðarbunga-veidivötn (hereafter Veidivötn), Grímsvötn, Kverkfjöll, Torfajökull and Reykjanes are considered the most active systems during the LGP (Fig. 1B) (e.g. Haflidason *et al.*, 2000; Bourne *et al.*, 2013, 2015; Voelker and Haflidason, 2015; Abbott *et al.*, 2016, 2018a). To identify the volcanic source of the tephra deposits recorded in GS16-204-22CC, we compared their geochemical composition to those of Icelandic volcanic systems using the database of Harning *et al.* (2018) and references therein. The former is based on modern to Holocene geochemistry of the volcanic systems. However, the geochemistry of volcanic systems evolves with time, and knowledge of the geochemical properties of these systems during the LGP is limited (Voelker and Haflidason, 2015). Therefore, there are uncertainties in the linkage of deposits to known volcanic systems when working with pre-Holocene tephra. This is especially true for the geochemically very similar Veidivötn and Reykjanes volcanic systems, as well as the Kverkfjöll and Grímsvötn volcanic systems.

Evaluating the isochronous integrity of tephra deposits

We evaluated the isochronous integrity of each tephra zone using the tephra deposit classification scheme outlined by Abbott *et al.* (2018b). Those relevant for this study are the Type 2A, 2B and 3 deposits. A Type 2 deposit is characterized by a distinct peak in shard concentration (100 s to 1000 s of shards per 0.5 g dry weight), with an upward and downward span of shards on either side of the main concentration peak. If the deposit is homogeneous it is characterized as a Type 2A deposit and was probably transported by sea ice or primary airfall. If the deposit is heterogeneous it is characterized as a Type 2B deposit and was probably transported by iceberg rafting. A Type 3 deposit has a flat-bottomed profile with an upward tail of shards caused by bioturbation and other secondary depositional mechanisms. The main concentration peak is homogeneous, and the most likely transportation mechanism was sea ice rafting or primary airfall. For most marine tephra deposits the main concentration peak is interpreted to represent the tephra isochron. However, post-depositional processes such as bioturbation and bottom-current reworking might increase the vertical spread of the deposit and mask the main concentration peak (Abbott *et al.*, 2018b). In such cases, providing a depth/age range for the tephra deposit might be more appropriate. In addition, we acknowledge that the term 'isochronous' should be taken with caution as one tephra deposit can cover 100 s of years due to low sedimentation rates and age model uncertainties.

During the LGP, large continental ice sheets such as the Greenland Ice Sheet (GIS), the Laurentide Ice Sheet (LIS) and Icelandic Ice Sheet (IIS) influenced the study site (Fig. 1A). However, the extents of these ice sheets have varied through time. For example, the LIS was much larger during the Last Glacial Maximum (LGM) compared to the period ca. 45–40 ka (Batchelor *et al.*, 2019) (Fig. 1A). The growth and decay of

continental ice sheets are reflected in the marine IRD record as icebergs act as the primary transport agent for IRD. Hence, at the core site, an increased occurrence of IRD indicates additional iceberg transport and melt. In addition to lithic material, icebergs also transport tephra shards that have been incorporated in the ice for up to several millennia (Brendryen *et al.*, 2010). This time delay between the volcanic eruption, iceberg calving and subsequent deposition on the ocean floor will compromise the isochronous integrity of the tephra deposit. Through the LGP, the GS16-204-22CC IRD record is characterized by a continuous IRD input, which indicates that icebergs were within the proximity of the study site at all times (Griem *et al.*, 2019). Therefore, we evaluate the combined record of IRD, geochemical composition and stratigraphic appearance signals when determining the transport mechanism of each tephra zone.

Tephrostratigraphy

The tephrostratigraphic record of GS16-204-22CC, spanning the period from ca. 65 to 5 ka, is based on 10 recorded levels of increased tephra shard concentrations (Fig. 2A,B). In the following text we define these levels as 'tephra zones (TZ)'. The most pronounced tephra deposits are recorded at

130–130.5 and 474–474.5 cm. The 130–130.5 cm layer represents the rhyolitic Vedde Ash tephra and the 474–474.5 cm layer NAAZ II (II-RHY-1) (Griem *et al.*, 2019; Rutledal *et al.*, 2020) (Supporting Information Fig. S1). Both horizons are in this study solely utilized as chronological tie-points, and hence not discussed further (see 'Chronology'). The remaining eight recorded tephra deposits are analysed here in terms of their shard profiles and concentration peaks, their geochemical composition, and any co-occurrence of IRD. The last of these is investigated to assess their (most likely) deposit type, transportation mechanism and volcanic source.

Tephra zone 1 (TZ-1): GS16-204-22CC, 530.25–524.25 cm (ca. 64.3–63.7 ± 0.5 ka b2k)

A stratigraphic level of increased tephra shard concentrations is identified between 530.25 and 524.25 cm. At 530.25 cm core depth, a clear tephra concentration peak is observed in all size fractions (Fig. 2A,B). This core depth has, according to the age model (Griem *et al.*, 2019), an age estimate of ca. 64.3 ± 0.5 ka b2k (Supporting Information Fig. S2). From the concentration peak, basaltic tephra material (150–500 and 63–106 µm), including a tuff fragment ca. 1.5 cm in diameter, was geochemically analysed. In addition, basaltic shards from a smaller concentration peak recorded at 524.25 cm, about 600 years

GS16-204-22CC (Labrador Sea)

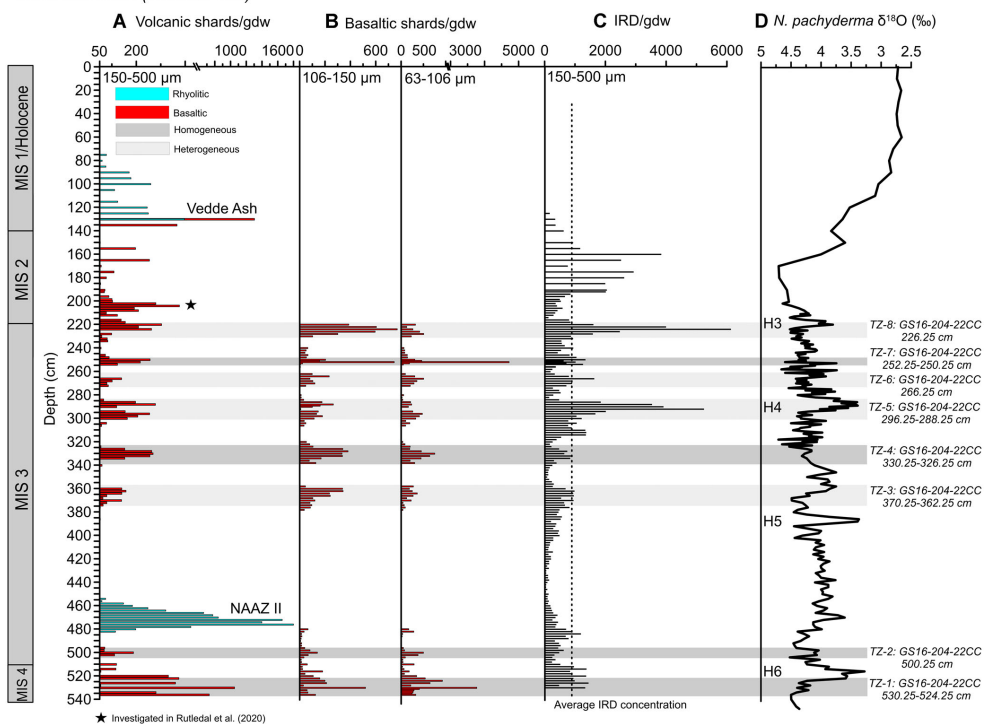


Figure 2. Tephrostratigraphic record from Labrador Sea core GS16-204-22CC, 0–540 cm versus depth (cm). (A) Occurrence of volcanic shards (basaltic and rhyolitic)/gram dry weight (gdw), 150–500 µm. (B) Occurrence of basaltic shards/gram dry weight (gdw), 106–150 µm and 63–106 µm. Please note that basaltic shards/gdw were only counted for selected intervals (i.e. TZ 1–8). (C) IRD (ice-rattled debris)/gdw from the size fraction 150–500 µm (Griem *et al.*, 2019). (D) $\delta^{18}\text{O}$ isotope record of the planktic foraminifera *N. pachyderma* (Griem *et al.*, 2019). Grey vertical bars mark the eight tephra zones described in the text, whereas Vedde Ash and NAAZ II are indicated by name. Vertical dotted line marks the average IRD concentration within the sediment core. H3–H6 = Heinrich events 3–6.

later in the record, at ca. 63.7 ± 0.5 ka b2k (Fig. S2a), was analysed to assess its relationship with the underlying peak at 530.25 cm. The analysed material from both depth intervals shows a fairly homogeneous basaltic composition (Fig. 3A) and a geochemical affiliation with the Veidivötn volcanic system in the EVZ (Harning *et al.*, 2018) (Fig. 4A,E). For this time period, there are no reports of a Veidivötn eruption in either the Greenland ice-core records or the North Atlantic marine tephra framework (e.g. Brendryen *et al.*, 2010; Bourne *et al.*, 2015; Abbott *et al.*, 2018a). The TZ-1 tephra shard concentration peak is a distinct single peak in both the coarse- and the fine-grained fractions, indicating a Type 2A deposit (Abbott *et al.*, 2018b). The tephra deposit co-occurs with increased IRD concentrations (Fig. 2C). However, because iceberg deposits often exhibit a heterogeneous geochemistry, this transport mechanism is considered unlikely. Instead, the combination of fairly homogeneous geochemistry and relatively high abundance of coarse-grained tephra indicates a near-instantaneous deposition of this tephra layer by drifting sea ice. The tephra shards were probably transported westwards off the Icelandic continental shelf by air, and then southwards by drifting sea ice along the East Greenland Current (EGC). This is in line with suggestions of an enhanced arctic export and strong EGC in this time interval (Griem *et al.*, 2019). The tephra concentration peak identified at 600 years later (524.25 cm) is stratigraphically less defined but shows the same geochemistry as the underlying peak at 530.25 cm. This tephra peak could have originated from either a later volcanic eruption from the same active system or reworking of material from the older and underlying deposit.

Tephra zone 2 (TZ-2): GS16-204-22CC, 500.25 cm (ca. 58.1 ± 0.8 ka b2k)

At the level of 500.25 cm (Fig. 2A,B) and an estimated age of ca. 58.1 ± 0.8 ka b2k (Supporting Information Fig. S2), a distinct peak in volcanic material is recorded. Tephra shards from the grain size fractions 150–500 and 63–106 μm show a homogeneous basaltic population in both grain sizes (Fig. 3A) with a geochemical composition affiliated to the Veidivötn volcanic system located in the EVZ (Harning *et al.*, 2018) (Fig. 4B,F). This geochemical spectrum does not resemble any established tephra

horizons within the Greenland ice-core tephra lattice or the North Atlantic tephra framework (e.g. Wastegård *et al.*, 2006; Bourne *et al.*, 2015; Abbott *et al.*, 2018a). TZ-2 occurs as an abrupt increase of tephra shards compared to background levels, with some up- and downward tailing of tephra shards. The tephra shards in the concentration peak show a homogeneous geochemistry, indicative of a Type 2A deposit (Abbott *et al.*, 2018b). The tephra zone does not accord with any increased levels of IRD (Fig. 2C). Due to the high concentration of relatively coarse-grained shards and homogeneous geochemistry, the tephra shards were probably transported and deposited near-instantaneously by drifting sea ice, in a similar manner as proposed for TZ-1 (ca. 6200 years older) and may be useful as a correlational tie-point for future studies.

Tephra zone 3 (TZ-3): GS16-204-22CC, 370.25–362.25 cm (ca. $46\text{--}45.3 \pm 0.5$ ka b2k)

Increased levels of tephra shards are observed in the interval between 370.25 and 362.25 cm (Fig. 2A), corresponding to an age estimate of ca. $46\text{--}45.3 \pm 0.5$ ka b2k (Supporting Information Fig. S2). Hence, the tephra shards were deposited shortly after H5 (Fig. 2d) and span a period of ca. 700 years (Fig. S2). Basaltic material (150–500 μm) from the tephra layer was geochemically analysed and showed a heterogeneous composition (Fig. 3B) with a predominantly Grímsvötn origin (Fig. 4C,G; Table 1), but 55% of the shards were collectively derived from the Katla, Hekla, Veidivötn (EVZ) and Kverkfjöll (NVZ) volcanic systems (Harning *et al.*, 2018). No tephra from the Katla, Hekla or Veidivötn volcanic systems is recorded in the Greenland ice-cores or North Atlantic marine tephra framework over this time period (e.g. Wastegård *et al.*, 2006; Bourne *et al.*, 2015; Voelker and Haflidason, 2015; Abbott *et al.*, 2018a). However, one Grímsvötn tephra horizon, known as FMAZ IV (ca. 46.8 ka BP), is recorded within the North Atlantic marine tephra framework (Griggs *et al.*, 2014; Wastegård and Rasmussen, 2014; Abbott *et al.*, 2018a). To investigate the geochemical similarity between the TZ-3 Grímsvötn shards and the FMAZ IV deposit recorded within different marine sediment cores (Fig. 1A; Table 1), we calculated the SC and SD, the former ranging from 0.95 to 0.98 and the latter from 1.48 to 5.13 (Table 1),

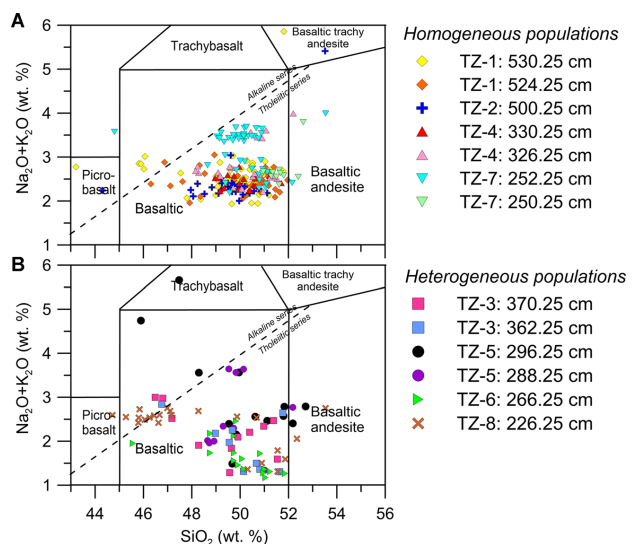


Figure 3 Total alkali silica (TAS) plot of the geochemical composition of tephra shards from GS16-204-22CC. A: Data from tephra zones with near-homogeneous composition (TZ 1, 2, 4, 7). B: Data from tephra zones with heterogeneous composition (TZ 3, 5, 6, 8). Chemical classification and nomenclature are from Le Maitre and Bateman (1989). [Color figure can be viewed at wileyonlinelibrary.com]

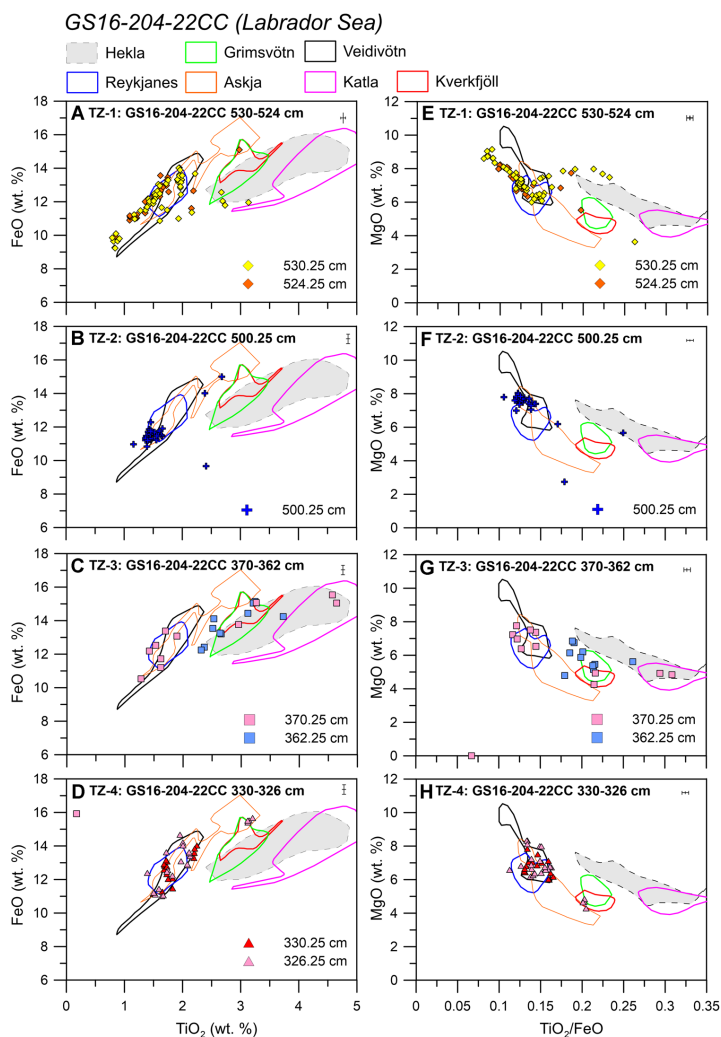


Figure 4. Visual biplot comparison (FeO versus TiO_2 and MgO versus TiO_2/FeO) of tephra shard analyses from marine sediment core GS16-204-22CC TZ 1–4. Geochemical envelopes of Icelandic volcanic systems after Harning *et al.* (2018). Error bars represent two standard deviations of replicate analysis of BCR2g reference glass. [Color figure can be viewed at [wileyonlinelibrary.com](https://onlinelibrary.wiley.com)]

indicating geochemical similarities that are also supported by the biplot graphics (Fig. 6A). We note that only geochemical data from Griggs *et al.* (2014) and Abbott *et al.* (2018a) were available for plotting, whereas statistical analysis was performed on data published by Griggs *et al.* (2014), Wastegård and Rasmussen (2014) and Abbott *et al.* (2018a). It is likely that the Grimsvötn tephra shards in TZ-3 originated from the same volcanic eruption(s) as the FMAZ IV deposit identified in multiple North Atlantic marine sediment cores (Griggs *et al.*, 2014; Wastegård and Rasmussen, 2014; Abbott *et al.*, 2018a). However, the transport mechanisms were different. The heterogeneous geochemistry of TZ-3, coupled with increased IRD concentrations (Fig. 2C), defines the deposit as a Type 2B deposit (Abbott *et al.*, 2018b), and the tephra

grains were probably transported by icebergs over a period of ca. 700 years. Consequently, deposition of TZ-3 was delayed by comparison with FMAZ IV deposition in other records, which are reported as primary (near-instantaneous) deposits.

Tephra zone 4 (TZ-4): GS16-204-22CC, 330.25–326.25 cm (ca. 42.4–42.1 ± 0.5 ka b2k)

Between 330.25 and 326.25 cm (ca. 42.4–42.1 ± 0.5 ka b2k, Supporting Information Fig. S2), corresponding to a time span of ca. 300 years, a distinct basaltic tephra deposit is observed (Fig. 2A,B). The main concentration peak occurs at 330.25 cm (ca. 42.4 ± 0.5 ka b2k). Basaltic shards (150–500 μm) from core depths 330.25 cm (ca. 42.4 ± 0.5 ka b2k) and 326.25 cm

Table 1. (Continued)

| | GRIP ^a | NGRIP ^a | NEEM ^a | MD99-2251 ^b | MD04-2829CQ ^b | MD04-2820CQ ^c | MD99-2284 ^d | GIK23415 (302-306 cm) ^b | LINK15 ^c | JM11-19PC 'FMAZ IV' ^e | MD95-2010 'FMAZ IV' ^b | SO82-05 'VZ 5' ^g |
|--|-------------------|--|---------------------------------|-------------------------|--|--------------------------|--|------------------------------------|---------------------|----------------------------------|----------------------------------|-----------------------------|
| GS16-204-22CC | 2207 m 1.53 | 2078.97 m 1.59 2079.40 m 1.20 2100.6 m 0.57 | - | - | 930-931 cm 1.10 | - | - | 0.59 | - | - | - | - |
| | SD | No match | - | - | - | - | - | - | - | - | - | - |
| | SC | Askja (26%) Katla (22%) | - | - | - | - | 3173-3174 (pop. 2) 0.98 3173-3174 (pop. 2) 2.79 | - | - | - | - | - |
| | SD | - | - | - | - | - | - | - | - | - | - | - |
| Tephra zone 6: GS16-204-22CC, 266.25 cm | - | - | - | 1713-1714 cm 0.98 | - | - | - | - | - | - | - | - |
| | SC | WVZ/RVB (28%) Grímsvötn (19%) | - | - | - | - | - | - | - | - | - | - |
| | SD | - | - | 1713-1714 cm 6.0 | - | - | - | - | - | - | - | - |
| | No match | - | - | - | - | - | - | - | - | - | - | - |
| | No match | - | - | - | - | - | - | - | - | - | - | - |
| | No match | - | - | - | - | - | - | - | - | - | - | - |
| Tephra zone 7: GS16-204-22CC, 250-252 cm | - | - | - | - | - | - | - | - | - | - | - | - |
| | SC | Veidivötn (39%) Veidivötn (88%) | - | - | - | - | - | - | - | - | - | - |
| | SD | Grímsvötn (71%) | - | - | - | - | - | - | - | - | - | - |
| Tephra zone 8: GS16-204-22CC, 226.25 cm | 2079.4 m 0.99 | 1929.95 m 0.98 | 1677.6 m 0.98 | 1680-1681 cm Table 1 | - | - | - | - | - | - | - | - |
| | SC | Katla (64%) | - | - | - | - | - | - | - | - | - | - |
| | SD | - | 1677.6 m 1677.6 m Table 1 | 1680-1681 cm Table 1 | - | - | - | - | - | - | - | - |
| | No match | - | 1.38 | 7.31 | - | - | - | - | - | - | - | - |
| | SC | Veidivötn (20%) Kverkfjöll (12%) | - | - | 800-801 cm (THOL-2) 0.98 800-801 cm (THOL-2) 1.41 | - | - | - | - | - | - | - |
| | SD | - | - | - | - | - | - | - | - | - | - | - |

(ca. 42.1 ± 0.5 ka b2k) were geochemically analysed for major elements. The results show a basaltic near-homogeneous geochemical population (Fig. 3A) indicating an affinity with the Veidivötn volcanic system in the EVZ (Harning *et al.*, 2018) (Fig. 4D,H). Veidivötn-type tephra does not appear in the Greenland ice-core records around that time (Bourne *et al.*, 2015). However, in a marine sediment core from the Goban Spur area [MD04-2820CQ, SW of Ireland (Fig. 1A)], a Veidivötn or Reykjanes tephra deposit was found at the Greenland stadial (GS) 12 to Greenland interstadial (GI) 11 transition (Abbott *et al.*, 2016). From the GICC05 chronology this transition is dated to 43.3 ka b2k (Rasmussen *et al.*, 2014). The Veidivötn tephra shards of this deposit represent a sub-population of a heterogeneous non-isochronous deposit (Abbott *et al.*, 2016). Statistical comparison between the geochemical analyses from MD04-2820CQ, 529–530 cm and TZ-4 results in an SC of 0.989 and an SD of 1.35, suggesting a clear geochemical match between both horizons in both sediment cores (Fig. 6B; Table 1). In addition, three Kverkfjöll shards from TZ-4 are geochemically similar to shards from an overlying peak in the same deposit (MD04-2820CQ, 524–525 cm), further supporting a link between the two deposits. The marine Goban Spur deposit is described as an ice-rafted tephra deposit with some reworked material, suggesting a delayed deposition following the volcanic eruption (Abbott *et al.*, 2016). By contrast, TZ-4 (ca. $42.4\text{--}42.1 \pm 0.5$ ka b2k) appears as a high-concentration peak with gradational up- and downward tailing of shards, indicative of a Type 2A deposit (Abbott *et al.*, 2018b). This tephra was probably deposited near-instantaneously by drifting sea ice and therefore is considered a potential useful isochron in future studies. Approximately 1000 years separate the Goban Spur (MD04-2820CQ, 529–530 cm) (Abbott *et al.*, 2016) horizon and TZ-4. Three possible explanations for this age discrepancy arise: (i) the deposits are from the same eruption, but deposition in the Goban Spur area was influenced by secondary transport mechanisms; (ii) the deposits represent two closely spaced eruptions from the same volcano; or (iii) the current age estimate for TZ-4 and/or the stratigraphic position from MD04-2820CQ, 529–530 cm, are inaccurate, and the two deposits are closer in time than the available data suggest.

Tephra zone 5 (TZ-5): GS16-204-22CC, 296.25–288.25 cm (ca. 39.4–38.7 ± 0.5 ka b2k)

Between 296.25 and 288.25 cm depth (ca. $39.4\text{--}38.7 \pm 0.5$ ka b2k, Supporting Information Fig. S2), elevated concentrations of tephra shards are observed (Fig. 2A,B). A first concentration peak is recorded at 296.25 cm (ca. 39.4 ± 0.5 ka b2k) and a second at 288.25 cm (ca. 38.7 ± 0.5 ka b2k). Geochemical analyses from both peaks show a heterogeneous basaltic composition (Fig. 3B) consisting of volcanic shards that can be affiliated with the Grímsvötn (EVZ), Askja (NVZ) and Katla (EVZ) volcanic systems according to Harning *et al.* (2018) (Fig. 5A,E; Table 1). TZ-5 occurs as two closely spaced peaks of increased tephra shards with a gradational tail on both sides, indicative of a Type 2B deposit (Abbott *et al.*, 2018b). The Askja shards do not match tephra layers recorded in either the Greenland ice-core records or the North Atlantic marine records (Bourne *et al.*, 2015; Voelker and Hafliðason, 2015; Abbott *et al.*, 2018a). The Katla shards do geochemically match a sub-population of a non-isochronous tephra horizon from the Nordic Seas (MD99-2284, 3173–3174 cm, Horizon F, population 2; Berben *et al.*, 2020) (Fig. 6C; Table 1), which was deposited during GS-9 and stratigraphically fits with the layer described in this study. Nonetheless, as the MD99-2284, 3173–3174-cm horizon shows

a heterogeneous geochemical composition and up- and downward tailing of shards, this deposit is considered to have been influenced by several secondary deposition mechanisms and an input of re-worked material (Berben *et al.*, 2020). Hence, it cannot be used as a time-parallel marker. In addition, the TZ-5 tephra shards assigned to the Grímsvötn volcanic system match several established horizons, as this system generated multiple ash deposits during this period, often grouped in marine ash zone FMAZ III. The FMAZ III ash zone was originally defined as a marine tephra deposit, but investigations in several Greenland ice-cores (Bourne *et al.*, 2013) detected tephra layers that fall within the broad geochemical compositional range of the marine FMAZ III. The results from the ice-cores indicated that the FMAZ III ash zone consists of several closely spaced eruption events, all of Grímsvötn volcanic type composition that could be separated and grouped by using minor variations in TiO₂ oxide content. Recently, a similar approach was attempted for a marine sediment core from the Nordic Seas (Berben *et al.*, 2020) that revealed, at least partially, a result similar to that obtained from the ice-cores. The TZ-5 Grímsvötn shards statistically match to three Grímsvötn-type eruptives which are recorded in the NGRIP ice-core (Bourne *et al.*, 2015) dating to the period 40.22–38.79 ka b2k (GI-9) (Table 1). The tephra shards from TZ-5 probably represent a mixture of these eruptives. When compared with the North Atlantic marine tephra framework, the Grímsvötn tephra shards are geochemically similar to two tephra populations identified by Abbott *et al.* (2018a): the GI-8 layer in MD04-2829CQ at 930–931 cm and the iceberg-rafted geochemical sub-population in GIK23415-9 at 302–306 cm (Fig. 1A), deposited during H4 (Fig. 6C; Table 1).

The TZ-5 tephra deposit coincides with increased IRD concentrations that represent H4 (Griem *et al.*, 2019). During H4, a collapse of adjacent continental ice sheets caused large amounts of icebergs to drift into the Labrador Sea. Hence, over a ca. 700-year time span (i.e. 296.25–288.25 cm) the tephra shards were probably transported in that manner, causing a delayed deposition. It is likely that the tephra-bearing icebergs originated from the IIS. Due to delayed deposition this deposit is not useful as a time-marker.

Regarding the geochemical signature of the TZ-5 deposit, the Katla shards geochemically match to a sub-population of a GS-9 deposit identified in the Nordic Seas (Berben *et al.*, 2020). Furthermore, TZ-5 contains tephra shards which geochemically resemble five identified Grímsvötn deposits in the time period between ca. 40 and 38 ka b2k, three of which are from the Greenland ice cores and two are marine deposits (Bourne *et al.*, 2015; Abbott *et al.*, 2018a). The latter are assigned to GI-8, while those in the ice-cores fall within GI-9. The TZ-5 Grímsvötn shards indicate a statistical match to all five of these deposits (Table 1), for which there are several possible explanations: (i) the age model from the marine deposits is off-set by one interstadial (ca. 2000 years) and the deposits were actually deposited closer in time than the current age model suggests; (ii) the marine and ice-core deposits represent two (or more) eruptions with very similar geochemistry, deposited in consecutive interstadials, and hence are not related; and (iii) the TZ-5 Grímsvötn shards were deposited after a delay due to iceberg transport which also captured shards from eruptions that occurred during GI-9 and GI-8, in which case the age model of GS16-204-22CC appears ~500 years too old [GI-8 (38.2 ka b2k; Rasmussen *et al.*, 2014)].

Tephra zone 6 (TZ-6): GS16-204-22CC, 266.25 cm (ca. 36.7 ± 0.5 ka b2k)

From level 266.25 cm (Fig. 2A,B) corresponding to ca. 36.7 ± 0.5 ka b2k (Supporting Information Fig. S2), basaltic

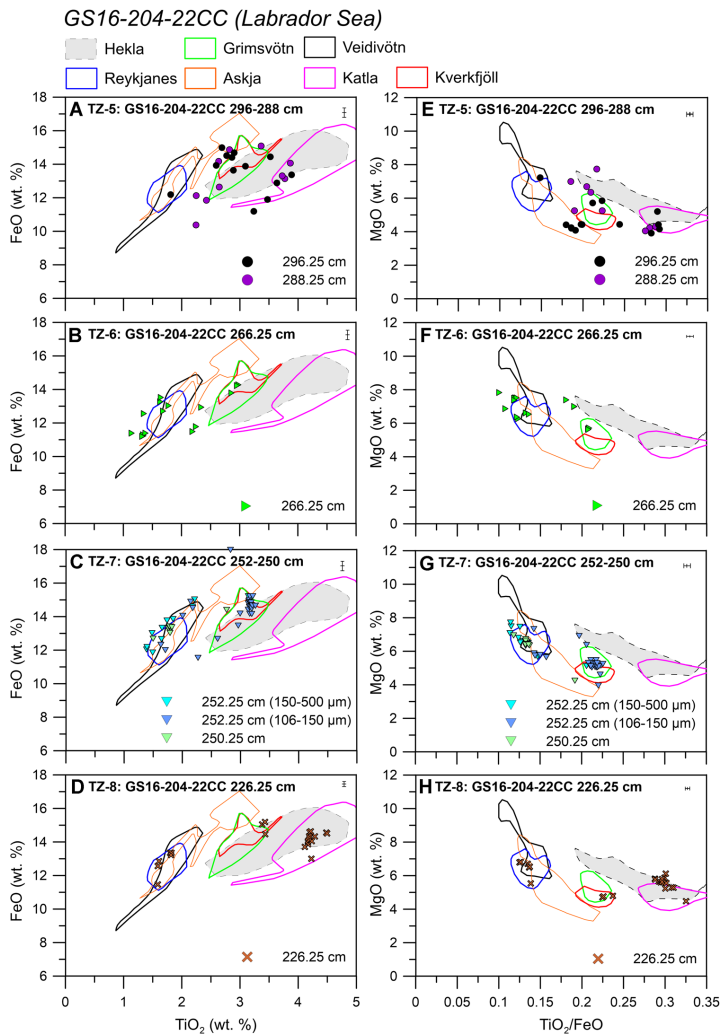


Figure 5. Visual biplot comparison (FeO versus TiO_2 and MgO versus TiO_2/FeO) of tephra shard analyses from marine sediment core GS16-204-22CC TZ 5–8. Geochemical envelopes of Icelandic volcanic systems are after Harning *et al.* (2018). Error bars represent two standard deviations of replicate analysis of BCR2g reference glass. [Color figure can be viewed at [wileyonlinelibrary.com](https://onlinelibrary.com)]

tephra shards (150–500 μm) were geochemically analysed. The analyses reveal a heterogeneous basaltic geochemistry (Fig. 3B) suggesting affinities to at least two different volcanic systems, Grímsvötn and Veidivötn (Harning *et al.*, 2018) (Fig. 5B,F; Table 1). There are no reports of Veidivötn eruptions around this time in either the North Atlantic marine records or the Greenland ice-core records (e.g. Wastegård *et al.*, 2006; Bourne *et al.*, 2015; Voelker and Hafliðason, 2015; Abbott *et al.*, 2018a). However, the geochemistry of the Grímsvötn shards resembles that of a sub-population in core MD99-2251 [1713–1714 cm (THOL-1)] from the Reykjanes Ridge area (Fig. 1A) deposited before H3 (Abbott *et al.*, 2018a) (Fig. 6D; Table 1).

TZ-6 appears as one main tephra concentration peak with a downward tail of shards, probably caused by bioturbation,

indicating a Type 3 deposit. The heterogeneous geochemical signature and evidence for increased IRD indicate a pulse of iceberg rafting. This transport mechanism is similar to that proposed for the geochemically matching sub-population in MD99-2251 (Abbott *et al.*, 2018a). Hence, deposition of TZ-6 was probably delayed and hence cannot serve as an isochronous marker.

Tephra zone 7 (TZ-7): GS16-204-22CC, 252.25–250.25 cm (ca. 34.8–34.5 \pm 0.4 ka b2k)

A zone of basaltic tephra is observed within the interval 252–250 cm (Fig. 2A,B) (34.8–34.5 \pm 0.4 ka b2k). Supporting Information Fig. S2a), which corresponds to a time span of ca.

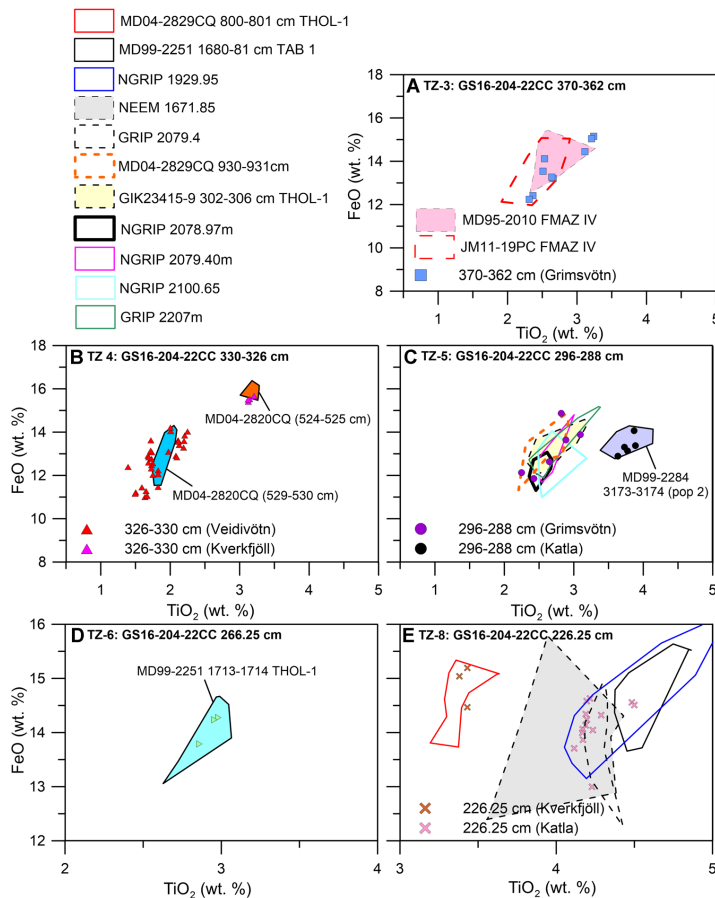


Figure 6. Visual biplot comparison of tephra shard analyses (major element oxides FeO and TiO₂) from tephra zones 3–6 and 8 in GS16-204-22CC to established tephra horizons. See Table 1 for references. [Color figure can be viewed at wileyonlinelibrary.com]

300 years. Within the analysed size fractions, the peak in the tephra concentration profile occurs at 252.25 cm (34.8 ± 0.4 ka b2k) (Fig. 2A,B). Nonetheless, basaltic shards from both 250.25 cm (34.5 ± 0.4 ka b2k, 150–500 μ m) and 252.25 cm (34.8 ± 0.4 ka b2k, 150–500 and 106–150 μ m) were geochemically analysed, to test for geochemical differences/similarities within the tephra zone. The analyses show two distinctly different populations: (i) within the coarse-grained size fraction (150–500 μ m) a homogeneous geochemical population from the Veidivötn volcanic system (Harning *et al.*, 2018) is found between 252.25 and 250.25 cm; and (ii) within the fine-grained size fraction (106–150 μ m), a homogeneous geochemical population (Fig. 3A) probably originating from the Grímsvötn volcanic system (Harning *et al.*, 2018) is observed (Fig. 5C,G). However, statistical analyses do not exclude Kverkfjöll as a potential alternative source. Neither of these tephra peaks geochemically match any previously established horizons within the Greenland ice-core records or the North Atlantic marine tephra framework (e.g. Wastegård *et al.*, 2006; Bourne *et al.*, 2015; Voelker and Hafliðason, 2015; Abbott *et al.*, 2018a) (Table 1). Both the

coarse- and the fine-grained deposits appear as one distinct tephra shard concentration peak, with some gradational upward and downward tailing consistent with a Type 2A deposit (Abbott *et al.*, 2018b). The deposit coincides with a small increase in IRD concentrations (Fig. 2C). It is therefore possible that the coarse-grained Veidivötn deposit was transported by sea ice rafting along the EGC, whereas the fine-grained Grímsvötn deposit is presumed to be of primary airborne material. Because both suggested transport mechanisms lead to near-instantaneous deposition of tephra, both peaks have the potential to serve as isochronous markers.

Tephra zone 8 (TZ-8): GS16-204-22CC, 226.25 cm (ca. 30.9 ± 0.4 ka b2k)

TZ-8 corresponds to a clear peak in the coarse-grained (150–500 μ m) tephra shard concentration profile (Fig. 2A,B). Geochemical analyses of shards from this interval reveal a heterogeneous basaltic composition (Fig. 3B) indicating three possible volcanic sources: predominantly from the Katla volcanic system, but also from the Veidivötn and Kverkfjöll

volcanic systems (Fig. 5D,H; Table 1) (Harning *et al.*, 2018). The Veidivötn population does not match any established tephra horizon. The TZ-8 Katla population geochemically matches the Katla horizon identified in GRIP (2079.40 m), NGRIP (1929.95 m) and NEM (1677.60 m) during GS-5.2 (31.4 ka b2k) yielding SCs between 0.98 and 0.99 and SDs between 0.97 and 1.41 (Fig. 6E; Table 1). In addition, TZ-8 geochemically matches the Katla isochron in MD99-2251 (1680–1681 cm, Table 1) (Abbott *et al.*, 2018a) deposited during H3. Furthermore, the TZ-8 Kverkfjöll shards geochemically resemble the MD04-2829CQ [800–801 cm (THOL-2)] (Fig. 1A) isochron (Fig. 6E; Table 1) from the eastern North Atlantic, deposited during GS-5.1 (Abbott *et al.*, 2018a). The TZ-8 tephra concentration profile shows a flat-bottom profile with an upward tailing of shards, indicating a Type 2B deposit (Abbott *et al.*, 2018b). The tephra deposit appears in conjunction with an IRD deposit which suggests iceberg rafting as the main transport agent. Thus, the deposit is not useful as an isochron. One of the populations is geochemically similar to a Katla eruption in the Greenland ice-core record that occurred around 31.4 ka b2k (Bourne *et al.*, 2015). If this was the source, it would imply a temporal delay of ~500 years between the Katla eruption in the Greenland ice-core record (Bourne *et al.*, 2015) and the deposition of the same material by icebergs in the Labrador Sea. The geochemical signature from a second population resembles a Kverkfjöll deposit identified in the eastern North Atlantic during the same time period (GS-5.1) (Abbott *et al.*, 2018a), but the two deposits were probably transported by different agents: near-instantaneous as suggested by Abbott *et al.* (2018a) and significantly delayed in the Labrador Sea (this study).

Discussion

Tephrochronological implications

We introduce five new tephra horizons with the potential to act as time-parallel markers for the Labrador Sea region in future studies. Four of the horizons originated from the Veidivötn volcanic system, whereas one was sourced from the Grímsvötn system. A summary of their key characteristics is provided in Table 2. These results suggest that although the prevailing wind-direction was probably eastwards (Halldason *et al.*, 2000; Lacasse, 2001), tephra shards from Iceland were near-instantaneously deposited in marine sediment sequences located west of Iceland. Furthermore, four of the new tephra deposits identified in this study do not geochemically match established tephra horizons from either the North Atlantic marine tephra framework or the Greenland ice-core tephra lattice (e.g. Bourne *et al.*, 2013, 2015; Abbott *et al.*, 2016, 2018a). We propose that,

after volcanic eruptions, the EGC rapidly transported Icelandic tephra material incorporated in the sea ice in a southward direction, to be deposited in southwestern regions of the North Atlantic. This mode of transportation might, however, confine deposition of these tephra layers to the Labrador Sea region, with little or no contemporaneous deposition to the east of Iceland, which have been the main focus area of previous marine North Atlantic marine tephra investigations.

The tephrostratigraphic record from core GS16-204-22CC is unique for both the area and the time period and offers the potential to make direct links between palaeoclimatic records from the Labrador Sea region and those from northern and eastern parts of the North Atlantic. However, this study has presented a continuous tephrostratigraphic record from the coarse-grained tephra fraction only, as examination of the fine-grained fraction was undertaken only for selected intervals. Hence, the full potential of the fine-grained ash component is not yet clear and should be the focus of future investigations.

Eruptive frequency of Icelandic volcanic systems during the LGP

Based on the tephrostratigraphic record from the Labrador Sea, we draw assumptions about the activity and eruptive frequency of several Icelandic volcanic systems during the LGP (Fig. 7). Throughout the record (65–30 ka b2k) the Veidivötn volcanic system consistently delivered material to the site, indicating that this system was very active during late MIS 4 and MIS 3. Before ca. 46 ka b2k, Torfajökull (NAAZ II-RHY-1) and Veidivötn appear to have been the only volcanic systems delivering material to the Labrador Sea. This is in line with previous studies that established an active Veidivötn system in MIS 4–5a, before the focused time interval of the present study (Brendryen *et al.*, 2010; Abbott *et al.*, 2011). However, in addition to Veidivötn, the Grímsvötn volcanic system was also active in the period before ca. 46 ka b2k, as shown by investigations in the northern Denmark Strait (Voelker and Halldason, 2015). Potentially, at that time, this part of Iceland (i.e. the EVZ) was covered by less continental ice or by a retreating ice sheet, producing meltwater favourable for explosive eruptions (Larsen and Eiríksson, 2008). During MIS 3, more of the Icelandic volcanoes were active compared to the glacial conditions of MIS 4. This is also indicated by tephra records obtained from the Greenland ice-cores (Bourne *et al.*, 2015). In the early MIS 3 we record increased activity of the Grímsvötn and Kverkfjöll volcanic systems. Following this, at around 40 ka b2k, the eruptive activity of the Katla and Askja volcanic systems increased. Lastly, it is apparent that Hekla was not particularly active prior to the widespread eruption known as FMAZ II dated to around

Table 2. Overview of potential tephra time-parallel markers identified in this study with respect to their estimated age, deposition type, transport mechanism, volcanic system and geochemical match to established horizons.

| Name of tephra horizon | Age (ka b2k) | Deposit type | Most likely transport mechanism | Match established horizon(s)? | Volcanic system |
|--|-----------------|--------------|---------------------------------|-------------------------------|-----------------|
| GS16-204-22CC, 530.25–524.25 cm | 64.3–63.7 ± 0.5 | Type 2A | Seasonal sea ice along the EGC | No | Veidivötn |
| GS16-204-22CC, 500.25 cm | 58.1 ± 0.8 | Type 2A | Seasonal sea ice along the EGC | No | Veidivötn |
| GS16-204-22CC, 330.25–326.25 cm | 42.4–42.1 ± 0.5 | Type 2A | Seasonal sea ice along the EGC | Yes, MD04-2829CQ (mixed) | Veidivötn |
| GS16-204-22CC, 252.25–250.25 cm (150–500 µm) | 34.8–34.5 ± 0.4 | Type 2A | Seasonal sea ice along the EGC | No | Veidivötn |
| GS16-204-22CC, 252.25 cm (106–150 µm) | 34.8 ± 0.4 | Type 2A | Primary airfall | No | Grímsvötn |

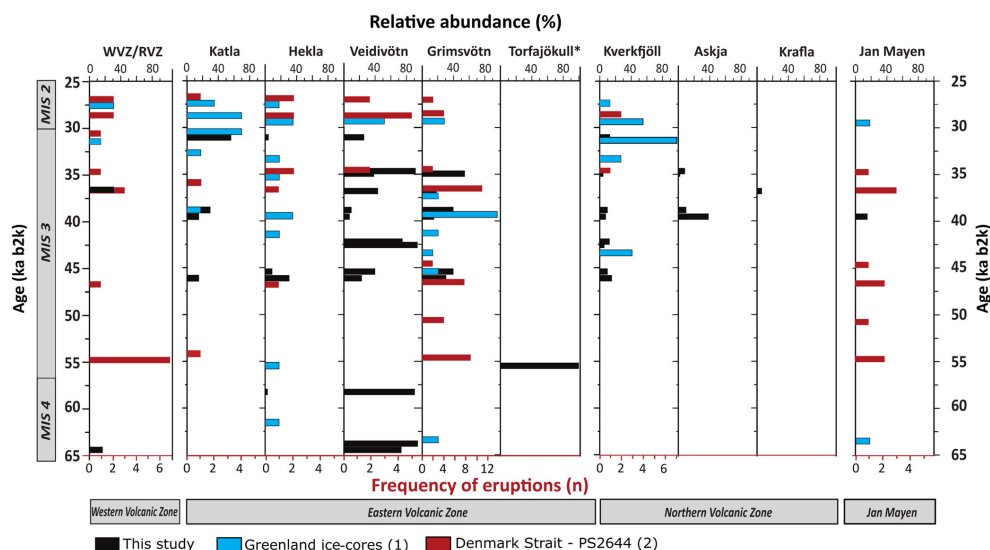


Figure 7. Estimated activity of selected Icelandic volcanoes based on the appearance in GS16-204-22CC (black bars), the Greenland ice-cores (blue bars) (Bourne *et al.*, 2013, 2015) and PS2644, Denmark Strait (red bars) (Voelker and Hafliðason, 2015). Note that black bars show relative abundance in the analysed sample (%) that relate to the top x-axis, whereas blue and red bars follow the number of eruptions on the bottom x-axis. WVZ = Western Volcanic Zone, RVB = Reykjanes Volcanic Belt. *Based on results in Rutledal *et al.* (2020). [Color figure can be viewed at wileyonlinelibrary.com]

26.7 ka b2k (e.g. Hafliðason *et al.*, 2000; Wastegård *et al.*, 2006; Davies *et al.*, 2008; Griggs *et al.*, 2014; Rutledal *et al.*, 2020).

The eruption sequences reflected in the Greenland ice-cores, marine core PS2644-5 and core GS16-204-22CC (Fig. 7) collectively suggest an eruption cyclicity of ca. 3–5 ka. This is most prominent for Veidivötn, but also in parts of the Grímsvötn record. This cyclical volcanic behaviour could reflect climate cycles that in turn modulated the volume of ice over Iceland, and/or changes in the transport pathway of ash to the Labrador Sea, Denmark Strait and Greenland. On that note, it is likely that the five primary deposits (TZ-1, -2, -4, -7 (106–150 µm and 150–500 µm), Table 2) reflect variability in the Icelandic eruptive frequency, while secondary deposits reflect changes in the transportation pathways to the Labrador Sea. Although intriguing, the proposed cyclicity needs to be substantiated by further, more detailed investigations, notably to establish the scale of delayed deposition of tephra by icebergs.

Conclusions

This first continuous stratigraphic record spanning the LGP from the Labrador Sea represents an initial stage in building a chronostratigraphic framework for this ocean sector. A total of eight tephra zones have been identified for the period 65–5 ka, five of which have the potential to serve as regional isochrons. However, at this point, these tephra isochrons do not geochemically match tephra horizons within the established North Atlantic tephra framework. The results show that the Veidivötn and Grímsvötn volcanic systems were most active during MIS 3. Prior to MIS 3 Veidivötn and Torfajökull were the only systems delivering material to the site. We find that the activity of the Veidivötn system during the studied interval shows a pattern of 3–5 ka cycles, which was also

noted in the record for Grímsvötn tephra, although not through the whole core sequence. It is not clear if these cycles reflect variability in the frequency of eruptions from the volcanic systems or changes in the ice transport pathways and/or depositional mechanisms in the Labrador Sea.

Supporting information

Additional supporting information may be found in the online version of this article at the publisher's web-site.

Figure S1. Visual biplot comparison of the rhyolitic tephra shards identified at 130–130.5 cm (150–500 µm) compared to the Vedde Ash geochemical envelope.

Figure S2. Tephrostratigraphic record from Labrador Sea core GS16-204-22CC, 0–540 cm, versus age (ka b2k).

Table S1. Age control points in sediment core GS16-204-22CC.

Supporting information.

Acknowledgement. S.R., S.M.P.B., L.G. and E.J. have received funding from the European Research Council under the European Community's Seventh Framework Program (FP7/2007–2013)/ERC grant agreement 610055 as part of the ice2ice project. H.H. has received funding from the Research Council of Norway under NRC agreement 255415 as part of the CHASE project. We thank Dr. Chris Hayward for his assistance using the electron microprobe at the Tephra Analysis Unit, University of Edinburgh. We would also like to thank R/V G.O. Sars and the ice2ice GS16-204 cruise crew members for retrieving the material used in this study. We thank John Lowe and Peter M. Abbott for their comprehensive reviews which greatly improved the manuscript.

Data availability statement

The data that support the findings of this study are available in the Supporting Information.

Abbreviations. EGC, East Greenland Current; EPMA, electron-probe microanalysis; FMAZ, Faroe Marine Ash Zone; GI, Greenland Interstadial; GIS, Greenland Ice Sheet; GS, Greenland Stadial; IIS, Icelandic Ice Sheet; IRD, ice-rafted debris; LGM, Last Glacial Maximum; LGP, Last Glacial period; LIS, Laurentide Ice Sheet; MIS, Marine Isotope Stage; NAAZ, North Atlantic Ash Zone; RVB, Reykjanes Volcanic Belt; SC, similarity coefficient; SD, statistical distance; TZ, tephra zone; WGC, West Greenland Current; WVZ, Western Volcanic Zone.

References

- Abbott PM, Bourne AJ, Purcell CS *et al.* 2016. Last glacial period cryptotephra deposits in an eastern North Atlantic marine sequence: exploring linkages to the Greenland ice-cores. *Quaternary Geochronology* **31**: 62–76.
- Abbott PM, Davies SM, Austin WEN *et al.* 2011. Identification of cryptotephra horizons in a North East Atlantic marine record spanning marine isotope stages 4 and 5a (~60,000–82,000 a b2k). *Quaternary International* **246**: 177–189.
- Abbott PM, Griggs AJ, Bourne AJ *et al.* 2018a. Tracing marine cryptotephra in the North Atlantic during the last glacial period: improving the North Atlantic marine tephrostratigraphic framework. *Quaternary Science Reviews* **189**: 169–186.
- Abbott PM, Griggs AJ, Bourne AJ *et al.* 2018b. Tracing marine cryptotephra in the North Atlantic during the last glacial period: protocols for identification, characterisation and evaluating depositional controls. *Marine Geology* **401**: 81–97.
- Batchelor CL, Margold M, Krapp M *et al.* 2019. The configuration of Northern Hemisphere ice sheets through the Quaternary. *Nature Communications* **10**: 3713.
- Berben SMP, Dokken TM, Abbott PM *et al.* 2020. Independent tephrochronological evidence for rapid and synchronous oceanic and atmospheric temperature rises over the Greenland stadial-interstadial transitions between ca. 32 and 40 ka b2k. *Quaternary Science Reviews* **236**(106277). <https://doi.org/10.1016/j.quascirev.2020.106277>
- Borchardt GA, Aruscavage PJ, Millard HTJR. 1972. Correlation of the Bishop Ash, a Pleistocene marker bed, using instrumental neutron activation analysis. *Journal of Sedimentary Petrology* **42**: 301–306.
- Bourne AJ, Cook E, Abbott PM *et al.* 2015. A tephra lattice for Greenland and a reconstruction of volcanic events spanning 25–45 ka b2k. *Quaternary Science Reviews* **118**: 122–141.
- Bourne AJ, Davies SM, Abbott PM *et al.* 2013. Revisiting the Faroe Marine Ash Zone III in two Greenland ice cores: implications for marine-ice correlations. *Journal of Quaternary Science* **28**: 641–646.
- Brendryen J, Hafliðason H, Sejrup HP. 2010. Norwegian Sea tephrostratigraphy of marine isotope stages 4 and 5: prospects and problems for tephrochronology in the North Atlantic region. *Quaternary Science Reviews* **29**: 847–864.
- Davies SM. 2015. Cryptotephra: the revolution in correlation and precision dating. *Journal of Quaternary Science* **30**: 114–130.
- Davies SM, Wastegård S, Rasmussen TL *et al.* 2008. Identification of the Fugloyarbanki tephra in the NGRIP ice core: a key tie-point for marine and ice-core sequences during the last glacial period. *Journal of Quaternary Science* **23**: 409–414.
- Davis JO. 1985. Correlation of late Quaternary tephra layers in a long pluvial sequence near Summer Lake, Oregon. *Quaternary Research* **23**: 38–53.
- Dokken TM, Cruise-Members. 2016. Ice2Ice Cruise GS16-204. In: Trond MD (ed.), Bjercknes Climate Data Centre.
- Feyling-Hanssen, RF. 1971. Weichselian interstadial foraminifera from the Sandnes-Jæren area. *Bulletin of the Geological Society of Denmark* **21**: 72–116.
- Griem L, Voelker AHL, Berben SMP *et al.* 2019. Insolation and glacial meltwater influence on sea-ice and circulation variability in the northeastern Labrador Sea during the Last Glacial period. *Paleoceanography and Paleoclimatology* **34**: 1689–1709.
- Griggs AJ, Davies SM, Abbott PM *et al.* 2014. Optimising the use of marine tephrochronology in the North Atlantic: a detailed investigation of the Faroe Marine Ash Zones II, III and IV. *Quaternary Science Reviews* **106**: 122–139.
- Hafliðason H, Eiríksson J, Kreveld SV. 2000. The tephrochronology of Iceland and the North Atlantic region during the Middle and Late Quaternary: a review. *Journal of Quaternary Science* **15**: 3–22.
- Harning DJ, Thordarson T, Geirsdóttir Á *et al.* 2018. Provenance, stratigraphy and chronology of Holocene tephra from Vestfirðir, Iceland. *Quaternary Geochronology* **46**: 59–76.
- Hayward C. 2012. High spatial resolution electron probe micro-analysis of tephra and melt inclusions without beam-induced chemical modification. *The Holocene* **22**: 119–125.
- Hesse R, Khodabakhsh S. 2016. Anatomy of Labrador Sea Heinrich layers. *Marine Geology* **380**: 44–66.
- Kvamme T, Mangerud J, Furnes H *et al.* 1989. Geochemistry of Pleistocene ash zones in cores from the North Atlantic. *Norsk Geologisk Tidsskrift* **69**: 251–272.
- Lacasse C. 2001. Influence of climate variability on the atmospheric transport of Icelandic tephra in the subpolar North Atlantic. *Global and Planetary Change* **29**: 31–55.
- Lackschewitz KS, Wallrabe-Adams H-J. 1997. Composition and origin of volcanic ash zones in Late Quaternary sediments from the Reykjanes Ridge: evidence for ash fallout and ice-rafting. *Marine Geology* **136**: 209–224.
- Larsen G, Eiríksson J. 2008. Late Quaternary terrestrial tephrochronology of Iceland – frequency of explosive eruptions, type and volume of tephra deposits. *Journal of Quaternary Science* **23**: 109–120.
- Le Maitre RW, Bateman P. 1989. *A Classification of Igneous Rocks and Glossary of Terms: Recommendations of the International Union of Geological Sciences Subcommittee on the Systematics of Igneous Rocks*. Blackwell Publishing: Oxford.
- Lowe DJ. 2011. Tephrochronology and its application: a review. *Quaternary Geochronology* **6**: 107–153.
- Pearce NJG, Alloway BV, Westgate JA. 2008. Mid-Pleistocene silicic tephra beds in the Auckland region, New Zealand: their correlation and origins based on the trace element analyses of single glass shards. *Quaternary International* **178**: 16–43.
- Perkins ME, Nash WP, Brown FH *et al.* 1995. Fallout tuffs of Trapper Creek, Idaho—a record of Miocene explosive volcanism in the Snake River Plain volcanic province. *Geological Society of America Bulletin* **107**: 1484–1506.
- Rasmussen SO, Bigler M, Blockley SP *et al.* 2014. A stratigraphic framework for abrupt climatic changes during the Last Glacial period based on three synchronized Greenland ice-core records: refining and extending the INTIMATE event stratigraphy. *Quaternary Science Reviews* **106**: 14–28.
- Rutledal S, Berben SMP, Dokken TM *et al.* 2020. Tephra horizons identified in the western North Atlantic and Nordic Seas during the Last Glacial period: extending the marine tephra framework. *Quaternary Science Reviews* **240**.
- Svensson A, Andersen KK, Bigler M *et al.* 2008. A 60 000 year Greenland stratigraphic ice core chronology. *Climate of the Past* **4**: 47–57.
- Thordarson T, Larsen G. 2007. Volcanism in Iceland in historical time: volcano types, eruption styles and eruptive history. *Journal of Geodynamics* **43**: 118–152.
- Voelker AHL, Hafliðason H. 2015. Refining the Icelandic tephrochronology of the last glacial period—the deep-sea core PS2644 record from the southern Greenland Sea. *Global and Planetary Change* **131**: 35–62.
- Voelker AHL, Samthein M, Grootes PM *et al.* 1998. Correlation of marine ¹⁴C ages from the Nordic Seas with the GISP2 isotope record; implications for ¹⁴C calibration beyond 25 ka BP. *Radio-carbon* **40**: 517–534.
- Wastegård S, Rasmussen TL. 2014. Faroe Marine Ash Zone IV: a new MIS 3 ash zone on the Faroe Islands margin. In *Geological Society, London, Special Publication 398*, Austin WEN, Abbott PM, Davies SM, Pearce NJG, Wastegård S (eds). Geological Society of London: London.
- Wastegård S, Rasmussen TL, Kuijpers A *et al.* 2006. Composition and origin of ash zones from Marine Isotope Stages 3 and 2 in the North Atlantic. *Quaternary Science Reviews* **25**: 2409–2419. <https://doi.org/10.1016/j.quascirev.2006.03.001>

Supplementary Information

“A continuous tephrostratigraphic record from the Labrador Sea spanning the last 65 ka”

Rutledal, S., Hafliðason, H., Berben, S. M. P., Griem, L., and Jansen, E.

2020, *Journal of Quaternary Science*, 35, 7, 855-868.

Table S1: Age control points in sediment core GS16-204-22CC. (1) This study, (2) Rutledal et al. (2020a), (3) Griem et al. (2019).

| Tuning tie-point | Depth (cm) | Age (ka b2k) | Error | Sedimentation rate (cm/ka) |
|---|------------|--------------|-------|----------------------------|
| $\delta^{13}\text{C}$ (opt.) ³ | 1.3 | 0.85 | 0.5 | 11.12 |
| $\delta^{13}\text{C}$ (opt.) ³ | 39.1 | 4.25 | 0.5 | 11.51 |
| Vedde Ash ¹ | 130.25 | 12.171 | 0.057 | 6.94 |
| AMS ^{14}C ³ | 150.5 | 15.09 | 0.353 | 4.81 |
| $\delta^{18}\text{O}$ (opt.) ³ | 221.25 | 29.79 | 0.5 | 4.29 |
| AMS ^{14}C ³ | 230.25 | 31.89 | 0.282 | 7.44 |
| $\delta^{18}\text{O}$ (opt.) ³ | 265.25 | 36.56 | 0.5 | 10.52 |
| $\delta^{18}\text{O}$ (opt.) ³ | 282.25 | 38.2 | 0.5 | 11.23 |
| $\delta^{18}\text{O}$ (opt.) ³ | 384.25 | 47.26 | 0.5 | 11.11 |
| NAAZ II ^{2,3} | 474.25 | 55.38 | 1.184 | 9.26 |
| $\delta^{13}\text{C}$ (opt.) ³ | 514.25 | 59.7 | 0.5 | 2.49 |
| $\delta^{18}\text{O}$ (opt.) ³ | 524.75 | 63.92 | 0.5 | 11.87 |
| $\delta^{13}\text{C}$ (opt.) ³ | 604.5 | 70.64 | 0.5 | 11.87 |

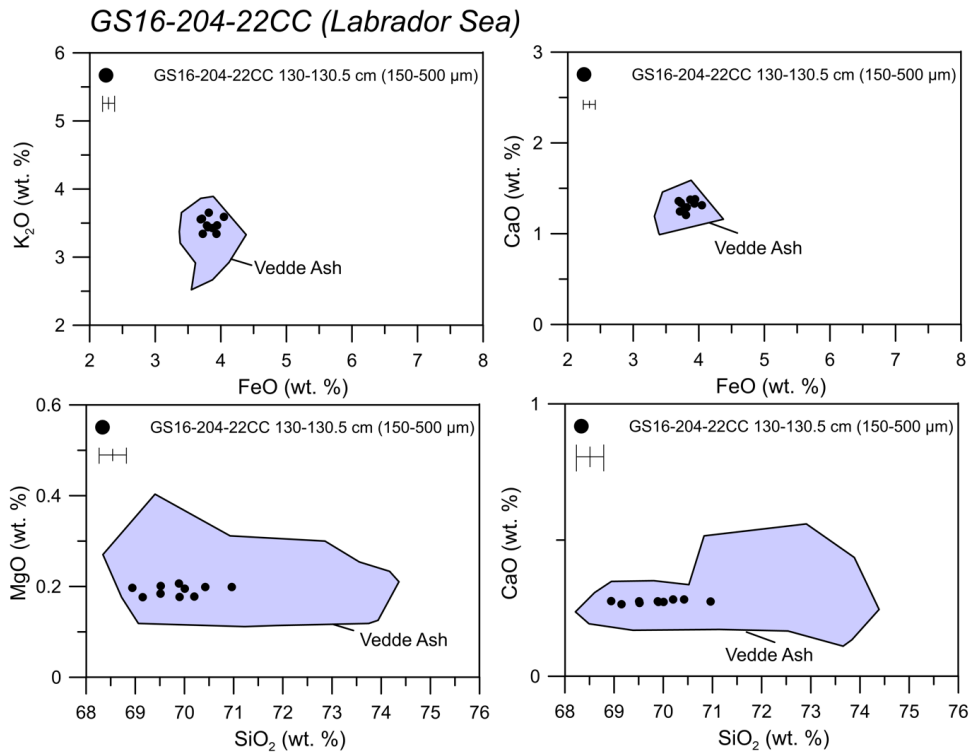


Figure S1: Visual biplot comparison of the rhyolitic tephra shards identified at 130-130.5 cm (150-500 μm) compared to the Vedde Ash geochemical envelope (Mangerud et al., 1984; Wastegård et al., 1998; Björck and Wastegård, 1999; Wastegård et al., 2000; Zillén et al., 2002; Pilcher et al., 2005).

GS16-204-22CC (Labrador Sea)

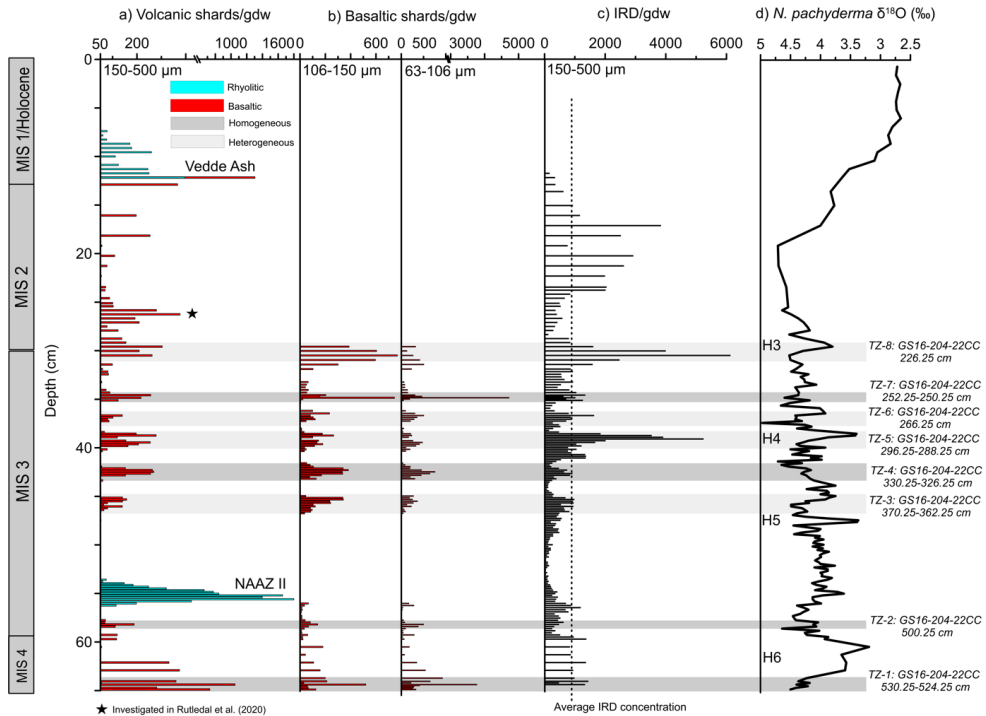


Figure S2: Tephrostratigraphic record from Labrador Sea core GS16-204-22CC 0-540 cm versus age (ka b2k). a) Occurrence of volcanic shards (basaltic and rhyolitic)/gram dry weight (gdw) 150-500 µm. b) Occurrence of basaltic shards /gram dry weight (gdw), 106-150 µm and 63-106 µm. Please note that basaltic shards/gdw were only counted for selected intervals (i.e., TZ 1-8). c) IRD (Ice rafted debris)/gdw from the 150-500 µm size fraction (Griem et al., 2019). d) $\delta^{18}\text{O}$ isotope record of the planktic foraminifera *Neogloboquadrina pachyderma* (*N. pachyderma*) (Griem et al., 2019). Grey vertical bars mark the eight tephra zones described in the text, whereas Vedde Ash and NAAZ II are indicated by name. Vertical dotted line marks the average IRD concentration within the sediment core. H3-H6 = Heinrich event 3-6.

References:

- Björck, J. & Wastegård, S. 1999. Climate oscillations and tephrochronology in eastern middle Sweden during the last glacial–interglacial transition. *Journal of Quaternary Science*, 14, 5, 399-410.
- Griem, L., Voelker, A. H. L., Berben, S. M. P., Dokken, T. M. & Jansen, E. 2019. Insolation and Glacial Meltwater Influence on Sea-Ice and Circulation Variability in the Northeastern Labrador Sea During the Last Glacial Period. *Paleoceanography and Paleoclimatology*, 34, 11, 1689-1709.
- Mangerud, J., Lie, S. E., Furnes, H., Kristiansen, I. L. & Lømo, L. 1984. A Younger Dryas Ash Bed in western Norway, and its possible correlations with tephra in cores from the Norwegian Sea and the North Atlantic. *Quaternary Research*, 21, 1, 85-104.
- Pilcher, J., Bradley, R. S., Francus, P. & Anderson, L. 2005. A Holocene tephra record from the Lofoten Islands, Arctic Norway. *Boreas*, 34, 2, 136-156.
- Rutledal, S., Berben, S. M. P., Dokken, T. M., van der Bilt, W. G. M., Cederstrom, J. M. & Jansen, E. 2020. Tephra horizons identified in the western North Atlantic and Nordic Seas during the Last Glacial Period: Extending the marine tephra framework. *Quaternary Science Reviews*, 240, 106247.
- Wastegård, S., Björck, S., Possnert, G. & Wohlfarth, B. 1998. Evidence for the occurrence of Vedde Ash in Sweden: radiocarbon and calendar age estimates. *Journal of Quaternary Science*, 13, 3, 271-274.
- Wastegård, S., Wohlfarth, B., Subetto, D. A. & Sapelko, T. V. 2000. Extending the known distribution of the Younger Dryas Vedde Ash into northwestern Russia. *Journal of Quaternary Science*, 15, 6, 581-586.
- Zillén, L. M., Wastegård, S. & Snowball, I. F. 2002. Calendar year ages of three mid-Holocene tephra layers identified in varved lake sediments in west central Sweden. *Quaternary Science Reviews*, 21, 1583-1591.

8. Appendix I

Mg/Ca based temperature reconstruction of surface and intermediate/deep-waters in the Labrador and Norwegian Sea during the GI-15 climate event

Sunniva Rutledal^{1*}, Amandine Tisserand², Sarah M. P. Berben¹, Trond M. Dokken² and Eystein Jansen^{1,2}

¹Department of Earth Science, University of Bergen, and The Bjerknes Centre for Climate Research, Bergen, Norway.

²Norwegian Research Centre (NORCE) and The Bjerknes Centre for Climate Research, Bergen, Norway

1. Introduction

Here we have reconstructed Mg/Ca based surface and intermediate/deep-water temperatures during the warm Greenland Interstadial (GI) 15. The material was collected from two North Atlantic marine sediment cores, located in the Norwegian (MD95-2010) and Labrador Sea (GS16-204-22CC), two key regions for deep-water formation and constituents of the AMOC today (Matsumoto, 2017).

We use the NAAZ II (II-RHY-1) tephra marker as a correlational tie-point. The NAAZ II (II-RHY-1) was initially identified as a marine rhyolitic tephra deposit (Bramlette and Bradley, 1941; Ruddiman and Glover, 1972) before it was correlated to the Greenland ice-cores (Grönvold et al., 1995). From the Greenland ice-cores, an age of $55\,380 \pm 1184$ b2k was assigned (Svensson et al., 2008). The tephra deposit has since been traced to the Torfajökull volcano (Moles et al., 2019) and is identified over a wide-spread area of the North Atlantic, making this an extremely useful correlational tie-point. According to the GICC05 chronology GI-15 covers the period from 55 800 to 54 900 a b2k, during early Marine Isotope Stage (MIS) 3 (Rasmussen et al., 2014). This period is punctuated by two short-lived stadials (GS 15.1 and GS 15.2), and NAAZ II (II-RHY-1) occur on exactly the transition from GI-15.2 to GS-15.2 (Figure A2) (Rasmussen et al., 2014).

2. Material and Methods

2.1 Marine sediment cores

The sediment core MD95-2010 was retrieved from the Vøring Plateau in the Norwegian Sea ($66^{\circ} 41.05' \text{ N}$; $04^{\circ} 33.97' \text{ E}$) at 1226 m water depth aboard R/V Marion Dufresne and the sediment core GS16-204-22CC was retrieved from the eastern Labrador Sea, south of Greenland ($58^{\circ} 02,83' \text{ N}$; $47^{\circ} 02,36' \text{ W}$) at 3160 m water depth during the Ice2Ice-2016 cruise aboard R/V G.O. Sars.

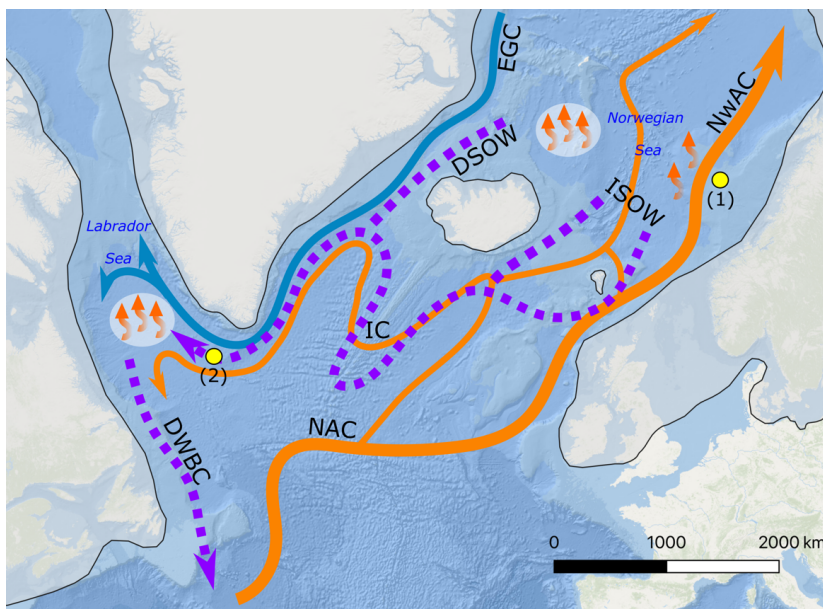


Figure A1: Map of study area. Core MD95-2010 (1) and core GS16-204-22CC (2) are marked. EGC = East Greenland Current, NwAC = Norwegian Atlantic Current, NAC = North Atlantic Current, IC = Irminger Current, DSOW = Denmark Strait Overflow Water, ISOW = Iceland Scotland Overflow Water, DWBC = Deep Western Boundary Current. Ice sheet margins by Batchelor et al. (2019).

2.2 Chronology

We apply the identification of the volcanic tephra marker NAAZ II (II-RHY-1) as a correlational tie-point to link the two marine sediment cores. In MD95-2010 (at 1000.5 cm), NAAZ II (II-RHY-1) was first visually described by Dokken and Jansen (1999) and was geochemically confirmed to be NAAZ II (II-RHY-1) by Abbott et al. (2018). In GS16-204-22CC, NAAZ II (II-RHY-1) was identified at 474.25 cm and is described by Rutledal et al. (2020). The horizons in both cores are considered near-instantaneously deposited.

In addition, we constrain the chronology to the Greenland ice-core record for both cores using magnetic susceptibility time-series to denote interstadial-stadial transitions (Table A1, Figure A2), with increased values marking GI periods (Voelker and Haflidason, 2015), and stable isotopes ($\delta^{18}\text{O}$ & $\delta^{13}\text{C}$) of planktonic foraminifera to denote Heinrich-events and the MIS 4/3 transition (Table A1, Figure A2).

3. Results

Dataset can be found in Table A2.

We measured Mg/Ca on *Neoglobiquadrina pachyderma* (*N. pachyderma*) (150-212 μm) (every 2 cm), *Cassidulina neoteretis* (*C. neoteretis*) (150-500 μm) (MD95-2010) and *Melonis barleanum* (*M. barleanum*) (150-500 μm) (GS16-204-22CC) (only samples containing sufficient material) (see Table A2). The habitat depth of *N. pachyderma* is driven by sea-ice and chlorophyll concentration and can thus be quite variable, but average around 100 m water depth (Greco et al., 2019), and therefore represent near-surface waters. *C. neoteretis* and *M. barleanum* are benthic shallow infaunal species (Corliss, 1985; Jansen et al., 1990) and represent intermediate/deep-waters.

The Mg/Ca temperatures of *N. pachyderma* were reconstructed using the modified calibration equation from Elderfield and Ganssen (2000) by Ezat et al. (2016). Mg/Ca temperatures of *C. neoteretis* were reconstructed using the modified calibration from Kristjánssdóttir et al. (2007) by Sessford et al. (2018). Lastly, Mg/Ca temperatures of

M. barleeanum were reconstructed using the calibration from Hasenfratz et al. (2017). The foraminifera shells were prepared for Mg/Ca analysis at the Trace Element Lab (TELab), NORCE, following procedures described in Sessford et al. (2018).

Table A1: Chronological tie-points used to establish the age chronology for both sediment cores used in this study. References are as follows: (1) (Voelker et al., 1998; Griem et al., 2019)– (2) Rasmussen et al. (2014), (3) Svensson et al. (2008). MS = magnetic susceptibility.

| Climate Event | Marine climate event indicator | Age ka (b2k) | GS16-204-22CC (depth cm) | Sedimentation rate (cm/ka) | MD95-2010 (depth cm) | Sedimentation rate (cm/ka) |
|--------------------|----------------------------------|--------------|--------------------------|----------------------------|----------------------|----------------------------|
| Start of GI-11 | MS | 43.34 (2) | - | - | 888.5 | 11.9 |
| Start of GI-12 | MS | 46.86 (2) | - | - | 930.5 | 9.5 |
| Heinrich event 5 | Planktonic $\delta^{18}\text{O}$ | 47.26 (1) | 386.25 | 7.5 | - | - |
| Start of GI-13 | MS | 49.28(2) | 401.25 | 11.1 | 953.5 | 8.1 |
| Start of GI-14 | MS | 54.22 (2) | 456.25 | 18.9 | 992.5 | 6.0 |
| Peak GI-15.1 | MS | 54.96 (2) | 470.25 | 9.5 | - | - |
| NAAZ II (II-RHY-1) | Tephra | 55.38 (3) | 474.25 | 14.3 | 1000.5 | 19.0 |
| Start of GI-15.2 | MS | 55.8 (2) | 480.25 | 8.7 | 1008.5 | 8.5 |
| Start of GI-16.2 | MS | 58.28 (2) | - | - | 1029.5 | 17.2 |
| Start of GI-17.2 | MS | 59.44 (2) | - | - | 1049.5 | 76.9 |
| MIS 4/3 transition | Planktonic $\delta^{13}\text{C}$ | 59.7(1) | 514.25 | 3.0 | 1068.5 | 76.9 |

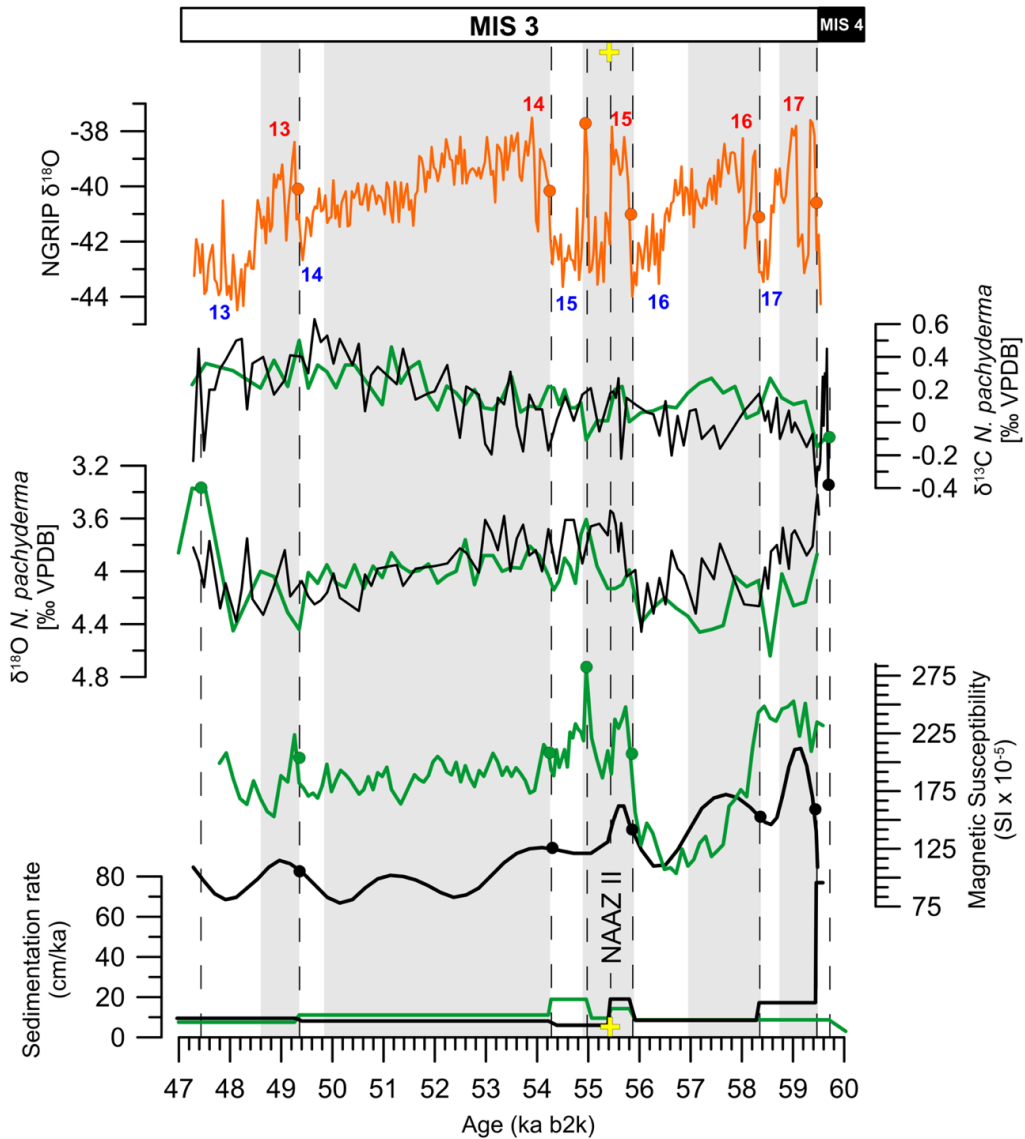


Figure A2: Chronology of cores MD95-2010 and GS16-204-22CC after tuned to NGRIP (NGRIP members et al., 2004) using tie-points listed in Table A1. Yellow cross marks the position of NAAZ II (II-RHY-1). Red and blue numbering denote GIs and GSs respectively. Green = GS16-204-22CC, Black = MD95-2010. MD95-2010 proxy records from Dokken and Jansen (1999). GS16-204-22CC proxy records from Griem et al. (2019).

Table A2: Mg/Ca (mmol/mol) measurements and reconstructed temperatures T ($^{\circ}\text{C}$). Replicated measurements are noted in brackets. Asterisk indicate combined samples of ± 1 cm. Preliminary and unpublished data.

| Core | Depth (cm) | <i>N. pachyderma</i> | | <i>M. barleaanum</i> (GS16-204-22CC) / <i>C. neoteretis</i> (MD95-2010) | |
|---------------|------------|----------------------|--------------------------|---|--------------------------|
| | | Mg/Ca (mmol/mol) | T ($^{\circ}\text{C}$) | Mg/Ca (mmol/mol) | T ($^{\circ}\text{C}$) |
| GS16-204-22CC | 450.25 | 0.402 | 0.04 | 0.774 | -0.16 |
| GS16-204-22CC | 451.25 | - | - | 0.813 | 0.19 |
| GS16-204-22CC | 452.25 | 0.447 | 1.10 | 0.905 | 1.00 |
| GS16-204-22CC | 453.25 | - | - | 0.848 | 0.50 |
| GS16-204-22CC | 454.25 | 0.422 | 0.55 | - | - |
| GS16-204-22CC | 455.25 | - | - | 0.901* | 0.96* |
| GS16-204-22CC | 456.25 | 0.397 | -0.08 | 0.810 | 0.16 |
| GS16-204-22CC | 458.25 | 0.329 | -1.95 | 0.786* | -0.06* |
| GS16-204-22CC | 460.25 | 0.458 | 1.36 | 0.651 | -1.25 |
| GS16-204-22CC | 461.25 | - | - | 0.797 | 0.04 |
| GS16-204-22CC | 462.25 | 0.396 | -0.10 | 0.704 | -0.78 |
| GS16-204-22CC | 464.25 | 0.462 | 1.44 | - | - |
| GS16-204-22CC | 466.25 | 0.497 [0.534] | 2.17 [2.9] | 1.006* | 1.89* |
| GS16-204-22CC | 468.25 | 0.387 | -0.34 | 0.966* | 1.54* |
| GS16-204-22CC | 470.22 | 0.487 | 1.96 | 0.884* | 0.81* |
| GS16-204-22CC | 472.25 | 0.446 | 1.09 | - | - |
| GS16-204-22CC | 473.25 | - | - | 0.863* | 0.63* |
| GS16-204-22CC | 474.25 | 0.450 | 1.18 | - | - |
| GS16-204-22CC | 475.25 | - | - | 0.795* | 0.02* |
| GS16-204-22CC | 476.25 | 0.403 | 0.09 | 0.794 | 0.02 |
| GS16-204-22CC | 477.25 | - | - | 0.914 | 1.08 |
| GS16-204-22CC | 478.25 | 0.380 | -0.51 | - | - |

| | | | | | |
|---------------|--------|---------------|--------------|--------|--------|
| GS16-204-22CC | 479.25 | - | - | 0.819* | 0.24* |
| GS16-204-22CC | 480.25 | 0.402 | 0.04 | 0.788 | -0.04 |
| GS16-204-22CC | 481.25 | - | - | 0.859 | 0.59 |
| GS16-204-22CC | 482.25 | 0.409 | 0.23 | 0.875 | 0.73 |
| GS16-204-22CC | 484.25 | 0.358 | -1.10 | 0.856 | 0.57 |
| GS16-204-22CC | 486.25 | 0.352 | -1.28 | 0.863* | 0.63* |
| GS16-204-22CC | 487.25 | - | - | 0.935 | 1.26 |
| GS16-204-22CC | 488.25 | 0.409 | 0.22 | - | - |
| GS16-204-22CC | 490.25 | 0.425 [0.514] | 0.60 [2.50] | - | - |
| GS16-204-22CC | 492.25 | 0.337 | -1.72 | - | - |
| GS16-204-22CC | 494.25 | 0.371 [0.671] | -0.76 [5.18] | 0.771* | -0.18* |
| GS16-204-22CC | 496.25 | 0.453 | 1.25 | - | - |
| GS16-204-22CC | 497.25 | - | - | 1.116 | 2.87 |
| MD95-2010 | 981.5 | - | - | 0.804 | 0.47 |
| MD95-2010 | 982.5 | 0.457 | 1.33 | - | - |
| MD95-2010 | 984.5 | 0.469 | 1.59 | 0.847 | 0.94 |
| MD95-2010 | 986.5 | 0.428 | 0.69 | 0.769 | 0.07 |
| MD95-2010 | 988.5 | 0.439 | 0.93 | - | - |
| MD95-2010 | 990.5 | 0.387 | -0.32 | 0.768 | 0.06 |
| MD95-2010 | 992.5 | 0.440 | 0.95 | 0.822 | 0.67 |
| MD95-2010 | 994.5 | 0.473 | 1.67 | 0.714 | -0.60 |
| MD95-2010 | 995.5 | - | - | 0.626 | -1.78 |
| MD95-2010 | 996.5 | 0.503 | 2.29 | 0.600 | -2.16 |
| MD95-2010 | 998.5 | 0.378 | -0.55 | 0.581 | -2.46 |
| MD95-2010 | 1000.5 | 0.426 | 0.62 | 0.610 | -2.02 |
| MD95-2010 | 1002.5 | 0.336 | -1.73 | 0.824* | 0.70* |
| MD95-2010 | 1004.5 | 0.408 | 0.20 | - | - |
| MD95-2010 | 1006.5 | 0.404 | 0.11 | 0.583 | -2.42 |
| MD95-2010 | 1007.5 | - | - | 0.657 | -1.34 |

| | | | | | |
|-----------|--------|---------------|-------------|-----------------------|-----------------------|
| MD95-2010 | 1008.5 | 0.476 [0.680] | 1.74 [5.31] | 0.673 [0.718] | -1.13 [-0.54] |
| MD95-2010 | 1010.5 | 0.459 | 1.37 | 0.706 [0.818] [0.816] | -0.71 [0.63] [0.61] |
| MD95-2010 | 1012.5 | 0.466 | 1.53 | 0.819 [0.911] | 0.64 [1.60] |
| MD95-2010 | 1013.5 | - | - | 0.705 | -0.71 |
| MD95-2010 | 1014.5 | 0.428 | 0.68 | - | - |
| MD95-2010 | 1015.5 | - | - | 0.719* | -0.53* |
| MD95-2010 | 1016.5 | 0.449 | 1.16 | - | - |
| MD95-2010 | 1018.5 | 0.430 | 0.71 | 0.594 [0.614] | -2.26 [-1.96] |
| MD95-2010 | 1020.5 | 0.418 | 0.44 | 0.678 [0.651] [0.682] | -1.06 [-1.43] [-1.02] |
| MD95-2010 | 1022.5 | 0.419 | 0.46 | - | - |
| MD95-2010 | 1025.5 | 0.406 | 0.16 | 0.672 | -1.14 |
| MD95-2010 | 1030.5 | 0.381 | -0.49 | - | - |

References:

- Abbott, P. M., Griggs, A. J., Bourne, A. J., Chapman, M. R. & Davies, S. M. 2018. Tracing marine cryptotephra in the North Atlantic during the last glacial period: Improving the North Atlantic marine tephrostratigraphic framework. *Quaternary Science Reviews*, 189, 169-186.
- Bramlette, M. N. & Bradley, W. H. 1941. Geology and Biology of North Atlantic Deep-Sea cores between Newfoundland and Ireland: 1. Lithology and Geologic interpretation. *U.S. Geological Survey Professional Paper*, 196-A, 1-34.
- Batchelor, C. L., Margold, M., Krapp, M., Murton, D. K., Dalton, A. S., Gibbard, P. L., Stokes, C. R., Murton, J. B., Manica, A. 2019. The configuration of Northern Hemisphere ice sheets through the Quaternary. *Nature Communications*, 10, 3713.
- Corliss, B. H. 1985. Microhabitats of benthic foraminifera within deep-sea sediments. *Nature*, 314, 6010, 435-438.
- Dokken, T. M. & Jansen, E. 1999. Rapid changes in the mechanism of ocean convection during the last glacial period. *Nature*, 401, 6752, 458-461.
- Elderfield, H. & Ganssen, G. 2000. Past temperature and $\delta^{18}\text{O}$ of surface ocean waters inferred from foraminiferal Mg/Ca ratios. *Nature (London)*, 405, 6785, 442-445.

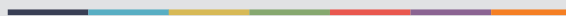
-
- Ezat, M. M., Rasmussen, T. L. & Groeneveld, J. 2016. Reconstruction of hydrographic changes in the southern Norwegian Sea during the past 135 kyr and the impact of different foraminiferal Mg/Ca cleaning protocols. *Geochemistry, Geophysics, Geosystems*, 17, 8, 3420-3436.
- Greco, M., Jonkers, L., Kretschmer, K., Bijma, J. & Kucera, M. 2019. Depth habitat of the planktonic foraminifera *Neogloboquadrina pachyderma* in the northern high latitudes explained by sea-ice and chlorophyll concentrations. *Biogeosciences*, 16, 17, 3425-3437.
- Griem, L., Voelker, A. H. L., Berben, S. M. P., Dokken, T. M. & Jansen, E. 2019. Insolation and Glacial Meltwater Influence on Sea-Ice and Circulation Variability in the Northeastern Labrador Sea During the Last Glacial Period. *Paleoceanography and Paleoclimatology*, 34, 11, 1689-1709.
- Grönvold, K., Óskarsson, N., Johnsen, S. J., Clausen, H. B., Hammer, C. U., Bond, G. & Bard, E. 1995. Ash layers from Iceland in the Greenland GRIP ice core correlated with oceanic and land sediments. *Earth and Planetary Science Letters*, 135, 1, 149-155.
- Hasenfratz, A. P., Schiebel, R., Thornalley, D. J. R., Schönfeld, J., Jaccard, S. L., Martínez-García, A., Holbourn, A., Jennings, A. E., Kuhnt, W., Lear, C. H., Marchitto, T. M., Quillmann, U., Rosenthal, Y., Yu, J. & Haug, G. H. 2017. Mg/Ca-temperature calibration for the benthic foraminifera *Melonis barleeanum* and *Melonis pompilioides*. *Geochimica et cosmochimica acta*, 217, 365-383.
- Jansen, E., Sjøholm, J., Bleil, U. & Erichsen, J. A. 1990. Neogene and Pleistocene Glaciations in the Northern Hemisphere and Late Miocene — Pliocene Global Ice Volume Fluctuations: Evidence from the Norwegian Sea. In: BLEIL U. & J., T. (eds.) *Geological History of the Polar Oceans: Arctic versus Antarctic. NATO ASI Series (Series C: Mathematical and Physical Sciences)*. Springer, Dordrecht.
- Kristjánsdóttir, G. B., Lea, D. W., Jennings, A. E., Pak, D. K. & Belanger, C. 2007. New spatial Mg/Ca-temperature calibrations for three Arctic, benthic foraminifera and reconstruction of north Iceland shelf temperature for the past 4000 years. *Geochemistry, Geophysics, Geosystems*, 8, 3, Q03P21-n/a.
- Matsumoto, K. 2017. Tantalizing evidence for the glacial North Atlantic bottom water. *PNAS*, 114, 11, 2794-2796.
- Moles, J. D., Mcgarvie, D., Stevenson, J. A., Sherlock, S. C., Abbott, P. M., Jenner, F. E. & Halton, A. M. 2019. Widespread tephra dispersal and ignimbrite emplacement from a subglacial volcano (Torfajökull, Iceland). *Geology*, 47, 6, 577-580.

- NGRIP Members, Andersen, K. K., Azuma, N., Barnola, J. M., Bigler, M., Biscaye, P., Caillon, N., Chappellaz, J., Clausen, H. B., Dahl-Jensen, D., Fischer, H., Fluckiger, J., Fritzsche, D., Fujii, Y., Goto-Azuma, K., Gronvold, K., Gundestrup, N. S., Hansson, M., Huber, C., Hvidberg, C. S., Johnsen, S. J., Jonsell, U., Jouzel, J., Kipfstuhl, S., Landais, A., Leuenberger, M., Lorrain, R., Masson-Delmotte, V., Miller, H., Motoyama, H., Narita, H., Popp, T., Rasmussen, S. O., Raynaud, D., Rothlisberger, R., Ruth, U., Samyn, D., Schwander, J., Shoji, H., Siggard-Andersen, M. L., Steffensen, J. P., Stocker, T., Sveinbjornsdottir, A. E., Svensson, A., Takata, M., Tison, J. L., Thorsteinsson, T., Watanabe, O., Wilhelms, F. & White, J. W. 2004. High-resolution record of Northern Hemisphere climate extending into the last interglacial period. *Nature*, 431, 147-151.
- Rasmussen, S. O., Bigler, M., Blockley, S. P., Blunier, T., Buchardt, S. L., Clausen, H. B., Cvijanovic, I., Dahl-Jensen, D., Johnsen, S. J., Fischer, H., Gkinis, V., Guillevic, M., Hoek, W. Z., Lowe, J. J., Pedro, J. B., Popp, T., Seierstad, I. K., Steffensen, J. P., Svensson, A. M., Vallelonga, P., Vinther, B. M., Walker, M. J. C., Wheatley, J. J. & Winstrup, M. 2014. A stratigraphic framework for abrupt climatic changes during the Last Glacial period based on three synchronized Greenland ice-core records: refining and extending the INTIMATE event stratigraphy. *Quaternary Science Reviews*, 106, 14-28.
- Ruddiman, W. F. & Glover, L. K. 1972. Vertical Mixing of Ice-Rafted Volcanic Ash in North Atlantic Sediments. *Geological Society of America Bulletin*, 83, 9, 2817-2835.
- Rutledal, S., Berben, S. M. P., Dokken, T. M., van der Bilt, W. G. M., Cederstrom, J. M. & Jansen, E. 2020. Tephra horizons identified in the western North Atlantic and Nordic Seas during the Last Glacial Period: Extending the marine tephra framework. *Quaternary Science Reviews*, 240, 106247.
- Sessford, E. G., Tisserand, A. A., Risebrobakken, B., Andersson, C., Dokken, T. & Jansen, E. 2018. High-Resolution Benthic Mg/Ca Temperature Record of the Intermediate Water in the Denmark Strait Across D-O Stadial-Interstadial Cycles. *Paleoceanography and Paleoclimatology*, 33, 11, 1169-1185.
- Svensson, A., Andersen, K. K., Bigler, M., Clausen, H. B., Dahl-Jensen, D., Davies, S. M., Johnsen, S. J., Muscheler, R., Parrenin, F., Rasmussen, S. O., Rothlisberger, R., Seierstad, I. K., Steffensen, J. P. & Vinther, B. M. 2008. A 60 000 year Greenland stratigraphic ice core chronology. *Climate of the Past*, 1, 47-57.
- Voelker, A. H. L., Sarinthein, M., Grootes, P. M., Erlenkeuser, H., Laj, C., Mazaud, A., Nadeau, M.-J., Schleicher, M., Mook, W. G. & Van Der Plicht, J. 1998. Correlation of marine (super 14) C ages from the Nordic Seas with the GISP2 isotope record; implications for (super 14) C calibration beyond 25 ka BP. *Radiocarbon*, 40, 1, 517-534.

- Voelker, A. H. L. & Hafliðason, H. 2015. Refining the Icelandic tephrochronology of the last glacial period – The deep-sea core PS2644 record from the southern Greenland Sea. *Global and Planetary Change*, 131, 35-62.
- Waelbroeck, C., Labeyrie, L., Michel, E., Duplessy, J. C., Mcmanus, J. F., Lambeck, K., Balbon, E. & Labracherie, M. 2002. Sea-level and deep water temperature changes derived from benthic foraminifera isotopic records. *Quaternary Science Reviews*, 21, 1-3, 295-305.



Graphic design: Communication Division, UIB / Print: Skjipes Kommunikasjon AS



uib.no

ISBN: 9788230859209 (print)
9788230864012 (PDF)